

University of Nebraska - Lincoln

DigitalCommons@University of Nebraska - Lincoln

---

Theses, Dissertations, and Student Research from  
Electrical & Computer Engineering

Electrical & Computer Engineering, Department of

---

Summer 7-30-2019

# Human-Cognition-in-the-Loop: A Framework to Include Decision Process in Closed Loop Control

Mehdi Firouznia

University of Nebraska-Lincoln, frouznia@gmail.com

Follow this and additional works at: <https://digitalcommons.unl.edu/elecengtheses>



Part of the [Electrical and Computer Engineering Commons](#)

---

Firouznia, Mehdi, "Human-Cognition-in-the-Loop: A Framework to Include Decision Process in Closed Loop Control" (2019).  
*Theses, Dissertations, and Student Research from Electrical & Computer Engineering*. 106.  
<https://digitalcommons.unl.edu/elecengtheses/106>

This Article is brought to you for free and open access by the Electrical & Computer Engineering, Department of at DigitalCommons@University of Nebraska - Lincoln. It has been accepted for inclusion in Theses, Dissertations, and Student Research from Electrical & Computer Engineering by an authorized administrator of DigitalCommons@University of Nebraska - Lincoln.

HUMAN-COGNITION- IN-THE-LOOP:  
A FRAMEWORK TO INCLUDE DECISION PROCESS IN CLOSED LOOP  
CONTROL

by

Mehdi Firouznia

A DISSERTATION

Presented to the Faculty of  
The College of Engineering at the University of Nebraska  
In Partial Fulfilment of Requirements  
For the Degree of Doctor of Philosophy

Major: Electrical Engineering

Under the Supervision of Professor Qing Hui

Lincoln, Nebraska

July, 2019

HUMAN-COGNITION- IN-THE-LOOP:  
A FRAMEWORK TO INCLUDE DECISION PROCESS IN CLOSED LOOP  
CONTROL

Mehdi Firouznia, Ph.D.

University of Nebraska, 2019

Adviser: Q.Hui

This thesis proposes a framework to include human cognitive process in making decision into control loop. Our approach in solving this problem is to add a complementary control which includes a model of human decision to the controller, capable of predicting human command accuracy in the near future. The outcome of decision unit can either be presented to the operator as a directive or may adjust the issued command toward better results. In order to construct human decision model, we combined three approaches of bio-physical connectionist, mathematical abstraction and behavioral cognitive models in the adaptive gain theory framework. We first extended the classic DDM to include a layer that represent the change of strategy from weighted additive to heuristics and proved that such model is mathematically sound and well defined. Then by the help of adaptive gain theory, we showed that by collecting feedback signals from operator, we are able to predict her decision quality.

We also presented a prototype for a supervisory controller that includes the dynamics of making decisions by humans in the control loop. A two-stage model for strategy selection and decision making was utilized to cover a range of situations, in which the operators are required to make proper decisions. A controller was designed to dispatch the tasks between the system and the operator to keep the operator close to the best performance region. A case study for a simple one-attribute task was

simulated to show the effectiveness of the proposed controller.

One major assumption in designing complementary control unit was that the feedback physiological signals can be mapped onto NE-LC gamma plane, hence the quality of decision at each time is known to controller. In the experiment section, we relaxed this assumption and showed that by using commercially available technologies, it is possible to infer the decision strategy and accuracy.

DEDICATION

*To Poupack and the one we are expecting...*

## ACKNOWLEDGMENTS

I would like to thank my advisor, Qing Hui, for all his help, advice, insights and patience over the course of this research. I also thank Jeffrey Stevens for all his advice and collaboration in the experiment part.

Many thanks go to my other committee members Jerry Hudgins and Sohrab Asgarpour. I also thank Fred Choobineh for giving me the opportunity to work under his supervision at the first part of my graduate school.

I thank Jessica Calvi at UNL Salivary Bioscience Laboratory for processing the bio-physiological data and Adam Caprez in the Holland Computer Center for his help and advice regarding neural model simulation. Many thanks to Chen Peng for his help in designing supervisory system and Elise Thayer for her help in analyzing E4 wristband data.

Bob Millikan, Ben Powel and my fellow volleyball teammates at the university recreation center helped me a lot to have a nice time during my graduate school in Lincoln. I thanked them all.

## Table of Contents

<b>List of Figures</b>	<b>ix</b>
<b>List of Tables</b>	<b>xii</b>
<b>1 Introduction</b>	<b>1</b>
<b>2 Neuro-Physiological models</b>	<b>5</b>
2.1 Electrophysiology of Neurons . . . . .	6
2.1.1 Gated Channels . . . . .	9
2.1.2 Hodgkin-Huxley Equations . . . . .	10
2.2 Integrate and Fire . . . . .	11
2.3 Simple Model . . . . .	12
2.3.1 Bifurcations . . . . .	13
2.3.2 Normal form . . . . .	18
2.4 Modeling Population of Neurons . . . . .	22
<b>3 Mathematical Abstractions</b>	<b>27</b>
3.1 SPRT approach . . . . .	28
3.1.1 Single-cue two-choice task . . . . .	28
3.1.2 Multi-cue two-choice task . . . . .	31
3.1.3 Single-cue multi-choice task . . . . .	32

3.1.4	Multi-cue multi-choice task . . . . .	33
3.2	Markov chain approach . . . . .	34
3.2.1	Multi-Choice tasks . . . . .	39
3.2.2	Autoregressive Model . . . . .	40
<b>4</b>	<b>Cognitive approach in modeling decision</b>	<b>46</b>
4.1	Behavioral models . . . . .	47
4.2	From WADD to Heuristics . . . . .	49
4.3	Adaptive Gain Control Theory . . . . .	51
4.3.1	LC-NE Framework . . . . .	52
4.4	Adaptive gain with strategy layer . . . . .	56
<b>5</b>	<b>Human Decision in the Loop</b>	<b>59</b>
5.1	Human-Cognition-in-the-Loop Supervisory Control . . . . .	61
5.1.1	Augmented supervisory system . . . . .	61
5.2	Case study . . . . .	63
5.2.1	Human decision accuracy . . . . .	65
5.2.2	Controller design . . . . .	67
<b>6</b>	<b>Experiment</b>	<b>70</b>
6.1	Effect of stress . . . . .	71
6.2	Experiment set-up . . . . .	72
6.2.1	Decision-making task . . . . .	73
6.2.2	Stressor task . . . . .	74
6.2.3	Biological data . . . . .	75
6.2.4	Method . . . . .	76
6.3	Stressor task results . . . . .	78

6.3.1	Visual analog scale (VAS) . . . . .	78
6.3.2	Inter-beat interval (IBI) . . . . .	80
6.3.2.1	Frequency domain analysis . . . . .	81
6.3.2.2	Time domain analysis . . . . .	82
6.3.3	Salivary Alpha-Amylase (sAA) . . . . .	83
6.3.4	Skin conductance (EDA) . . . . .	84
6.3.5	Effect of stressor; Discussion . . . . .	85
6.3.6	Decision task results . . . . .	88
6.3.6.1	Decision task results; Discussion . . . . .	93
<b>7</b>	<b>Conclusion</b>	<b>95</b>
<b>A</b>	<b>Expectation and variance of multi-cue multi-choice model</b>	<b>98</b>
A.1	Paracontraction . . . . .	99
A.2	Asymptotic Analysis of Discrete-Time Systems . . . . .	101
A.2.1	Discrete-time switched linear systems . . . . .	101
A.2.2	Homogeneous subsystem . . . . .	103
A.2.3	Non-homogeneous subsystem . . . . .	112
A.3	Asymptotic Approximation of Mean-Value Multi-Cue Multi-Choice Tasks	118
A.3.1	Asymptotic approximation of expectation . . . . .	118
A.3.2	Asymptotic approximation of variance . . . . .	123
	<b>Bibliography</b>	<b>126</b>

## List of Figures

2.1	Ion concentration and Nernst equilibrium potential [1] . . . . .	6
2.2	Equivalent electrical circuit representation of a neuron . . . . .	8
2.3	Saddle node bifurcation in $I_{Na,p} + I_K$ model. $I = 0$ above, $I = 4.51$ middle, $I > 4.51$ below [1] . . . . .	15
2.4	Supercritical Anronov-Hopf bifurcation in $I_{Na,p} + I_K$ model [1] . . . . .	17
2.5	Different spiking regime, produced by simple model [1] . . . . .	23
2.6	Populations of neurons and their interconnection . . . . .	24
4.1	Change of LC mode based on long and short term utilities. . . . .	55
4.2	Brain parts that govern decision process . . . . .	55
4.3	Schematic diagram of decision model . . . . .	57
4.4	Proposed adaptive gain control and strategy selection framework . . . . .	58
5.1	Common Human-in-the-loop control scheme . . . . .	62
5.2	Human-cognition-in-the-loop control framework . . . . .	64
5.3	The region of operator high performance in $\Gamma$ plane for moving dot task with complexity 50% . . . . .	66
5.4	$\Gamma$ gain plain trajectory of operator . . . . .	68
5.5	Human operator's accuracy $a_H$ . . . . .	69
5.6	Overall accuracy $a$ . . . . .	69

6.1	choice task screen . . . . .	74
6.2	Time line of experiment . . . . .	77
6.3	VAS results . . . . .	78
6.4	Estimated distribution of differences and effect size, Highest Posterior Density (HPD) Interval is selected to be 94% . . . . .	79
6.5	Change of the average value of stress level in VAS; group1: before stress, group2: after stress. Difference of mean = $18.05 \pm 6.51$ , Difference of stds = $1.34 \pm 1.84$ . . . . .	80
6.6	Sample frequency domain analysis of IBI in 400 seconds period . . . . .	82
6.7	Change of frequency measures in three 400 sec. intervals; baseline, stress and end . . . . .	83
6.8	Estimated distribution of difference (group1-group2) average, standard deviation and effect size of LFnorm (top) and HFnorm (middle) and LF/HF ratio (bottom) in IBI trail; group1: baseline, group2: stress . . . . .	84
6.9	Estimated distribution of difference (group1-group2) average, standard deviation and effect size of LFnorm (top) and HFnorm (middle) and LF/HF ratio (bottom) in IBI trail; group1: baseline, group2: end . . . . .	85
6.10	Estimated difference (group1-group2) of mean and its standard deviation for LFnorm, HFnorm and LF/HF ratio in IBI trail; group1: baseline, group2: end . . . . .	86
6.11	Estimated difference (group1-group2) of mean and its standard deviation for SDNN and RMSSD; group1: baseline, group2: end . . . . .	87
6.12	Box plot of sAA . . . . .	87
6.13	Sample EDA graphs for two participants; red line indicates the start of stressor task . . . . .	88

6.14	Time and frequency of retrieving data, summed over all participants, choice tasks 1 and 2 . . . . .	90
6.15	Time and frequency of retrieving data for each decision task, summed over all participants, choice tasks 1 and 2 . . . . .	91
6.16	Sum of time and frequency of retrieving data, averaged for each participant, choice tasks 1 and 2. The value of cues decreases from left to right . . . . .	91
6.17	Search index of participants in session 1 and 2 . . . . .	93

## List of Tables

2.1	Neuron dynamics classifications . . . . .	19
4.1	Decision strategies spectrum [2] . . . . .	48
4.2	Cue information for hiring example . . . . .	50
4.3	Cue information with different weight factors . . . . .	51
4.4	Candidate values recalculated . . . . .	51
5.1	Accuracy of the augmented decision-making process . . . . .	65
6.1	Attributes and benefits for choice task . . . . .	73
6.2	Summary of choice task results . . . . .	94

## Chapter 1

### Introduction

On September 8, 2011, the largest power outage in California’s history occurred because a technician erroneously shut down a power line. None of the automated control and protection systems could prevent this incident because the human operator had the authority to override autonomy. While fool-proofing complex cyber-physical networks with unprecedented emergency scenarios is a common approach, the important lesson learned from such an incident is that a comprehensive solution to system control should include human behavior in the loop. In the current “human-in-the-loop” perspective, researchers provide only a rough caricature of actual human cognition and decision making. Without cognitively realistic models of human decision making, one cannot appropriately model these systems and develop decision tools to help human operators cope with abrupt changes and unprecedented situations. Thus, a fundamental need exists to bridge this critical gap in understanding of human operator decision making in CPS.

The *ultimate goal* of this project is to improve the expected performance of CPS, considering human factors in the control loop. This includes robustness and resilience of CPS against catastrophic failures. The physical system, human operators, and the control system together form a so-called human-in-the-loop supervisory control

system. The proposed research aims to optimize this human-in-the-loop supervisory control system by mainly controlling the parts that affect human performance. In other words, the project aims to achieve the goal by affecting human operators status instead of only controlling physical systems parameters. For this purpose, the first step is to develop appropriate models for human roles in CPS by integrating cognitive science perspectives on human decision making. Then, one can focus on searching reasonable decision-making strategies for the human-in-the-loop supervisory control system. The proposed research can refine these two steps into the following objectives:

**Objective 1:** Develop and simulate models for human decision making process, interacting with cyber-physical network specially under internal and external stress factors such as emergencies.

**Objective 2:** Propose a control strategy to maximize the average success rate of human decision making for CPS.

Furthermore, in order to model actual human decision making, an experiment is design to empirically validate the theoretical results. That is, in addition to investigate theoretically, which classes of models perform well, this study aims to test whether these models capture the decisions that people actually make. The main feature of the experiment is using commercialized technology to establish the closed loop control scheme, including the data required from physical and emotional state of decision maker. In this way, minimal set of effecting factors, i.e. stress and fatigue were chosen and their effect on decision models investigated.

In Chapters 2, we first review approaches in modeling human decision making process known as biophysics-based models. Spiking neural network (SNN) models is neuron-level approach to mimic the process of decision making in the brain by simulating the dynamics that govern a single neuron activity as well as the dynamics of synaptic connections. Spiking neural networks mostly use the *leaky integrate-*

*and-fire* (LIF) model for each single neuron, which is essentially a one-dimensional model without the capability of producing the diverse and intricate range of neuronal spiking behavior. For that reason, we decided to choose *simple model* which is two dimensional dynamical model and by help of mathematical tools, specifically bifurcation theory, can produce a diverse range of neuronal spiking regimes. Later in Chapter 5, we simulated the behavior of population of neurons, each modeled with simple model to get a measure of human decision performance for a sample task.

In Chapter 3, mathematical abstraction methods in describing decision process are investigated. This approach is built on drift diffusion model (DDM). A DDM is a mathematical abstraction in which the continuum limit of the sequential probability ratio test is employed in the sense that it captures the optimal decision time, assuming a fixed accuracy rate and initial conditions. It can account for how behavioral performance improves over time as a result of the accumulation of information, and has been successfully applied to predict human accuracy and reaction time. Two separate approaches in deriving continuous and discrete DDM processes are introduced and a complete model for multi-cue multi-choice task with strategy selection layer is proposed. Through mathematically rigorous process, we proved that the proposed model is well defined and converge in first and second statistical moments.

Chapter 4 deals with the notation of strategy selection which is a common term in behavioral science. In general, strategy selection is a tool to cope with situation that flow of information and/or the decision process itself undergo changes that deviate from optimal practice. One good example is the level of stress in decision maker that affect her performance in a great deal. Here we specifically focus on locus coeruleus-norepinephrine (LC-NE) framework, a process in human brain that plays a complex and specific role in judgment and decision. Combining our proposed DDM model with LC-NE process and strategy selection practice, we construct a closed loop feedback

model to mimic the human decision process in an enterprise level control platform.

Chapter 5 gives an example of supervisory and control system that utilize the proposed decision model. Our purpose in building such example is to show that constructed model can be used in conjunction with modern AI technologies to enhance the performance of the system in a great deal. Though some assumptions are made, specially in terms of biological feed back data ( excitatory-inhibitory gain level) which are not collectible with today's commercial technologies. To address this shortcoming, in Chapter 6 we design an experiment to show that with more accessible data such as hear-beat variability we can estimate the state of decision maker in terms of using different strategies in stressful condition. Therefore, even with today's commercialized technologies it is viable to use the human cognition in the loop framework for enhanced system control.

The innovation of the current study stems from the integration of three different approaches in modeling human process, namely bio-physically inspired models, mathematical abstract models and behavioral models into one comprehensive framework which is capable to pair with system autonomy and improve the overall performance specifically under stress condition. Having such model in hand and validate it through experiment, the proposed research may be able to inspire the development of a network supervisory control scheme that facilitates better operator decision making by helping reduce operator's error specially during emergency situations.

## Chapter 2

### Neuro-Physiological models

Finding a complete description of nervous system dynamics is still a far fetching goal, however considerable advancements have happened in recent years to construct a mathematical model that can emulate the physiological properties of a single neuron. Neurons produce action potential or *spike* to communicate with each other. Spike is an abrupt and transient change of membrane voltage. Inputs which are received through dendritic tree or synapses cause trans-membrane currents and consequently post-synaptic potentials (PSPs) that tend to change the membrane potential of the neuron. Large PSPs can be amplified by the voltage sensitive processes embedded in the neuronal membrane and lead to generation of spike. A typical neuron receives input from more than 10,000 other neurons and fire spikes with different regimes. So the fundamental question is why the response of neurons to their inputs are so much different. Is there a simple model that can describe the response with acceptable accuracy?

In this chapter we investigate models that are based on of electrophysiology of neurons which primarily focused on dynamics of membrane voltage in the classic approach. Then using the mathematical tools provided by dynamical systems and bifurcation theory, we proceed to know more involved model, named simple model [1].

The core concept is treating neurons as dynamical systems and using mathematical tools such as phase analysis and bifurcation theory to find a minimal model, capable of describing the wide range of neural activities. But first let's take a quick look at neuronal electrophysiology to have a better understanding of the dynamics of a neuron.

## 2.1 Electrophysiology of Neurons

Neurons use ionic currents to conduct their electrical activities. The transmembrane ionic currents mostly include one of the four ions, namely sodium( $\text{Na}^+$ ), potassium( $\text{K}^+$ ), calcium ( $\text{Ca}^{2+}$ ), or chloride ( $\text{Cl}^-$ ). The concentration of ions is different on the inside and the outside of a cell, which is the driving force of their movement. As depicted in Fig. 2.1, the concentration of ( $\text{Na}^+$ ) and ( $\text{Cl}^-$ ) is high in extracellular medium while inside the cell there is more concentration of ( $\text{K}^+$ ) and negatively charged molecules denoted by ( $\text{A}^-$ ).

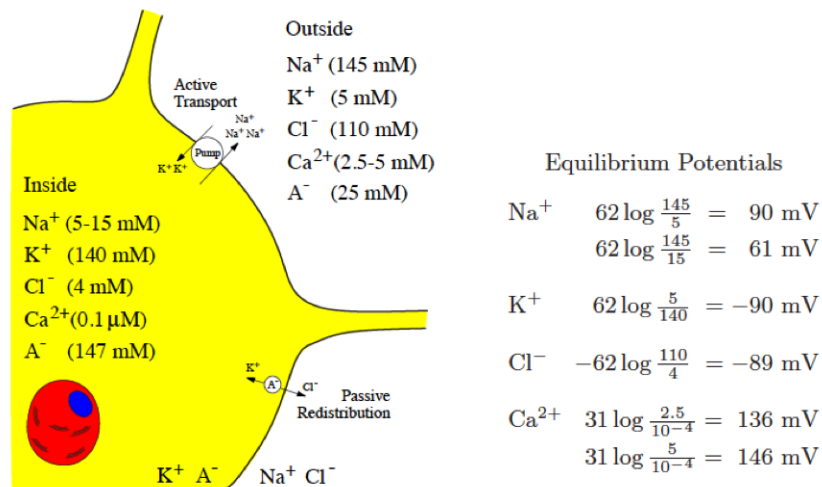


Figure 2.1: Ion concentration and Nernst equilibrium potential [1]

Active (pumping of ions via ionic pumps ) and passive (attraction of ( $\text{K}^+$ ) and

repelling of ( $\text{Cl}^-$ ) by impermeable ( $\text{A}^-$ ) ) redistribution of ions through membrane protein channels maintain the stability of membrane voltage in the rest state. The process involves two opposite forces. For instance, consider ( $\text{K}^+$ ) ions. Since the concentration is lower on the outside, the ions start to flow outward and make the inside medium more negative. This induces an increasing voltage difference on two sides of membrane which makes it harder for ( $\text{K}^+$ ) currents to flow outward. At one point the equilibrium is achieved when concentration gradient and electric potential gradient cancel each other and the net current becomes zero. The value of equilibrium potential depends on the ionic species and called the *Nernst* potential. Based on that the net current is given by:

$$I_{\text{K}} = g_{\text{K}}(V - E_{\text{K}}) \quad (2.1)$$

In which  $V$  is membrane potential in volts,  $g_{\text{K}}$  is the ( $\text{K}^+$ ) conductance in ( $\text{mS}/\text{cm}^2$ ) and  $E_{\text{K}}$  is the Nernst potential of ( $\text{K}^+$ ). The same type of equation can describe other ionic currents which lead to the equivalent circuit of Fig. 2.2, for a single neuron. Note that the capacitance of membrane is in ( $\mu\text{F}/\text{cm}^2$ ). Based on electrical equivalent circuit of Fig. 2.2, the equation that describes the ionic currents is:

$$\begin{aligned} C\dot{V} &= I - I_{\text{Na}} - I_{\text{Ca}} - I_{\text{K}} - I_{\text{Cl}} \\ &= I - g_{\text{Na}}(V - E_{\text{Na}}) - g_{\text{Ca}}(V - E_{\text{Ca}}) - g_{\text{K}}(V - E_{\text{K}}) - g_{\text{Cl}}(V - E_{\text{Cl}}) \end{aligned} \quad (2.2)$$

If there is no additional source or injected current then  $I = 0$ . In this case the membrane potential is typically bounded by :

$$E_{\text{K}} < E_{\text{Cl}} < V_{\text{rest}} < E_{\text{Na}} < E_{\text{Ca}} \quad (2.3)$$

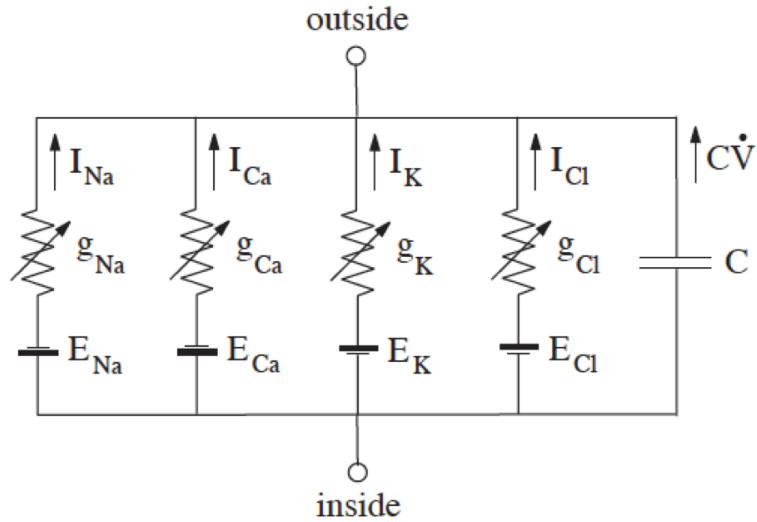


Figure 2.2: Equivalent electrical circuit representation of a neuron

Also note that  $I_{Na}$ ,  $I_{Ca} < 0$  (inward currents) that make the membrane potential more positive or cause depolarization while  $I_K$ ,  $I_{Cl} > 0$  (outward currents) that make the membrane potential more negative or cause hyperpolarization. At  $V_{rest}$  we have  $\dot{V} = 0$  and hence:

$$V_{rest} = \frac{g_{Na}E_{Na} + g_{Ca}E_{Ca} + g_K E_K + g_{Cl}E_{Cl}}{g_{Na} + g_{Ca} + g_K + g_{Cl}} \quad (2.4)$$

The denominator of 2.4 is the total input conductance,  $g_{inp}$ , of the neuron. The quantity  $R_{inp} = 1/g_{inp}$  is called the input resistance. The bigger value of resistance results in larger displacement from  $V_{rest}$  due to injection of DC current  $I$ .

The input resistance is a function of membrane voltage and time. The common experiment to see the relationship is holding the membrane voltage at fixed value  $V_c$  by means of voltage-clamp. Then reset the value of voltage to  $V_s$  and measure the instantaneous and asymptotic currents. The instantaneous I-V curves usually has non-monotone N-shape curve which shows the nonlinear positive feedback trans-

membrane process and can be assumed fast enough to have instantaneous kinetic [3]. The steady state I-V relation can be monotone or not depending on the properties of membrane current.

### 2.1.1 Gated Channels

Ionic channels are large transmembrane protein that facilitate the flow of ions through the membrane. The electrical conductance of the channel may be controlled by gating particles which switch the channels between close and open states [4]. The net current generated by large population of identical channels can be described by the equation

$$I = \bar{g}p(V - E) \quad (2.5)$$

in which parameter  $p$  is the average proportion of channels in open state. If the channel is selective for a single ion, the value of  $E$  will be the relevant Nernst potential. When the gating variable is sensitive to the membrane voltage the channels are called voltage-gated. Also the gates are divided to activation gates and inactivation gates. The probability of an activation gate is being open is denoted by variable  $m$  and the probability of inactivation gate in open state is denoted by variable  $h$ . Therefore

$$p = m^a h^b \quad (2.6)$$

where  $a$  and  $b$  are the number of activation and deactivation gates respectively. Some channels do not have inactivation gates ( $b = 0$ ). Such channels do not inactivate which results in persistent currents. In contrast channels with inactivation results in transient currents. The dynamic of activation variable is given by a first order

differential equation [3]:

$$\dot{m} = (m_\infty(V) - m)/\tau(V) \quad (2.7)$$

The values of steady state activation function and time constant can be measured experimentally. Likewise the dynamics of inactivation variable is described by first order differential equation

$$\dot{h} = (h_\infty(V) - h)/\tau(V) \quad (2.8)$$

Inactivation kinetics is usually slower than activation kinetics.  $h_\infty(V)$  has the same sigmoid shape of  $m_\infty(V)$ .

### 2.1.2 Hodgkin-Huxley Equations

Using experimental techniques, Hodgkin and Huxley (1952) determined that giant squid axon carries three major currents : voltage gated persistent  $K^+$  current with four activation gates, voltage gated transient  $Na^+$  current with three activation gates and one inactivation gate, and ohmic leak current which carried mostly by  $Cl^-$ . The model is described by the following set of equations [5].

$$\begin{aligned} C\dot{V} &= I - \bar{g}_K n^4 (V - E_K) - \bar{g}_{Na} m^3 h (V - E_{Na}) - \bar{g}_L (V - E_L) \\ \dot{n} &= (n_\infty - n)/\tau_n(V) \\ \dot{m} &= (m_\infty - m)/\tau_m(V) \\ \dot{h} &= (h_\infty - h)/\tau_h(V) \end{aligned} \quad (2.9)$$

Where the steady state and time constant values of gating variables are function of  $V$  and time. It is common to approximate the steady state activation curve by

Boltzmann function [3], e.g. for  $m$

$$m_{\infty}(V) = \frac{1}{1 + \exp\{(V_{1/2} - V)/k\}} \quad (2.10)$$

The parameter  $V_{1/2}$  satisfies  $m_{\infty}(V_{1/2}) = 0.5$  and  $k$  is the slope factor (negative for  $h$ ). Smaller values of  $|k|$  results in steeper curves. The time constant is approximated by Gaussian function

$$\tau(V) = C_{\text{base}} + C_{\text{amp}} \exp \frac{-(V_{\text{max}} - V)^2}{\sigma^2} \quad (2.11)$$

Hodgkin-Huxley model is constructed based on evidence gathered from a single experiment. However for more general modeling purpose, a normal form that universally describes the neuron behavior is required.

## 2.2 Integrate and Fire

The most popular neural model is known as integrate-and-fire [6]. In this model, neurons are integrator units that sum up the incoming PSPs and compare the sum with a threshold value. If the sum is greater than the threshold, neuron will fire a spike and then the membrane potential reset to a rest value. In other words, spikes are generated whenever the membrane potential  $u$  crosses the threshold value  $\vartheta$ . The firing time is defined as the crossing moment, i.e.  $u(t^f) = \vartheta$ .

The standard equation of linear leaky integrate-and-fire neuron is given by [6]:

$$\tau_m \frac{du}{dt} = -u(t) + RI(t) \quad (2.12)$$

in which  $\tau_m = RC$  is membrane time constant and  $R$  and  $C$  are equivalent resistance

and capacitance (see Fig 2.2). When  $u(t^{(f)}) = \vartheta$ , the spike is emitted and the potential resets to the rest value,  $u_r$ , after spending refractory period,  $\Delta_{abs}$ . If it is assumed that the last spike was emitted at  $\hat{t}$ , the value of  $u(t)$  is given by:

$$u(t) = u_r \exp\left(-\frac{t - \hat{t}}{\tau_m}\right) + \frac{1}{C} \int_0^{t - \hat{t}} \exp\left(-\frac{s}{\tau_m}\right) I(t - s) ds \quad (2.13)$$

In general, parameters of the model can be seen as voltage dependent functions which leads to nonlinear model as follows:

$$\tau \frac{du}{dt} = F(u) + G(u)I \quad (2.14)$$

The input current is sum of external stimuli and postsynaptic current pulse. We will get back to model the postsynaptic current in the upcoming sections.

## 2.3 Simple Model

Theoretically, the integrator model is based on Hodgkin-Huxley model of spike generation in squid giant axon. However, further investigations showed that both integration and threshold notions are not applicable for the wide range of neural activities. Surprisingly even for the Hodgkin-Huxley model the threshold value is not well defined. Based on understanding of neuronal behavior given by Hodgkin-Huxley model, and employing dynamical systems and bifurcation theory, a simple normal model is constructed as we describe in following sections.

### 2.3.1 Bifurcations

Before deriving the minimal model let us briefly review the concept of bifurcation in planar systems [7]. Consider the following two dimensional dynamical system

$$\begin{aligned}\dot{x} &= f(x, y) \\ \dot{y} &= g(x, y)\end{aligned}\tag{2.15}$$

Functions  $f$  and  $g$  describe the evolution of two dimensional state variables  $(x(t), y(t))$  on the phase plane. The system 2.15 defines a vector field on the phase plane, since the direction of change of  $(x(t), y(t))$  is defined at each point. The set of points where  $f(x, y) = 0$  is called  $x$ -nullcline. The  $x$ -nullcline partitions the phase plane into two regions where  $x$  moves in opposite directions.  $y$ -nullcline is defined in the same fashion. The intersection of nullclines is equilibrium point. There are three major types of equilibria namely node, saddle and focus. The equilibrium is a *node* if the eigenvalues of the Jacobian matrix of the model, calculated at the equilibrium point are both real and have the same sign. If they are negative, the node is stable. The trajectories tend to converge or diverge from the node along the eigenvector corresponding the eigenvalue having the smallest absolute value. If the sign of real eigenvalues are not the same the equilibrium is a *saddle*. Saddles are unstable. Complex conjugate eigenvalues means the equilibrium is a *focus*. The imaginary part of the eigenvalue determines the frequency of rotation of trajectories around the focus.

A trajectory that forms a closed loop in the phase plane is called *periodic orbit*. Sometimes the orbit is isolated and sometimes it is part of a continuum. An isolated periodic orbit is called *limit cycle*. Limit cycles can be stable that attract all trajec-

tories close enough or unstable that repel the nearby trajectories. Note that there is always at least one equilibrium inside any limit cycle.

To explain the concept of bifurcation, we use two dimensional neuronal model with state variables  $(V, n)$ . Remember that  $n$  is the activation variable of  $I_K$ . We assume that variable  $m$  is fast enough and can be replaced by its steady state value. We also neglect the effect of  $h$ . The state equations of resulted  $I_{Na,p} + I_K$  model is give by [1]:

$$\begin{aligned} C\dot{V} &= I - \bar{g}_K n(V - E_K) - \bar{g}_{Na} m_\infty(V - E_{Na}) - \bar{g}_L(V - E_L) \\ \dot{n} &= (n_\infty - n)/\tau_n(V) \end{aligned} \quad (2.16)$$

Where  $I$  is injected current. First we investigate the process of saddle-node bifurcation. The phase portrait of the model is depicted in Fig 2.3. When the injected current is small, there are two equilibria in low voltage range, a stable node corresponding to the rest state and a saddle. Increasing the parameter  $I$  will move the V-nullcline upward and at some value of  $I$  the saddle and the node coalesce. Further increase of  $I$  results in disappearance of the low voltage equilibria and remaining of only a limit cycle attractor corresponds to repetitive firing state. This process is called saddle-node bifurcation.

Finding  $I - V$  relationship is another common way to analyze the bifurcation. In the equilibria, we have

$$0 = I - \bar{g}_K n_\infty(V - E_K) - \bar{g}_{Na} m_\infty(V - E_{Na}) - \bar{g}_L(V - E_L) \quad (2.17)$$

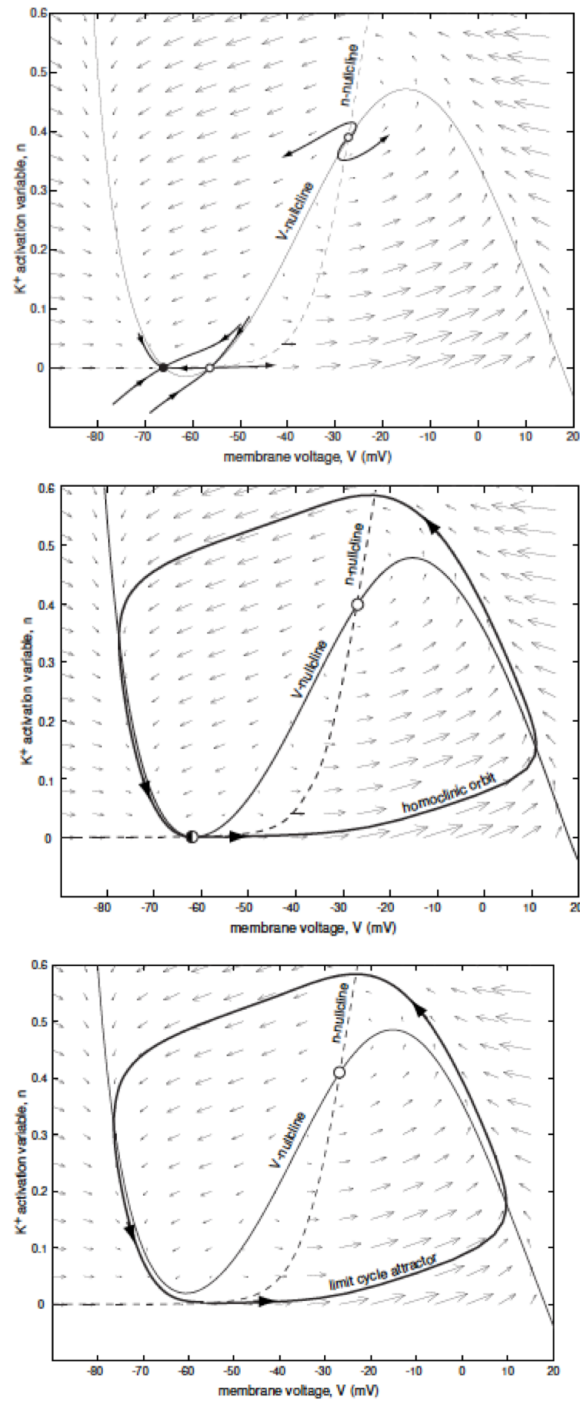


Figure 2.3: Saddle node bifurcation in  $I_{Na,p} + I_K$  model.  $I = 0$  above,  $I = 4.51$  middle,  $I > 4.51$  below [1]

Using  $V$  as free parameter we get

$$I = \bar{g}_K n_\infty (V - E_K) + \bar{g}_{Na} m_\infty (V - E_{Na}) + \bar{g}_L (V - E_L) \quad (2.18)$$

The right hand side of 2.18 can be interpreted as steady state current  $I_\infty(V)$ .

Saddle-node on invariant circle bifurcation is a standard saddle-node bifurcation with one additional condition. The post bifurcation limit cycle attractor happens to be an invariant homoclinic circle (originate and terminate at the same annihilation point of saddle-node). This type of bifurcation happens in our  $I_{Na,p} + I_K$  model when the  $K^+$  current has long time constant. When the current is fast, it activates during upstroke and decreases the amplitude of the action potential. Also it is fast enough to deactivate during the downstroke, resulting in overshoot and creating another upstroke. In contrast, slow current can not be deactivated fast enough during downstroke and cause undershoot, with  $V$  going below resting state. The result is a limit cycle attractor with infinite period, or firing in zero frequency.

If in the model 2.16, the  $K^+$  has lower threshold of activation voltage, the behavior of neuron changes due to the change of bifurcation to Andronov-Hopf bifurcation. The phase portrait of Fig 2.4 shows that for small values of  $I$  there is just one stable focus corresponding to rest state. By increasing the input value, the focus loses its stability and gives birth to a small-amplitude limit cycle attractor. The amplitude of the limit cycle grows as  $I$  increases.

To get the bifurcation diagram, for each input  $I$ , the transient period is neglected and both values of  $\min V(t)$  and  $\max V(t)$  is plotted. When  $I$  is small, the solution converges to the stable equilibrium and both maximum and minimum values are equal to the resting voltage. By increasing the input, the values start to diverge meaning the existence of a limit cycle attractor with increasing amplitude

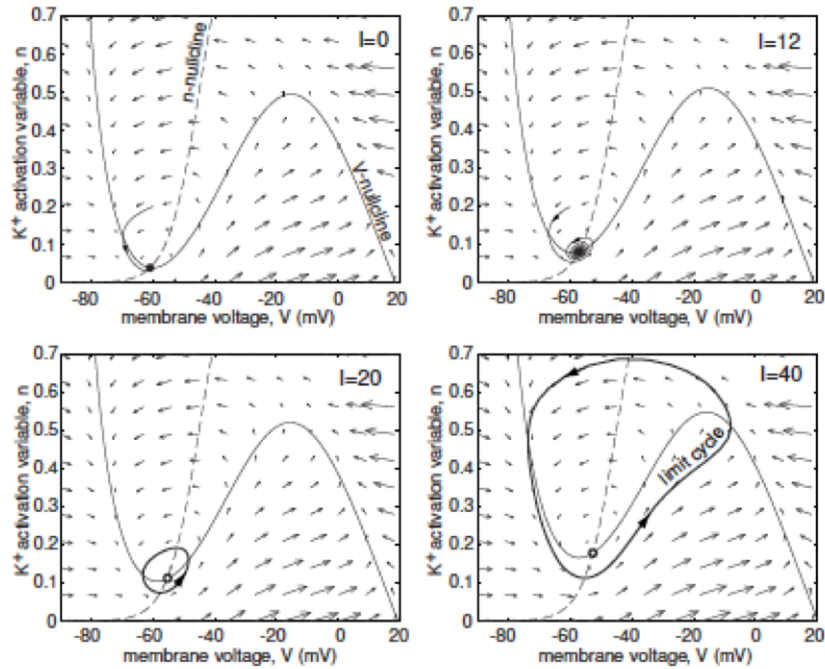


Figure 2.4: Supercritical Andronov-Hopf bifurcation in  $I_{Na,p} + I_K$  model [1]

$I_{Na,p} + I_K$  model with low threshold and steep activation curve of  $K^+$  can exhibit subcritical Andronov-Hopf bifurcation. The stable equilibrium in this system is surrounded by an unstable limit cycle which is often surrounded by another stable limit cycle. As the input increases, the unstable limit cycle shrinks to the stable equilibrium and makes it lose stability. Which remains is large stable limit cycle attractor, results in tonic spiking activity.

In contrast the saddle-node and Andronov-Hopf bifurcation result in dramatically different neurocomputational properties. Particularly, neurons near saddle-node bifurcation act as integrators, that fire sooner if the frequency of input goes higher. On the other hand, near Andronov-Hopf bifurcation the system poses damped oscillations and acts as a resonator, prefers input with the same frequency of damped oscillation. Note that exact mathematical definition of bifurcation in multidimensional system is

not the concern of this study and can be found in related mathematical texts (e.g. [3]).

### 2.3.2 Normal form

Typically, state variables that describe neuron dynamics are classified into four classes according to their functionality and time scale. The first class is the membrane voltage which is the indicator of cell activity. The second class are *excitation variables* which are responsible for the upstroke, e.g. activation of  $\text{Na}^+$  current. The third class are *recovery variables* that facilitate the downstroke through repolarization process ,e.g. inactivation of  $\text{Na}^+$  current or activation of fast  $\text{K}^+$  current. and finally *adaptation variables* which build up during prolonged spiking and can affect excitability in the long term.

From the dynamical system point of view, the transition from rest to spike is correspondent to occurring of a bifurcation, i.e. the qualitative change of phase portrait of the system. Different type of bifurcations result in different excitability patterns. neurons are considered either *integrator* or *resonator*. Showing damped oscillation of membrane potential is the sign of resonators. This phenomenon does not exist in integrators. Also, some neurons exhibit the coexistence of resting and spiking states, while others do not. The latter are named *monostable* while the former are called *bistable*. There is one-to-one correspondence among each of four possible neuron groups and four type of bifurcation as summarized in Table 2.1.

As seen in previous chapter, all four types of bifurcations mentioned in Table 2.1 can be amenably visualize and analyzed in two dimensional (planar) systems using phase plane methods. So reducing Hodgkin-Huxley four dimensional model to two dimensional minimal model, with variables having electrophysiological meaning is helpful. But to remove one or more gating variables from the basic model, one

Table 2.1: Neuron dynamics classifications

		co-existence of resting and spiking states	
		YES (Bi-stable)	NO (Mono-stable)
subthreshold oscillation	NO	saddle - node	saddle-node invariant circle
	YES	subcritical Andronov-Hopf	supercritical Andronov-Hopf

should consider the capability of reduced model in describing all major characteristics of neuronal activities of four general types of neurons, i.e resonator/integrator, monostable/bistable. However we should not expect that understanding such minimal models provides exhaustive information about all electrophysiological aspects of neuronal activities.

To build the planar model, we start from minimal model comprising of one amplifying and one resonant gating variable (plus ohmic leak current). The amplifying gating variable is the activation variable  $m$  for inward current or the inactivation variable  $h$  of outward current. A small depolarization increases  $m$  and decreases  $h$  which in turn cause more depolarization. Similarly, a small hyperpolarization decrease  $m$  and increase  $h$  resulting in less inward current and more hyperpolarization. This positive feedback loop performs amplifying task.

Inactivation of  $h$  for inward current or activation of  $n$  for outward current have resonating effect. A small depolarization decreases  $h$  and increase  $n$  which in turn decreases inward and increases outward current and produces net current that resists the depolarization. Currents with amplifying gating variables can result in bistability, while resonant gating variables have one stable equilibrium with possible damped oscillation. A model with at least one amplifying and one resonant gating variable

should produce all four types of neuronal activities.

Time constants of gating variables are also play an important role. To get spike, the positive feedback should act faster than negative feedback process. On the other hand, if an amplifying variable has a slow time constant, fast fluctuations can not be followed and the cell acts as a low pass filter. Fast resonant gating variables will damp input fluctuations (sooner than be amplified) and results in stable rest state and shows a band pass filter characteristics. In practice, the amplifying gating variables such as  $m$  has relatively fast kinetics and can be replaced by the steady state value,  $m_\infty(V)$  in the model. This allows to reduce the dimension of the minimal model by one.

Most of the time it is not easy to find a simple equivalent replacement that describes the original system in its whole domain, but we can restricts ourselves to a small critical neighborhood with the most significant effect on the system behavior. If we assume that all neuronal current models can be reduced to two-dimensional system with N-shape for voltage and sigmoid nullcline for recovery variable, the decision of fire would be made in the bifurcation region. Then to model the sub-threshold behavior and initial segment of upstroke, we need to consider only a small neighborhood of the left knee of voltage nullcline. The voltage nullcline in the bifurcation region can be approximated by a quadratic function. Also we approximate the gating variable with a linear function. The resulted simple model [1]:

$$\dot{v} = I + v^2 - u \quad \text{if } v \geq 1, \text{ then} \quad (2.19)$$

$$\dot{u} = a(bv - u) \quad c \rightarrow v, u + d \rightarrow u \quad (2.20)$$

where  $v$  and  $u$  are membrane voltage and gating variables. The model has four dimensionless parameters. Depending on the values of  $a$  and  $b$  it can be an integrator or

resonator. Parameters  $c$  and  $d$  effect the after spike transient behavior by controlling the high-threshold voltage gated current during the spike. When the spike dynamics started, the voltage rises quickly until it reaches the maximum value (normalized at  $v = 1$ ) and then resets to the after spike value. Equations (2.19) and (2.20) can be written in more convenient form.

$$C\dot{v} = k(v - v_r)(v - v_t) - u + I \quad \text{if } v \geq v_{\text{peak}}, \text{ then} \quad (2.21)$$

$$\dot{u} = a[b(v - v_r) - u] \quad c \rightarrow v, u + d \rightarrow u \quad (2.22)$$

where  $C$  is the membrane capacitance,  $v_r$  is the resting potential and  $v_t$  is the instantaneous threshold potential. Parameters  $k$  and  $b$  are dependent to neuron's rhobase and input resistance. The sign of parameter  $b$  determines that wether gating variable is amplifying ( $b < 0$ ) or resonant ( $b > 0$ ). The recovery time constant is  $a$ .  $v_{\text{peak}}$  is spike cutoff value and  $c$  is the voltage reset value. The parameter  $d$  is the net amount of currents activated during the spike and affecting the after-spike behavior. The output of simulation of simple model and experimental spike curve are shown in Fig.???. According to the phase portrait, injection of  $I = 70\text{pA}$  shifts the  $V$  nullcline upward and makes the resting state disappear. The trajectory tends to spiking limit cycle attractor and when it reaches the  $v_{\text{peak}} = 35\text{mV}$  it is reset to the after-spike value, resulting in periodic spiking behavior. Slow afterhyperpolarization (AHP) is due to the dynamic of recovery variable. Depending to the parameters, the model can exhibit other type of activities.

At this stage, comparing the dynamics of simple model with well-known integrate-and-fire model would be useful. In integrate-and-fire model, when the membrane voltage reaches the preset threshold value, the neuron is said to fire spike. Then

the potential is reset to a new value and the spike is drawn by hand. In contrast, in simple model, generating spike is due to the dynamics of voltage equation. The firing threshold is not a parameter but the property of dynamical system near the bifurcation point. Depending on the type of bifurcation, the firing threshold may not be well defined as in case of many conductance base models. To summarize, simple model of 2.21 and 2.22 are capable to produce diverse range of neuronal dynamics as shown in Fig. 2.5.

## 2.4 Modeling Population of Neurons

In general, neurons act in large populations. Their collective behavior can be modeled in two ways. One way is to derive a system of simultaneous differential equations in the form of 2.21 and 2.22 for each neuron and add the dynamics of intra cellular agents as well. For large populations, this method will give a sophisticated system of equations which are very time and space expensive to solve. Another method is using mathematical techniques such as averaging or mean-field to reduce the dimension of model. In this section we review a famous method developed by Wong [8] to model the perceptual decision two choice task by several populations of neurons. As depicted in Fig. 2.6 red and blue populations are selective to choice A and B. There is larger population of non-selective neurons that selective populations tries to recruit them act in their favor. The forth group are inhibitory cells that suppress the outputs of other groups. The underlying assumption that all neurons receive noisy inputs. Also each neuron is either inhibitory characterized by GABA mediated current or excitatory with AMPA and NMDA mediated current. Each selective pool accumulates information related to one of two possible decisions. Mutual inhibition creates winner takes all dynamics between two competing accumulator.

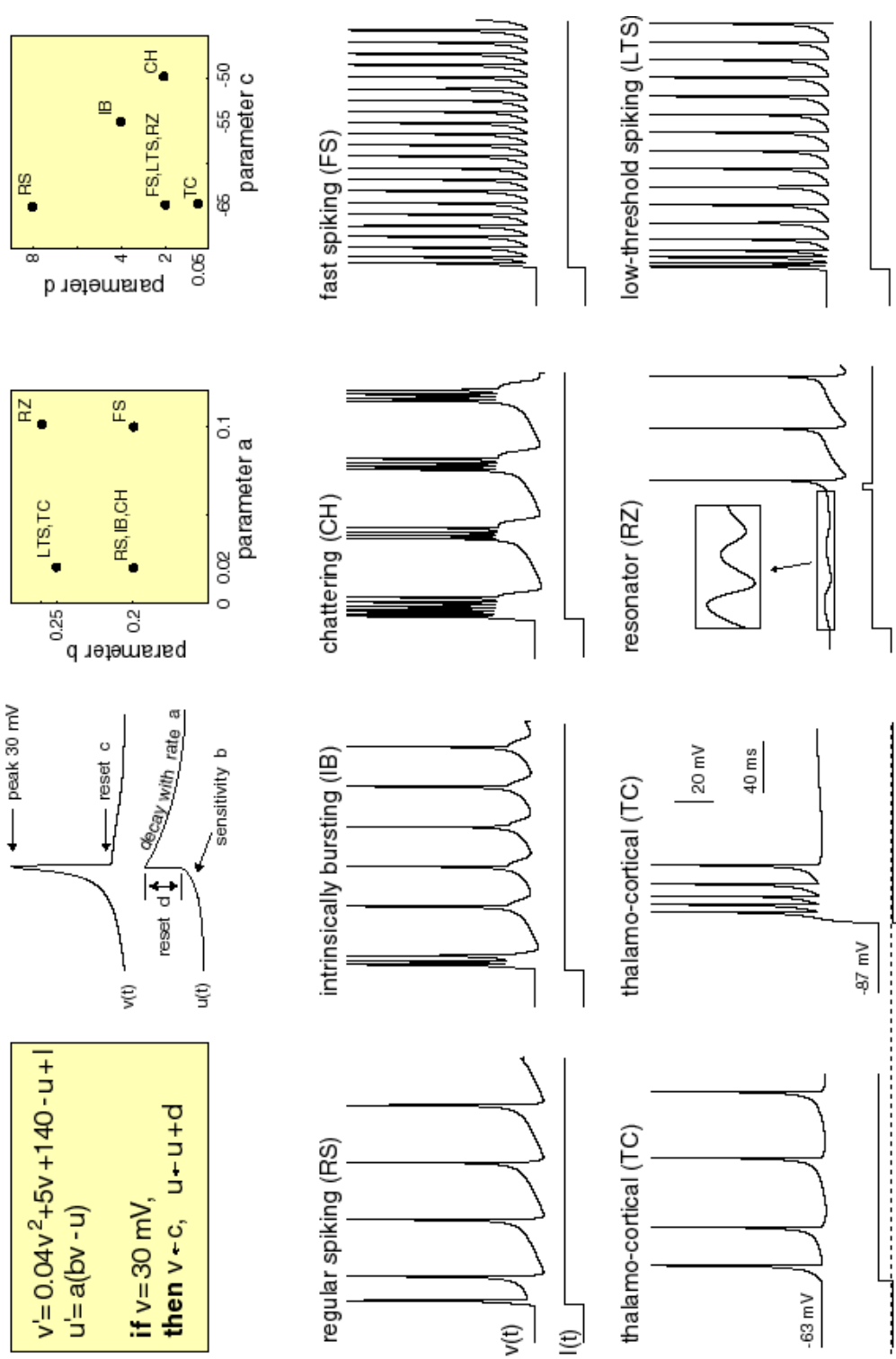


Figure 2.5: Different spiking regime, produced by simple model [1]

Electronic version of the figure and reproduction permissions are freely available at [www.izhikevich.com](http://www.izhikevich.com)

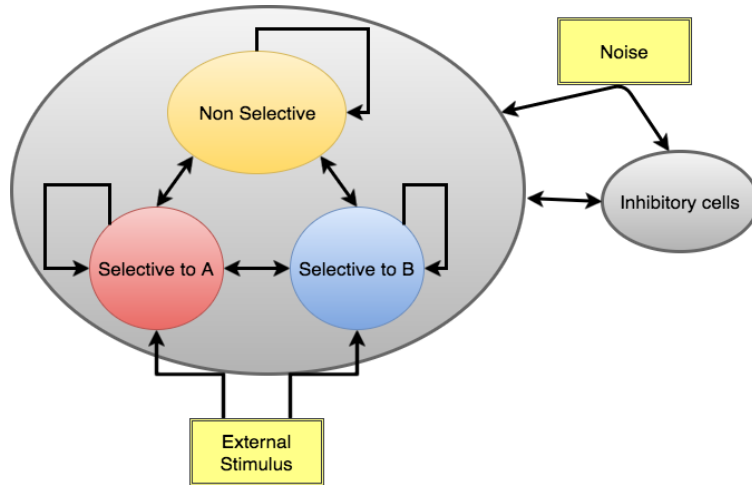


Figure 2.6: Populations of neurons and their interconnection

We will simulate the dynamics of this model later in Chapter 5. But here, we show that by using averaging techniques, the system of equations can be reduced to famous drift-diffusion abstract model. If the activity of groups A and B is presented by the average firing rate, the pool equation can be represented by [8]:

$$\frac{dx_1}{dt} = -\frac{x_1}{\tau_x} + (1 - x_1)\gamma r_1 \quad (2.23)$$

$$\frac{dx_2}{dt} = -\frac{x_2}{\tau_x} + (1 - x_2)\gamma r_2 \quad (2.24)$$

where  $x_1$  and  $x_2$  are decision variables and  $r$  is the firing rate of two competing pools. Note that firing rate is a function of input current to each neuron  $r_i = \phi(I_{in})$  which itself is a function of both  $r_1$  and  $r_2$  and noise. One important relation that needs to be known is the cell input-output relation denoted by  $H$ .

$$r_1 = H(i_1, i_2) \quad (2.25)$$

$$r_2 = H(i_2, i_1) \quad (2.26)$$

where

$$i_1 = J_1x_1 - J_2x_2 + I_0 + I_1 + I_{noise1} \quad (2.27)$$

$$i_2 = J_2x_2 - J_1x_1 + I_0 + I_2 + I_{noise2} \quad (2.28)$$

where  $J_i$  is coupling term and  $I_i$  is the stimulus current related to input data

$$\begin{aligned} \frac{dx_1}{dt} &= -\frac{x_1}{\tau_x} + (1 - x_1)\gamma H(i_1, i_2) \\ \frac{dx_2}{dt} &= -\frac{x_2}{\tau_x} + (1 - x_2)\gamma H(i_2, i_1) \end{aligned} \quad (2.29)$$

Having the reduced model of 2.29 in hand, the question is how this model can explain the change of performance in decision tasks.

Cortical neural circuits receive dynamic inputs from other structures as well as neuromodulator transmitters. Neuromodulator include dopamine, serotonin, norepinephrine. Their effect on single neuron are not completely known but one of their mechanisms is to change the neuronal gain. Remember the fire rate of a neuron is function of its input currents which is called neuron gain e.g.  $H$  in Wong reduced model. One way to model the change of performance is to modulate inhibitory and excitatory gains independently and observe the effect on some performance measure. One common performance criteria is Reward Rate [9]. If a two choice task is performed several times and the decision time and outcome is collected, the following performance measure can be defined:

$$\text{Reward Rate} = \frac{\langle \text{Acc} \rangle}{\text{DT} + \text{NDT} + \text{RSI}} \quad (2.30)$$

where  $\langle \text{Acc} \rangle$  is the fraction of trials with correct decision, DT is the time duration from the onset of stimulus to making the decision in brain, NDT is the sensory and motor delays and RSI is the time between trials. It is evident that by changing the voltage controlled conductances  $g_{type}$  related to each reversal potential and leak conductances  $g_L$ , neuron gain can be manipulated. Let's name the excitatory gain  $\gamma_E$  and inhibitory gain  $\gamma_I$ . Note that Dale's principle force each neuron to be either one or the other not both. Running model simulation or solving the analytical reduced model with reward rate criteria will show the effect of modulating the excitatory and inhibitory gains on decision performance. We will get back to this tasks in upcoming chapters.

## Chapter 3

### Mathematical Abstractions

In the previous chapter, we introduced bio-physiologically inspired model of the decision process. We also investigated models of populations of neurons. We showed that by means of model reduction techniques and averaging, high dimensional models can be summarized into efficient low dimensional, and even for two choice task to one dimensional model. In this Chapter, we tackle the modeling problem in pure mathematical abstract way. Starting with simple two choice task, we show that drift diffusion model can capture the dynamics of collecting information and making decision accordingly. Moving toward more complicated multi-cue multi-choice tasks, we introduce our extension to traditional model and provide mathematically sound model to mimic the decision making dynamics. In the same way, we extend the discrete Markov chain approach to multi-cue multi-choice task, using multi-variate Markov chains and autoregressive models to give an approximation of the process.

### 3.1 SPRT approach

#### 3.1.1 Single-cue two-choice task

Mathematical abstract models to describe the process of making decision in human brain start by analyzing the simple two-alternative forced choice (2AFC) decision task [9]. Consider a 2-choice task and assume  $e$  stands for evidence presented to decision maker. Let the conditional probabilities  $p(e|S1)$  and  $p(e|S2)$  denotes the probabilities of observing evidence  $e$  given  $S1$  or  $S2$  is true. The first and second moments of the probability function are  $\mu$  and  $\sigma$ . Depending on the similarity of two decisions,  $(\mu_1 - \mu_2)$  and signal to noise ratio,  $\mu/\sigma$  the two PDFs overlap. According to Bayes law a posteriori probability  $p(S1|e)$  is given by:

$$p(S1|e) = \frac{p(e|S1)p(S1)}{p(e)}$$

Define likelihood ratio as :

$$LR(e) = \frac{p(e|S1)}{p(e|S2)}$$

If equal priors are assumed, i.e.  $p(S1) = p(S2)$ , then likelihood ratio greater than one means  $S1$  is more likely to be correct. Hence choosing  $S1$  is the optimal decision in the sense that it provides overall lower error rates. Now assume multiple piece of evidence  $e_1, \dots, e_N$  are presented sequentially to the observer. Assuming independent evidences we have:

$$LR(e) = \frac{p(S1|e_1 \dots e_N)}{p(S2|e_1 \dots e_N)} = \prod_{n=1}^N \frac{p(e_n|S1)}{p(e_n|S2)} \quad (3.1)$$

Taking logarithm of 3.1 will give:

$$I^n = I^{(n-1)} + \log \frac{p(e_n|S1)}{p(e_n|S2)} \quad (3.2)$$

where:

$$I^{(n-1)} = \sum_{n=1}^{n-1} \log \frac{p(e_n|S1)}{p(e_n|S2)} \quad (3.3)$$

Now let  $\delta I^r$  has mean  $\mu$  and variance  $\sigma^2$  which assumed to be finite. Define a family of random functions, indexed by  $M = 1, 2, \dots$  of  $t \in [0, T]$ , where  $T$  is large enough, as follows:

$$I^M(t) = \frac{1}{\sqrt{M}} \sum_{r=1}^k (\delta I^r - \mu) + \frac{1}{M} \sum_{r=1}^k \delta I^r \quad \text{where } k = \lfloor Mt/T \rfloor \quad (3.4)$$

For any  $M$ ,  $I^M(t)$  has the mean value of  $\mu \lfloor t/T \rfloor$  and variance  $\sigma^2 \lfloor t/T \rfloor$ . According to Donsker invariance principle [10] and the law of large number we get:

$$I^M \xrightarrow[f]{} \sigma W(t) + \mu t \quad \text{as } M \rightarrow \infty \quad (3.5)$$

where convergence is in the sense of distribution. In other words the process  $I(t)$  satisfies the following stochastic differential equation:

$$dI = \mu dt + \sigma dW(t) \quad (3.6)$$

which is the expected drift-diffusion process (DDM). The drift and diffusion constants are dependent to the  $p_i(e_i|S_i)$  distributions. In the case of Gaussian, the solution of

3.6 with initial condition  $I(0) = 0$  is given by:

$$p(e_i|S1) = \frac{1}{\sqrt{2\pi\sigma^2}} \exp\{-(e_i - \mu_1)^2/2\sigma^2\} \quad (3.7)$$

$$p(e_i|S2) = \frac{1}{\sqrt{2\pi\sigma^2}} \exp\{-(e_i - \mu_2)^2/2\sigma^2\} \quad (3.8)$$

Assuming  $\mu_1 > \mu_2$ , we have:

$$\delta I_r = \log \frac{p_1(e_i|S1)}{p_2(e_i|S1)} = \frac{\mu_1 - \mu_2}{\sigma^2} \left( e_i - \frac{\mu_1 + \mu_2}{2} \right) \quad (3.9)$$

Taking the first and second moment of 3.9 gives the values of  $\mu_i$  and  $\sigma^2$  as it is assumed. In particular by assuming  $\mu_1 = -\mu_2 = \mu$  the accumulated information is given by:

$$I^n = \sum_{r=1}^n \delta I_r = \frac{2\mu}{\sigma^2} \sum_{r=1}^n e_i \quad (3.10)$$

Thus, the decision variable for a noisy evidence can be modeled by one-dimensional Wiener process bounded by positive and negative thresholds,  $\theta_A$  and  $\theta_B$ , in which an integrator accumulates the difference of evidences between two choices [9]. In order to reflect the effect of bounded accuracy and forgotten information, the DDM integrators are considered not perfect but leaky as follows:

$$dx(t) = (\mu - \lambda x)dt + \sigma d\mathbf{W}(t) \quad (3.11)$$

in which  $x(t) \in \mathbb{R}$  is the decision variable,  $\mu$  is the drift,  $\sigma$  is the diffusion rate,  $\mathbf{W}(t)$  is the standard Wiener process,  $d\mathbf{W}(t)$  is the standard white noise, and  $\mathbb{R}$  denotes the set of real numbers. The term  $\lambda$  represents the leak and  $\lambda > 0$  leads to a stable Ornstein-Uhlenbeck (O-U) process. The drift rate  $\mu$  represents the capability of input

information in discrimination between choices A and B, which in behavioral studies are known as quality of cue (attribute). For example, in the random dot motion task designed in [11], the cue is the direction of dots and its quality alters by changing the proportion of dots moving in the left or right direction.  $\lambda$  tunes the drift based on the current state and is often connected to memory processes (e.g., primacy and recency effects), conflict situations (e.g., approach-avoidance), or similarities between choice alternatives. In the free response paradigm, whenever the decision variable reaches the positive or negative thresholds, the decision is made, while in interrogation protocol, after spending the specific amount of time, the decision is made based on the value of gathered information. DDM has the capability to capture the characteristics of 2AFC in terms of speed or accuracy of decision.

### 3.1.2 Multi-cue two-choice task

For 2AFC, only one cue, e.g., the direction of dots is concerned. In real world, always several cues, such as color, sound, and texture, are involved. One method is to combine and integrate all cues in favor of each choice into single source of evidence and this source is being used throughout the decision process. More involved treatment includes separate processes for each cue. In this approach the order of considering the cues and the process time devoted to each cue are two important aspects. The time frame of the decision process is divided into subintervals with different lengths during which the attention focus is only one cue. The order of cues can be assumed to be deterministic or probabilistic. Let  $\mathcal{M} = \{1, 2, \dots, M\}$  be the index set of cues. Following the method of [12], we assume that the evidence for cues is accumulated

by a piecewise O-H process, i.e.

$$\begin{aligned} dx(t) &= (\mu_m - \lambda_m x(t))dt + \sigma d\mathbf{W}_m(t) \\ m &\in \mathcal{M}, \quad t_{l-1} \leq t < t_l \end{aligned} \quad (3.12)$$

in which the parameters identified by index  $m$  are the characteristics of the  $m$ th cue. If finite decision time span is divided into  $L$  consecutive time intervals,  $[t_{l-1}, t_l]$  for  $l = 1, \dots, L$ , we assume that one cue is processed in each time interval based on the given order schedule. The process of making decision in free response time or interrogation is the same as a single cue task.

### 3.1.3 Single-cue multi-choice task

In order to model multi-choice tasks, a more general race model, which is comprised of separate leaky competing integrators, representing each choice, with mutual inhibition, was proposed by [13]. Each integrator gathers information in favor of or against the associated choice based on the value of cue. We assume that the dynamic of each integrator is governed by the O-H process. Consider  $K$  integrator pools, one for each choice, accumulating the incoming noisy evidence  $S_i$  in favor of choice  $i$ . Each pool is described by the following form:

$$dx_i = (-kx_i - \sum_{j \neq i} wx_j + S_i)dt + \sigma_i d\mathbf{W}_i \quad (3.13)$$

where  $w$  is the mutual inhibition strength among pools. There are two different categories of decision criteria in choosing among the pools which give the same asymptotically optimal results. One way is to assign a threshold  $\theta_i$  to each pool and select the

one that reaches the threshold sooner under the free response protocol or at the fixed time choose the pool with higher value of decision variable. Other methods consider the ratio of the output of the pools such as max-versus-next and max-versus-average. Reference [12] showed that under a particular parameter range, two-dimensional race model can be expressed as one dimensional DDM.

### 3.1.4 Multi-cue multi-choice task

In this study we propose a model for multi-cue multi-choice task which considers the condition that a decision maker faces different situations and prioritizes some tasks by weighing associated choices differently based on different choices. The mathematical model reads:

$$\begin{aligned} dx_i(t) = & \left( -k_{i,m(t)}x_i(t) - \sum_{j \neq i} w_{i,j,m(t)}x_j(t) + S_{i,m(t)} \right) dt \\ & + \sigma_i d\mathbf{W}_i(t), \quad m(t) \in \mathcal{M}, \quad t_{l-1} \leq t < t_l \end{aligned} \quad (3.14)$$

where  $k_{i,m}$  depends on both choice  $i$  and cue  $m$ ,  $w_{i,j,m}$  depends on choice  $i$ , choice  $j$ , and cue  $m$ , and  $w_{i,j,m} = w_{j,i,m}$ .

It is known that the O-H process 3.11 has the following asymptotic approximations on expectation and variance in the long run:  $\lim_{t \rightarrow \infty} E[x(t)] = \mu/\lambda$  and  $\lim_{t \rightarrow \infty} E[x^2(t)] = \sigma^2/(2\lambda)$ , where  $E$  denotes the expectation operator. Now a natural question about the multi-cue multi-choice task model 3.14 is that whether or not it has a similar asymptotic approximations of expectation and variance in the long run. Unlike 3.11 which is a linear scalar stochastic differential equation (SDE), since 3.14 is a multivariable SDE with a piecewise time-dependent switching between different cues, the theoretical discussion will be much more involved. In Appendix A, we inves-

tigated the asymptotic behavior of expectation and variance of 3.14. With some mild assumptions, it is shown that the model has well defined asymptotic approximation for its first and second moments.

### 3.2 Markov chain approach

In this section a method to construct a discrete version of multi-cue multi-choice Ornstein-Uhlenbeck (O-U) decision model based on the discrete time Markov process is presented. First, let us review the basics concepts of birth-death chain in simple single cue two forced choice task(2AFC) which starts with the following random walk process.

Consider a Markov process  $X_n$ , which is a random variable over time interval  $[0,t]$ . The time is divided into subintervals of length  $\tau$ . Suppose the process make a step change at  $\tau, 2\tau, 3\tau, \dots$ . The size of steps are assumed to be  $\pm\Delta = \sqrt{t}$  with probabilities  $p_{ij}$ . The state space of the process is given by  $S = \{-k\Delta, \dots, -\Delta, 0, +\Delta, \dots, +k\Delta\}$  where  $k$  is the number of time steps and  $\pm k\Delta$  are the boundaries showing the decisions S1 and S2 respectively. Transition probability matrix of the process is as follows:

$$P = \left[ \begin{array}{c|c} P_I & 0 \\ \hline R & Q \end{array} \right]$$

where states number 1 and  $m$  are correspondent to absorbing states associated with decisions S1 and S2 and  $m = 2k + 1$ . Assuming the initial condition of  $Z$ , the

$$\begin{array}{c}
\begin{array}{cccccccc}
& & 1 & & m & & 2 & & 3 & & \dots & & m-2 & & m-1 \\
& 1 & | & 1 & & 0 & | & 0 & & 0 & & \dots & & 0 & & 0 \\
& m & | & 0 & & 1 & | & 0 & & 0 & & \dots & & 0 & & 0 \\
= & 2 & | & p_{21} & & 0 & | & p_{21} & & p_{23} & & \dots & & 0 & & 0 \\
& 3 & | & 0 & & 0 & | & p_{321} & & p_{33} & & \dots & & 0 & & 0 \\
& \vdots & | & \vdots & & \vdots & | & \vdots & & \vdots & & \dots & & \vdots & & \vdots \\
& m-2 & | & 0 & & 0 & | & 0 & & 0 & & \dots & & p_{m-2,m-2} & & p_{m-2,m-1} \\
& m-1 & | & 0 & & p_{m-1,m} & | & 0 & & 0 & & \dots & & p_{m-1,m-2} & & p_{m-1,m-1}
\end{array}
\end{array}$$

probability and expected time to reach each decision is given by [12]:

$$[Pr(S1), Pr(S2)] = Z.(I - Q)^{-1}.R \quad (3.15)$$

$$[E(T/S1), E(T/S2)] = \tau.[Z.(I - Q)^{-2}.R]./[Pr(S1), Pr(S2)] \quad (3.16)$$

where ./ indicates element wise operation. The increment of the process from time  $n$  to  $n + 1$  is given by:

$$X_{n+1} - X_n = Z_{n+1}, \quad n = 1, 2, 3, \dots$$

Take  $X_{t/\tau} = \sum_{i=1}^{t/\tau} Z_i$ . Since  $Z_i$  are independently and identically distributed, if we assume  $Pr[Z_i = +\Delta] = Pr[Z_i = -\Delta] = 0.5$  we get  $E(X_{t/\tau}) = 0$  and  $Var(X_{t/\tau}) = (t/\tau)Var(Z_i) = t\Delta^2/\tau = t$ . Now if we let  $\tau \rightarrow 0$  the random walk converges in distribution to standard Wiener process  $W(t)$  which from central limit theorem has normal distribution with mean zero and variance  $t$ . In general, Markov processes with continuous time set and continuous state space are called *diffusion processes* and the standard Wiener process is the simplest diffusion process [14]. The Wiener process with drift is given by:

$$V(t) = \mu t + \sigma W(t) \quad (3.17)$$

where  $\sigma$  is a positive number. Also

$$dV(t) = V(t + \tau) - V(t) = \mu\tau + \sigma dW(t) \quad (3.18)$$

in which  $V(t)$  is normally distributes with mean  $\mu t$  and variance  $\sigma^2 t$ . To derive more general form where the probability of stepping up and down at each time step are not equal, we define infinitesimal first and second moment of the process as follows:

$$\mu(x, t) = \lim_{\tau \rightarrow 0} \frac{E[dX(t)|X(t) = x]}{\tau} \quad (3.19)$$

$$\sigma^2(x, t) = \lim_{\tau \rightarrow 0} \frac{E[dX(t)^2|X(t) = x]}{\tau} \quad (3.20)$$

note that by finding these two moments which are called drift and diffusion terms, the process  $V(t)$  is determined. The drift and diffusion coefficients for the Wiener process are simply  $\mu(x, t) = \mu$  and  $\sigma^2(x, t) = \sigma^2$ . In cognitive tasks the drift term is related to stimulus intensity, since larger drift may results in less decision time and diffusion term in related to the noise intensity in presented stimulus. For the sake of discretization the transition probabilities of the Markov process is given by [12]:

$$p_{i,i-1} = \frac{1}{2} \left( 1 - \frac{\mu}{\sigma} \sqrt{\tau} \right) \quad (3.21)$$

$$p_{i,i+1} = \frac{1}{2} \left( 1 + \frac{\mu}{\sigma} \sqrt{\tau} \right) \quad (3.22)$$

with  $\sqrt{\tau} = \Delta/\sigma$  and  $(-1/\sqrt{\tau}) \leq \mu/\sigma \leq (+1/\sqrt{\tau})$  to keep the  $p$  between zero and one. Note that here it is assumed  $p_{ii} = 0$  or the process is not allowed to stay in the current stage at the next time step. However if this is not the case, the process can still characterized by drift-diffusion form [15]. In this case the Markov chains is

known as Birth-Death process and characterized in continuous domain by Ornstein-Uhlenbeck (O-U) process. Here, the velocity of information accumulation is assumed to be damped proportional to the current state while the new random information is added, leads to:

$$X(t + \tau) = (1 - \tau\gamma)X(t) + V(t + \tau) \quad (3.23)$$

or in difference form:

$$dX(t) = -\tau\gamma X(t) + V(t + \tau) \quad (3.24)$$

Let  $V(t)$  be a Wiener process with drift  $\delta$  and diffusion coefficient  $\sigma^2$ . According to 3.18, it follows:

$$dX(t) = (\delta - \gamma X(t))\tau + \sigma dW(t) \quad (3.25)$$

In O-U process, the drift rate  $\mu(x, t) = \delta - \gamma x$ , comprises of two parts. The constant part determines the direction of the process while the linear part causes the decay of the process depending on the current state. Again the transition probabilities can be determined as follows [12]:

$$p_{i,j} = \begin{cases} \frac{1}{2\alpha} \left( 1 - \frac{\delta - \gamma(-k\Delta + (i-1)\Delta)}{\sigma^2} \sqrt{\tau} \right) & \text{if } j - i = -1 \\ \frac{1}{2\alpha} \left( 1 + \frac{\delta - \gamma(-k\Delta + (i-1)\Delta)}{\sigma^2} \sqrt{\tau} \right) & \text{if } j - i = +1 \\ 1 - \frac{1}{\alpha} & \text{if } j = i \\ 0 & \text{otherwise} \end{cases} \quad (3.26)$$

where  $\Delta = \alpha\sigma\sqrt{\tau}$  and  $\alpha > 1$  is a free parameter. Accordingly the first passage time

distribution for reaching the boundaries for choices S1 or S2 is given by:

$$[Pr(T = t|S2, Pr(T = t|S1))] = ZQ^{n-1}R./Z(I - Q)^{-1}R \quad (3.27)$$

where  $t = n\tau$ .

To investigate the multi-cue task, the drift rate within the trail is not constant. More valid cues are represented by larger drift rates. The change of drift rate can be deterministic, i.e. based on predetermined schedule, or probabilistic. In the latter case a probability distribution should be assign to the drift rate. Here we consider the deterministic version, since we propose a theory on changing strategy and deterministic cue schedule and time will fit to it.

Assume decision time interval  $[0,t]$  is divided to set of  $L$  consecutive time intervals, namely  $\{[t_{l-1}, t_l]\}$  for  $l = 1, 2, \dots, L$ . Note that this time partitioning should not be confused with time discretization variable  $\tau$ . Consider a set of cues  $\mathcal{M} = \{m_k\}$  are available with  $k = 1, 2, 3, \dots, K$  and at the start of each time partition  $t_l$  the attentions focus will be changed to one of the cues namely  $c_l$ . Since each cue represents a drift rate, the process is a piecewise (O-H). In terms of transition probability matrix  $P$ , at each switching time, the elements of matrices  $R$  and  $Q$  would change which is denoted by subscript  $l$ . If the switching times replaced by  $n_l = \lfloor t_l/\tau \rfloor$  the probability of selecting  $S1$  is determined by extending 3.16 as follows [12]:

$$\begin{aligned} Pr(S1) \approx & Z \sum_{i=1}^{n_1} Q_{c_1}^{i-1} R_{S1,c_1} \\ & + ZQ_{c_1}^{n_1} \sum_{i=n_1+1}^{n_2} Q_{c_2}^{i-(n_1+1)} R_{S1,c_2} + \dots \\ & + ZQ_{c_1}^{n_1} \dots Q_{c_{L-1}}^{n_{L-1}-n_{L-2}} \sum_{i=n_{L-1}+1}^{n_L} Q_{c_L}^{i-(n_{L-1}+1)} R_{S1,c_L} \end{aligned} \quad (3.28)$$

in which  $R_{S_1}$  is the first column of matrix  $R$  and  $Z$  is the initial probability vector.  $Q_{c_k}$  are the transition matrix block based on the specification of cue  $c_k$  as defined before. Similarly the time required to reach the decision is given by [12]:

$$\begin{aligned}
E[T_{S_1}|S_1] \approx & \frac{\tau}{Pr(S_1)} \left( \sum_{i=1}^{n_1} Q_{c_1}^{i-1} R_{S_1, c_1} \right. & (3.29) \\
& + Z Q_{c_1}^{n_1} \sum_{i=n_1+1}^{n_2} Q_{c_2}^{i-(n_1+1)} R_{S_1, c_2} + \dots \\
& \left. + Z Q_{c_1}^{n_1} \dots Q_{c_{L-1}}^{n_{L-1}-n_{L-2}} \sum_{i=n_{L-1}+1}^{n_L} Q_{c_L}^{i-(n_{L-1}+1)} R_{S_1, c_L} \right)
\end{aligned}$$

Expressions for probability of making decision  $S_2$  and related expected time can be derived by replacing the vector  $R_{S_1}$  with  $R_{S_2}$ .

### 3.2.1 Multi-Choice tasks

Consider the following system of equations based on 3.23:

$$X_1(t + \tau) = ((1 - \tau\gamma_1)X_1(t) - \tau\gamma_2 X_2(t)) + V_1(t + \tau) \quad (3.30)$$

$$X_2(t + \tau) = (-\tau\gamma_2 X_1(t) + (1 - \tau\gamma_1)X_2(t)) + V_2(t + \tau) \quad (3.31)$$

Let  $X_1$  represents accumulating data for choice  $S_1$  and  $X_2$  for choice  $S_2$  with  $V_1 + V_2 = 0$ . Assuming that any information for one choice acts against the other choice, i.e.  $X_1 + X_2 = 0$ , the system is representing two choice task with drift rate of  $\gamma_2 - \gamma_1$ .

Now assume there are  $S$  choices and the process of accumulations are governed

by equations of the form 3.30. In the vector form:

$$d\mathbf{X}(t) = \mathbf{X}(t + \tau) - \mathbf{X}(t) = -\tau\Gamma(t)\mathbf{X}(t) + \mathbf{V}(t + \tau) \quad (3.32)$$

Let each  $V_i$  process has the mean of  $\delta_i$  and variance of  $\sigma_i^2$  to get:

$$d\mathbf{X}(t) = (\delta\mathbf{e}_s - \Gamma\mathbf{X}(t))\tau + \Sigma d\mathbf{W}(t) \quad (3.33)$$

where  $\mathbf{X} \in \mathbf{R}^S$  is column vector,  $\Gamma$  and  $\Sigma \in \mathbf{R}^{S \times S}$  are  $S$  by  $S$  matrices and  $\mathbf{e}_s$  is a  $1 \times s$  column vector with all elements equal to one.

If we take the same approach of discretization as we did in two- choice model, we get a conventional  $S$ -th order Markov chain of  $m$  states which has  $O(m^S)$  states and therefore parameters. The number of transition probabilities (to be estimated) increases exponentially with respect to the order  $S$  (the number of choices) of the model. Therefor we propose to follow the approach of [16] for multi -choice task modeling.

### 3.2.2 Autoregressive Model

By definition an autoregressive process is a random process that its value in each time step is linearly dependent on its own previous values plus a stochastic term [17]. The notion  $AR(p)$  indicates an autoregressive process of order  $p$  defined as:

$$X(t) = c + \sum_{i=1}^p \phi_i X_{t-i} + W(t) \quad (3.34)$$

in which  $\phi_i$  are the parameters of the model,  $c$  is a constant and  $W(t)$  is white noise. It is easy to see that (O-U) process in discrete time can be modeled by  $AR(1)$  by rearranging 3.23.

$$X(t+1) = \mu t + (1 - \gamma)X(t) + \sigma W(t) \quad (3.35)$$

Knowing this fact, it is rational to consider a model in the order of  $AR(n)$  for discrete version of multi-choice task. The model for multi-variate Markov chains proposed by [16] and later extended by [18] employs this approach. The following assumptions are required to estimate multi-variate Markov chains. Let  $\mathbf{x}(n)^{(k)}$  be the state probability distribution vector of the  $k$ th sequence at time  $n$ . If the  $k$ -th sequence is in state  $j$  with probability one then we state:

$$\mathbf{x}(n)^{(k)} = \mathbf{e}_j = (0, \dots, 0, \underbrace{1}_{j\text{-th}}, 0, \dots, 0)^T \quad (3.36)$$

Moreover, assume:

$$\mathbf{x}(n+1)^{(j)} = \lambda_{jj}P^{(jj)}\mathbf{x}(n)^{(j)} + \sum_{k=1, k \neq j}^S P^{(jk)}\lambda_{jk}\mathbf{x}(n)^{(k)}, \quad \text{for } j = 1, 2, \dots, S \quad (3.37)$$

where

$$\lambda_{jk} \geq 0, \quad 1 \leq j, k \leq S, \quad \sum_{k=1}^S \lambda_{jk} = 1 \quad \text{for } j = 1, 2, \dots, S \quad (3.38)$$

These assumptions mean that the state probability distribution of the  $j$ -th chain at time  $(n+1)$  depends only on the weighted average of itself,  $P^{(jj)}\mathbf{x}(n)^{(j)}$ , and other chains,  $P^{(jk)}\mathbf{x}(n)^{(k)}$ , at time  $n$ . Here  $P^{(ij)}$  is one step transition matrix of the states

from the  $j$ th sequence to the states of the  $i$ th sequence. In vector form:

$$\begin{aligned} \mathbf{X}(n+1) &\equiv \begin{pmatrix} \mathbf{x}^{(1)}(n+1) \\ \mathbf{x}^{(2)}(n+1) \\ \vdots \\ \mathbf{x}^{(S)}(n+1) \end{pmatrix} = \begin{pmatrix} \lambda_{11}P^{(11)} & \lambda_{12}P^{(12)} & \dots & \lambda_{1S}P^{(1S)} \\ \lambda_{21}P^{(21)} & \lambda_{22}P^{(22)} & \dots & \lambda_{2S}P^{(2S)} \\ \vdots & \vdots & \vdots & \vdots \\ \lambda_{S1}P^{(S1)} & \lambda_{S2}P^{(S2)} & \dots & \lambda_{SS}P^{(SS)} \end{pmatrix} \begin{pmatrix} \mathbf{x}^{(1)}(n) \\ \mathbf{x}^{(2)}(n) \\ \vdots \\ \mathbf{x}^{(S)}(n) \end{pmatrix} \\ &\equiv Q\mathbf{X}(n) \end{aligned} \quad (3.39)$$

The proof is based on Perron-Frobenius theorem and is given in [18]. It requires that  $P^{(jj)}$  and  $\Lambda = [\lambda_{jk}]^T$  are irreducible. Since all  $\lambda_{ij}$  are assumed to be non-negative, the model only considers positive correlation among sequences. This means an increase in a state probability in any of the sequences at time  $n$  can only increase the state probabilities at time  $n+1$ . Let's define variable  $z$  be negatively correlated with  $\mathbf{x}$  as follows:

$$z(n+1) = \frac{1}{m-1}(\mathbf{1} - \mathbf{x}(n+1))$$

Here  $\mathbf{1}$  is a vector of all ones and  $(m-1)$  is for normalization factor for number of state  $m \geq 2$ . We extend the model 3.39 to consider both negative and positive correlation as follows:

$$\begin{pmatrix} \mathbf{x}^{(1)}(n+1) \\ \mathbf{x}^{(2)}(n+1) \\ \vdots \\ \mathbf{x}^{(S)}(n+1) \end{pmatrix} = \Lambda^+ \begin{pmatrix} \mathbf{x}^{(1)}(n) \\ \mathbf{x}^{(2)}(n) \\ \vdots \\ \mathbf{x}^{(S)}(n) \end{pmatrix} + \frac{1}{m-1} \Lambda^- \begin{pmatrix} 1 - \mathbf{x}^{(1)}(n) \\ 1 - \mathbf{x}^{(2)}(n) \\ \vdots \\ 1 - \mathbf{x}^{(S)}(n) \end{pmatrix} \quad (3.40)$$

with

$$\Lambda^+ = \begin{pmatrix} \lambda_{1,1}P^{(11)} & \lambda_{1,2}I & \dots & \lambda_{1,S}I \\ \lambda_{2,1}I & \lambda_{2,2}P^{(2,2)} & \dots & \lambda_{2,S}I \\ \vdots & \vdots & \vdots & \vdots \\ \lambda_{S,1}I & \lambda_{S,2}I & \dots & \lambda_{SS}P^{(SS)} \end{pmatrix} \quad (3.41)$$

and

$$\Lambda^- = \begin{pmatrix} \lambda_{1,-1}P^{(11)} & \lambda_{1,-2}I & \dots & \lambda_{1,-S}I \\ \lambda_{2,-1}I & \lambda_{2,-2}P^{(2,2)} & \dots & \lambda_{2,-S}I \\ \vdots & \vdots & \vdots & \vdots \\ \lambda_{S,-1}I & \lambda_{S,-2}I & \dots & \lambda_{SS}P^{(SS)} \end{pmatrix} \quad (3.42)$$

for  $\lambda_{(i,j)} \geq 0$  for  $i = 1, 2, \dots, S$  and  $j = \pm 1, \pm 2, \dots, \pm S$  and  $\sum_{-S}^{+S} \lambda_{i,j} = 1$ .

Equivalently:

$$\mathbf{X}(n+1) = \mathbf{H} \times \mathbf{X}(n) + \frac{1}{m-1} \mathbf{J} \times \mathbf{1} \equiv M_s \mathbf{X}(n) + \mathbf{b} \quad (3.43)$$

where

$$H_{ij} = \begin{cases} (\lambda_{i,j} - \frac{\lambda_{i,-j}}{m-1})P^{(ii)} & \text{if } i = j \\ (\lambda_{i,j} - \frac{\lambda_{i,-j}}{m-1})I & \text{otherwise} \end{cases} \quad (3.44)$$

and

$$J_{ij} = \begin{cases} \lambda_{i,-j}P^{(ii)} & \text{if } i = j \\ \lambda_{i,-j}I & \text{otherwise} \end{cases} \quad (3.45)$$

Using 3.43 recursively we get:

$$\mathbf{X}(n+1) = M_S^{(n+1)}\mathbf{X}(0) + \sum_{k=0}^n M_S^k \mathbf{b} \quad (3.46)$$

where  $M_S^0 = I$ . If for certain matrix norm, we have  $\|M_S\| < 1$  then the model 3.43 reaches to a stationary distribution. For instance by considering  $\|\cdot\|_\infty$  norm which defined as:

$$\|M\|_\infty = \max_i \left( \sum_{j=1}^n |M_{ij}| \right)$$

we have:

$$\lim_{n \rightarrow \infty} \mathbf{X}(n) = \lim_{n \rightarrow \infty} \sum_{k=0}^n M_S^k \mathbf{b} = (I - M_S)^{-1} \mathbf{b} \quad (3.47)$$

Also note that :

$$\|M_S\|_\infty \leq \max_{1 \leq k \leq S} \left\{ m \left| \lambda_{k,k} - \frac{\lambda_{k,-k}}{m-1} \right| + \sum_{k \neq i} \left| \lambda_{k,i} - \frac{\lambda_{k,-i}}{m-1} \right| \right\} \quad (3.48)$$

which helps to control the rate of convergence by setting the right hand side of 3.48 less than specific value  $\alpha$ . To estimate the parameters of model 3.43 the final stationary distribution, namely  $\hat{\mathbf{X}}$  and state transition probability matrices,  $P^{(ii)}$  should be given. These parameters can be calculated from previously recorded data of the sequences. Knowing them the following linear program should be solved to get parameters of  $\Lambda$ .

$$\min_{\lambda} \sum_i \left| \left[ b_{j,k} - \hat{\mathbf{x}}^{(j)} \right]_i \right| \quad (3.49)$$

subject to:

$$b_{j,k} = \sum_{k=1}^S \left( \left( \lambda_{j,k} - \frac{\lambda_{j,-k}}{m-1} \right) \Delta_{j,k} \hat{\mathbf{x}}^{(k)} + \frac{1}{m-1} \lambda_{j,k} \Delta_{j,k} \mathbf{1} \right) \quad (3.50)$$

$$\sum_{k=-S}^S \lambda_{j,k} = 1, \quad \forall j = 1, 2, \dots, S. \quad (3.51)$$

$$\lambda_{j,k} \geq 0, \quad \forall k = \pm 1, \dots, \pm S, j = 1, 2, \dots, S \quad (3.52)$$

$$m \left| \lambda_{k,k} - \frac{\lambda_{k,-k}}{m-1} \right| + \sum_{k \neq i} \left| \lambda_{k,i} - \frac{\lambda_{k,-i}}{m-1} \right| \leq \alpha \quad \text{for } k = 1, 2, \dots, S. \quad (3.53)$$

$$\Delta_{jk} = \begin{cases} P^{(jj)} & \text{if } j = k \\ I & \text{if } j \neq k \end{cases} \quad (3.54)$$

Note that by choosing  $\|\cdot\|_1$  we need to solve linear program 3.49 for each Markov process  $i$  to find proper  $\lambda$ 's. To do this, the preliminary estimates of final stationary distribution and state transition matrices are required.

## Chapter 4

### Cognitive approach in modeling decision

In this Chapter, we introduce the third approach in modeling decision process which is widely used by behavioral scientists. Here, effective factors and patterns in human behavior and performance are studied to construct normative models [19]. The advantage of this approach is the capability of including strategy selection feature into the process of decision making. In other words, the strategy layer provides tools to understand how the process of making decision, as a whole, can be effected by changing the strategy. After reviewing the main concept of cognitive approach, we focus on constructing a model that can take advantage of bio-physical modeling, mathematical abstraction and cognitive modeling approaches. We claim that such model is capable to satisfy the basic requirements of closed loop control system.

Recently, some research has been aimed at unifying three approaches of bio-physical model, mathematical abstraction and cognitive models, specifically in the locus coeruleus-norepinephrine (LC-NE) framework [20]. The locus coeruleus (LC) is a part of the human brain that plays a complex and specific role in the control of behavior. Norepinephrine (NE) is a neurotransmitter released by LC that adjusts the function of layers of neurons. The LC-NE system is believed to be an essential part of the brain in the process of decision making [21]. In this chapter we specifically used

the *adaptive gain theory framework* to propose a feedback control model, includes the human decision process.

## 4.1 Behavioral models

In classical multi-cue multi-choice theories, it assumed that humans shall process all available information, namely cues and their validities, and by carefully computing the weighted sum associated with each choice, make a correct judgment [22]. This view known as weighted additive (WADD) and dominated literature for a long time. The core concept behind the wide acceptance of this approach is “*more information is always better*”. Accordingly any procedure that relies on employing less amount of information for the sake of saving time of cognitive effort is inherently less accurate in results (accuracy-effort trade-off).

Starting in late 1990’s, this classical view challenged by series of studies that shown relying on one good reason and ignoring the rest can produce more accurate results, e.g. [23]. In other words, using heuristics might be somewhat more efficient than rational decision. Those findings were in stark contradiction with the view of heuristics are best to avoid. Surprisingly, less information and computation can actually lead to higher accuracy, or *less-is-more* effect holds. In that sense, the word *heuristics* is congruent with its Greek origin “serving to find out or discover”. It is worthy to note less-is-more dose not imply that the less information one uses, the better accuracy is expected. Rather, it means there is a point that more information and computation becomes counterproductive.

There are two general ways to depart from linear regression (WADD) to heuristics. The passage is summarized in Table 4.1. We can either ignore weights associated with each cue or neglect some cues themselves. The former is called *Tallying* in which

Table 4.1: Decision strategies spectrum [2]

Strategy	Description
Weighted Additive (WADD)	Linear summation of cues multiplied by weight
Tallying	Equal wights for all cues
Eliminated by aspects (EBA)	Eliminate all choices that do not exceed a specified value on the first cue
Lexicographic (LEX)	Select a choice with highest cue on the cue with highest validity
Take The Best (TTB)	Special case of LEX for two choices with binary cue value

equal or random weights are assigned to all cues. The latter in its extreme case becomes *take-the-best* strategy, which means ignoring all cues but the most valid one. Heuristics would overcome WADD in the case of low predictability of a criterion, small sample sizes relative to the number of available cues, and dependency between cues, which are not infrequent in environment, specifically in the case of emergencies [24]. One important assumption is the existence of so called *adaptive toolbox* [25], which comprised of collection of heuristics and building blocks an individual has at its disposal for construction heuristics. Mental capacities such as recognition memory are used to construct heuristics constantly. The extend that one uses heuristics are brilliantly defined by Simon’s scissors analogy: “Human rational behavior (and the rational behavior of all physical symbol systems) is shaped by a scissors whose two blades are the structure of task environments and the computational capabilities of the actor”. In our work this analogy translated to indigenous human factors and exogenous system characteristics during emergencies. According to [26] environmental

structures that might affect the strategy selection include:

1. Uncertainty: How well a criterion can be predicted
2. Redundancy: The correlation between cues
3. Sample size: Number of observation compare to number of cues
4. Variability in wights: The distribution of the cue weights

Higher values of uncertainty, redundancy and variability increase the success rate of heuristics while low sample size has the same effect.

## 4.2 From WADD to Heuristics

Behavioral scientists have introduced normative models to explain the process of decision-making in multi-cue tasks. In normative models, each cue is assumed to have a utility or validity  $[q_m]$  which is defined as the conditional probability that a choice based on this cue is correct, given that the cue discriminates between the choice alternatives [27]. Each cue also has a value  $[c_{m,i}]$  in favor of or against the choice represented by pool  $i$  which for simplicity is assumed to be 1 or 0. Validity of each cue is multiplied by its value and the sum for each choice is calculated. The choice with the largest sum is selected. As mentioned earlier WADD is defined as a subsection of larger category named compensatory methods which in essence are the discretized versions of race model 3.13 without noise, where cue validity is equivalent to binary drift rate. Another approach called non-compensatory or heuristics employs only a limited number of cues and ignores others. The decision to select which of these two approaches is called *strategy selection*. In other words strategy is defined as a

Table 4.2: Cue information for hiring example

	Cues				
	con.	int.	ini.	cre.	com.
Cue validity	0.706	0.688	0.667	0.647	0.6
Cue value for choice 1	1	0	0	0	1
Cue value for choice 2	0	1	1	0	0
Cue value for choice 3	0	1	0	1	0

decision on how to make decisions. For better understanding of strategy selection, let us illustrate the method with the following example.

Assume a manger has to make a decision of hiring a new employee. There are five distinct criteria: *conscientiousness*, *intelligence*, *initiative*, *creativity*, *communication skills* (multi-cue task) and three finalists to choose from (multi-choice). The company have a good estimation of a probability of a good hire if the hiring is made based on one specific cue (cue validity). Using WADD approach and Table 4.2 information we calculated the value of each candidate as follows:

$$V_j = \sum_1^5 q_i c_{i,j}$$

$$V1 = 1.0306 \quad V2 = 1.355 \quad V3 = 1.335$$

The algorithm will results in hiring candidate 2. To add strategy layer to the model, let's assume the manager has control by defining a custom **weight** factor,  $\beta$  for each department that redistributes validities based on soft-max rule:

$$w_j = \frac{e^{\beta q_j}}{\sum_1^5 e^{\beta q_i}}$$

Larger values of  $\beta$  changes the validity distribution in favor of larger values. Cue weights with two different weight factor are presented in Table 4.3. Using WADD

Table 4.3: Cue information with different weight factors

	Cues				
	con.	int.	ini.	cre.	com.
Cue validity	0.706	0.688	0.667	0.647	0.6
Cue value for choice 1	1	0	0	0	1
Cue value for choice 2	0	1	1	0	0
Cue value for choice 3	0	1	0	1	0
Cue weight ( $\beta = 5$ )	0.211	0.193	0.174	0.157	0.124
Cue weight ( $\beta = 35$ )	0.501	0.267	0.128	0.063	0.012

Table 4.4: Candidate values recalculated

	base	$\beta = 5$	$\beta = 35$
V1	1.0306	0.335	0.513
V2	1.355	0.367	0.395
V3	1.335	0.330	0.330

with weight factors results in different choices as shown in Table 4.4.

$$V_j = \sum_1^5 w_i^\beta c_{i,j}$$

By controlling  $\beta$  the manager can change the strategy from *compensatory* that fairly considers all cues based on their validities to *non-compensatory* that heavily leans towards large validities and ignores others.

### 4.3 Adaptive Gain Control Theory

Intuitively, human performance on most tasks is best with an intermediate level of arousal and is worse with too little or too much arousal or stress. This inverted U-shape relationship is confirmed by the classic Yerkes-Dodson curve [28]. The underlying brain mechanism that controls phenomena such as arousal and motivation is provided by several brain stem neuromodulatory nuclei with wide distribution and ascending projection to the neocortex. These neurons play crucial roles in cogni-

tive behavior by releasing neurotransmitters, such as dopamine (DA), serotonin, and norepinephrine (NE). Any disturbance in such basic and pervasive functions causes trouble in cognition, emotion, and behavior. In addition to their direct effect on post synaptic neurons in the form of excitation or inhibition, these neurotransmitters modulate the effect of other neurotransmitters such as glutamate and gamma amino butyric acid (GABA) by change of neuronal gain or activity function [29]. Our focus in this study is to model the role of locus coeruleus (LC) neurons which release NE, and its different modes of activities during the process of decision-making. In particular, we focus on *adaptive gain control theory* proposed by [21] and try to formulate it in the control framework.

Experiments showed two distinguished modes of activity in LC neurons. In *tonic* mode, an elevated baseline activity is recognized without any bursts, while in *phasic* mode bursts of activities have been recorded during moderate baseline. Accurate decision processes are usually accompanied by bursts in the phasic mode [30]. By increasing the level of baseline activity in LC, engagement in the specific task and consequently the performance decrease. This is the LC tonic mode which is associated with more destructibility and greater tendency to respond to not relevant stimuli. These findings lead to hypothesis that LC phasic activity can be modeled as a temporal attentional filter which facilitates behavioral responses in the task-related decision process. However the information-processing function that the tonic mode may serve needs more speculation.

#### 4.3.1 LC-NE Framework

Studies on neuromodulatory effect of NE on the performance of making decision given by [31] showed that the decision network can move from unaroused states through high

performance to impulsive states and eventually lose the inhibition driven race model behavior by varying the gain of inhibitory and excitatory neurons. Furthermore, after making the decision in decision layer, the temporary increase in the gain  $\gamma_E$  of neurons in behavioral layer makes them act as a binary units to reduce the effect of noise and delay in eliciting response. In other word, the phasic bursts make the multilayer complex decision network to act as a single layer network when there exists a strong evidence in favor of the decision. In contrast, LC tonic mode, due to elevated baseline activity, causes indiscriminate persistent increase in gain that renders more sensitivity to irrelevant stimuli. With respect to the current task, such distraction is clearly disadvantageous, however it paves the road for exploration of other opportunities and accumulates evidence toward other decisions.

Using a detailed population-level model of LC neurons and abstract connectionist network, Reference [30] showed that change in electrical coupling among LC neurons can produce the above mentioned two modes of activity. Within LC, increased coupling gain, resulted from activation of the target decision unit, facilitates phasic mode, which in turn causes the alternation of gain function in neurons receiving NE in each layer of the behavioral network, namely input, decision layer itself, and response layer. This positive feedback loop leads to better performance. In contrast, reduced coupling strength in LC neurons causes a modest increase in baseline activity due to non-decisive random input into the LC neuron and diminished bursting activity. Employing this mechanism, decision maker optimizes the performance in a broader sense, which is the trade-off between exploitation of current utility or exploration of other opportunities. The question is what will drive the gain change or baseline excitatory drive to change the mode of LC neurons?

LC neurons have strong projection on two other frontal brain areas, namely orbitofrontal cortex (OFC) and anterior cingulate cortex (ACC), which are responsible

for evaluation of reward and cost [32]. OFC neurons are activated by rewarding stimuli and their response varies in proportion to the amount of reward. ACC is responsive to a variety of negatively valenced signals from pain to perceived errors in performance, in addition to task difficulty and conflicts in processing. The main feature which plays a significant role in decision making is the ability of integration of rate of reward over extended periods. Due to mutual projection between LC and OFC and ACC, it has been suggested that OFC and ACC may drive the LC activation in phasic mode. They also regulate the transition between phasic and tonic modes [21]. When evaluations in ACC and OFC indicate that the current task utility decreases steadily, they facilitate transition to the tonic mode to search for other possible sources instead of focusing on the current task. This is done by diminishing the phasic bursts that render concentration on the current task. In case that ACC evaluates the utility is adequate enough, the phasic mode would continue.

The dilemma of either exploitation of current resource or exploration of other opportunities requires both long-term and short-term evaluation of utility. It is assumed that OFC and ACC outputs are integrated over two time scales in order of seconds and minutes respectively [21]. For example, for 2AFC a simple engagement index is defined as:

$$E_i = \left(1 - \frac{1}{1 + e^{u_s}}\right) \frac{1}{1 + e^{u_l}} \quad (4.1)$$

in which  $u_l$  and  $u_s$  are long and short term utilities of the decision.  $E_i$  sets a threshold for changing the mode of LC neurons as depicted in Fig. 4.1.

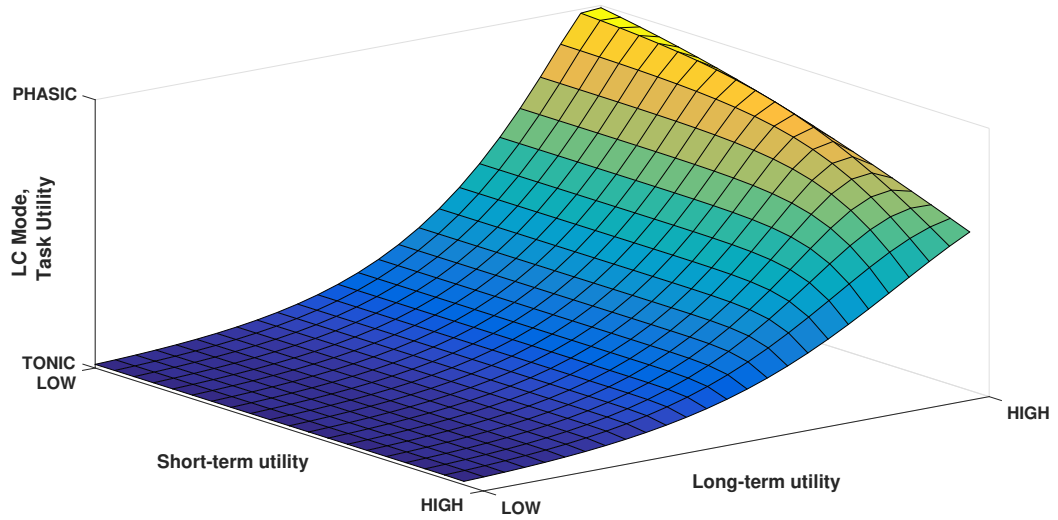


Figure 4.1: Change of LC mode based on long and short term utilities.

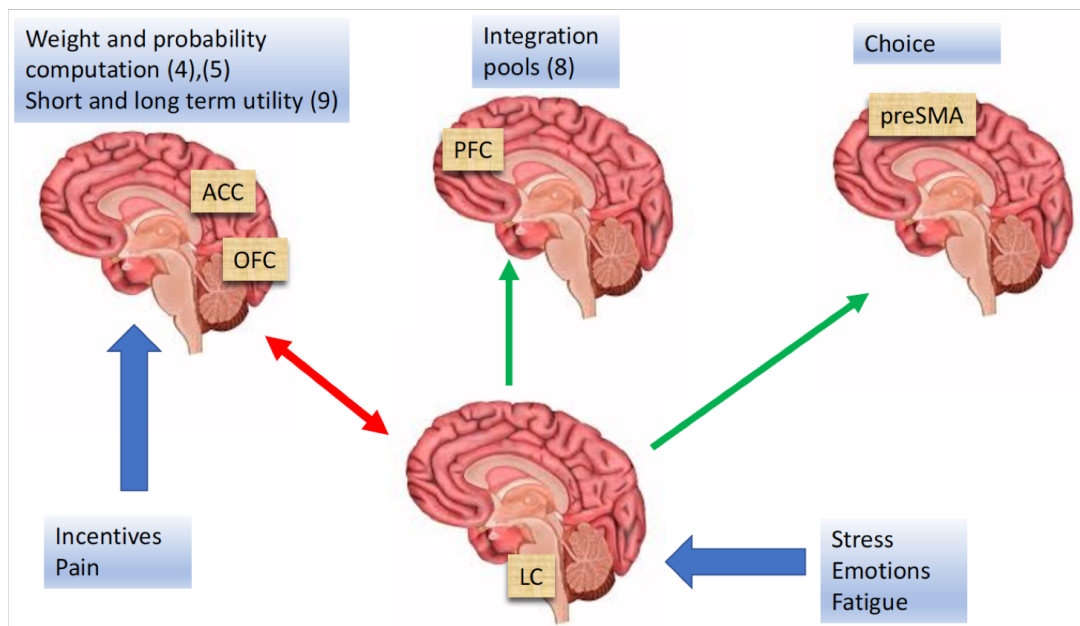


Figure 4.2: Brain parts that govern decision process

#### 4.4 Adaptive gain with strategy layer

To fit the strategy selection into adaptive gain theory, it is hypothesized that ACC and OFC also calculate the cue weight factor  $[w_m]$  on the basis of initial cue validities  $[q_m]$  [20]. LC neurons on their phasic mode facilitate adjustments of the weights factors in favor of most valid cues by tuning the linear gains  $\gamma_E$  and  $\gamma_I$ . It has been believed that attentional controls such as cue order schedule and processing time are performed in prefrontal cortex (PFC) [33]. Hence, the cue order schedule and process time distribution are determined in PFC. The projection of NE to all these areas ratifies the role of LC neurons in attention and making decisions. Figure 4.2 summarized the roles of each part of brain in LC-NE framework.

Returning to our multi-cue multi-task race model, the strategy selection problem is a process that controls the probability distribution of considering each cue and the time assigned to it in the order schedule. We employ the idea presented in [20] to find such probability distribution. Assume that a weight factor is initially assigned to each cue on the basis of given initial cue validities. Then the weight factors are calculated according to the following softmax rule:

$$a_m = \frac{e^{\gamma_I q_m}}{\sum_{i=1}^M e^{\gamma_I q_i}} \quad (4.2)$$

in which  $\gamma_I$  is the linearized inhibitory gain factor. We use the normalize vector  $[w_m]$  as the probability distribution of cue processing time and order:  $p_m = a_m / \max [a_m]$ .

Note that by increasing  $\gamma_I$ , the probability of choosing the cue with highest validity and the time interval assigned to it increase. Here, the gain can be interpreted as the control parameter that changes the strategy from compensatory to heuristics. To explain the propose model, we assume that the decision maker acquire information in

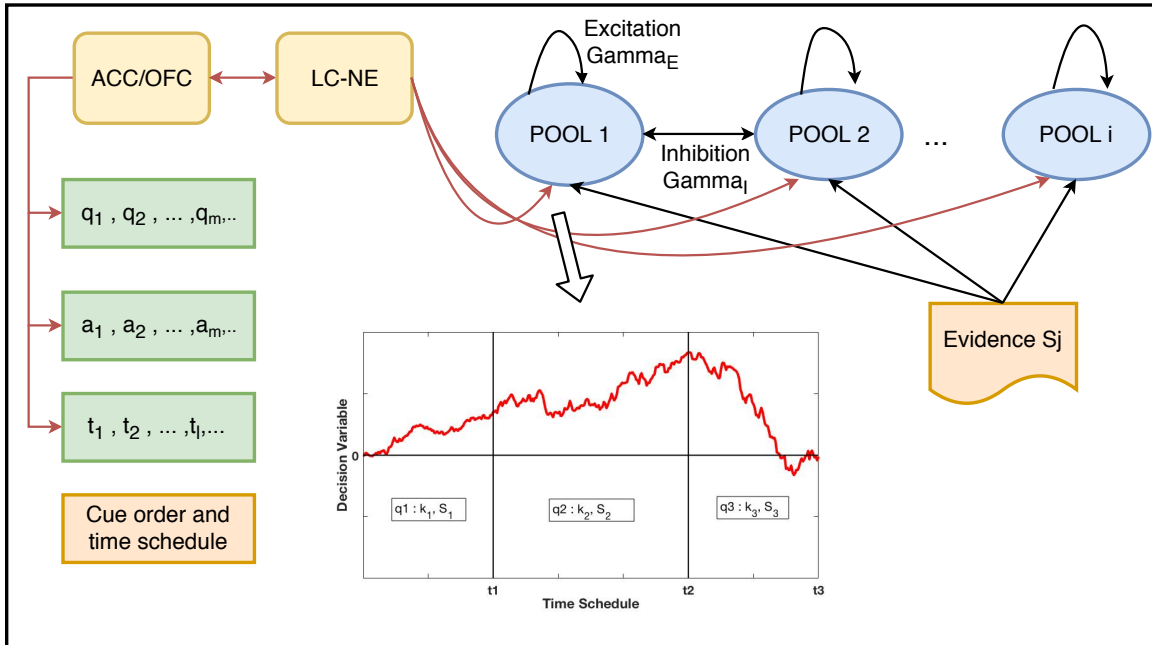


Figure 4.3: Schematic diagram of decision model

sequential manner, similar to DDM. Cue validities are determined by OFC and ACC based on past associations. The OFC and ACC relay their activation to LC which in turn tune the gain tuple  $[\gamma_E, \gamma_I]$ . As discussed in chapter 1, this neuro-modulation process can change the performance of decision maker which is shown in terms of reward rate. Figs.4.3 depicts the schematic diagram of the proposed model with decision process modeled by DDM.

The big advantage of proposed model in control is giving measures that moderate the performance of decision maker LC activity has large correlation with non-cognitive factors such as arousal, affect and stress For instance by controlling the environmental factors and recording the stress level, one can estimate the mode of LC Having this modeling tool in hand, it is viable to think about having human decision model in the control loop. Our proposed model features can be summed up as follows.

- The model uses both DDM formalization and physiologic models

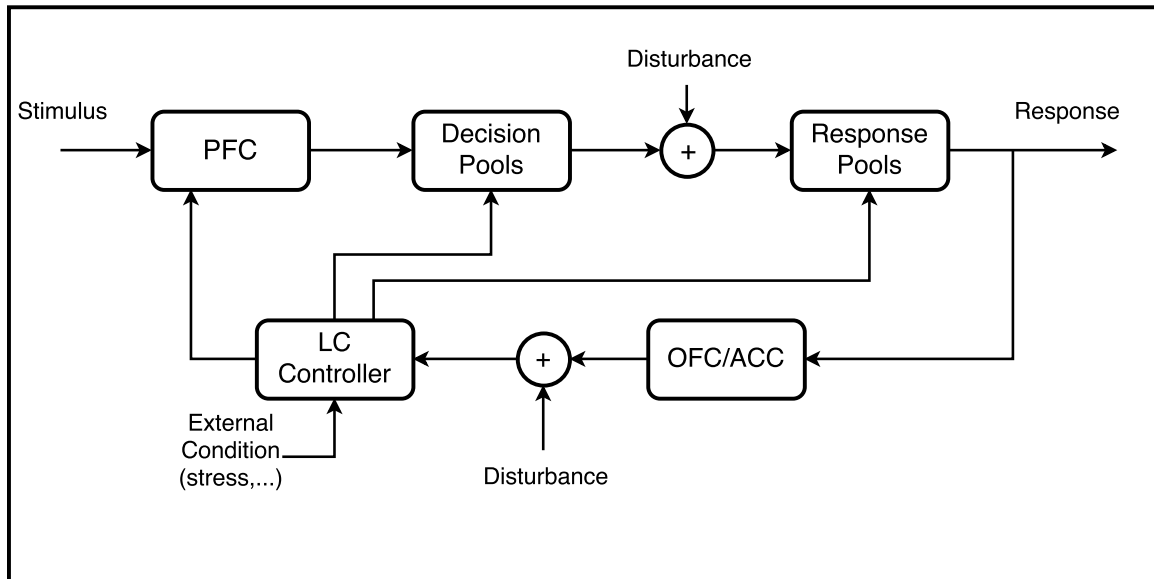


Figure 4.4: Proposed adaptive gain control and strategy selection framework

- Connects abstract notation of decision making to measurable control signals
- By capturing the LC mode, the decision strategy can be estimated
- By controlling the factors such as stress and fatigue, it is possible to keep the performance near its optimum value
- This idea is a way to put more realistic decision model in to the plant control loop

Fig.4.4 summarize the extended adaptive gain theory with strategy selection layer. In the next Chapter we use this closed-loop model to mimic the process of decision in an enterprise level supervisory and control system.

## Chapter 5

### Human Decision in the Loop

The goal in this chapter is to propose a modeling approach in conjunction with supervisory-control-and-data-acquisition (SCADA) actions (human responses and autonomous controls) and non-SCADA actions to facilitate the integration of the proposed human decision-making scheme into cyber-physical network control loop.

Although the SCADA control center typically possesses a multi-echelon hierarchical architecture, seeking an appropriate tool to address such hierarchical control with humans in the loop tends to be challenging. One approach in solving the problem is assigning weight to autonomy and human decision based on factors like threat level [34]. However it is hard to justify that higher level of autonomy in high threat levels would result in better control outcome or vice versa. Also since there is no human decision model involved, it is assumed that the trained operator in healthy condition would issue eligible commands.

Second approach is to design a complementary control, namely *decision unit* which adds a model of human decision to the controller that can predict human command in the near future. The outcome of decision unit can either be presented to the operator as a directive or may adjust the issued command toward better results. Thus far some research have been conducted in the latter area using model-predictive control

(MPC) framework [35]. To predict the human decision, common practice is assuming a given probability distribution for decisions in different condition, based on previous recorded data.

As part of the human-system integration, here we proposed a two-step approach. In this context, it is assumed that a human operator may influence the system in different levels as a function of indigenous system states or exogenous factors such as emergencies. Thus, the system should possess *sliding levels of autonomy* [36]. It is also assumed that in a normal situation, plant can complete the designated task autonomously. However the trained human operator has the authority to differ from the automation and issue commands that change the plant state trajectories. Traditional control scheme requires that the operator be constantly aware of the states of the plant and notice any anomaly sufficiently soon so that the issued corrections guarantee safe operation. Such a condition does not hold during emergencies, and the assumption that vindicates the human operator's full authority is invalid. To overcome this issue, an augmented control system architecture will be proposed so that it can evaluate the operator's decision together with other synthesized control solutions generated by computational control models, considering the human operator's working condition/states, such as stress, fatigue, etc.

The goal of the augmented control system is to enable an optimal selection of multiple strategies, including both the operator's decision and the control model's adjusted decision, so that even in critical emergency situations, the supervisory control system can judge the reliability of the operator's decision and select an optimal solution.

## 5.1 Human-Cognition-in-the-Loop Supervisory Control

In this section, we give an application scenario for the human decision model introduced in the previous sections. Specifically, we describe a human-cognition-in-the-loop control system that pursues two main tasks: The first task is to employ the proposed human decision model to evaluate the reliability of the human operator's decision, and then to combine it with the decision given by a decision support system. The second task is to dispatch the work loads specifically in critical situation between the human operator and decision support system in a way that the operator remains close to his/her best performing condition.

### 5.1.1 Augmented supervisory system

Consider a regular industrial plant, e.g., a manufacturing plant, whose states are affected by external variables (uncontrollable) and the control signal input. Generally, when the plant is simple enough, the control signal can be given by a controller (implemented with a control algorithm); and thus the plant and the controller form a control loop which makes sure the industrial process operates normally. In addition, this process may be monitored by one or several human operators, who are responsible for intervening in the automated process whenever they think it is necessary. This paradigm is adopted in almost every automatic industrial process, such as supervisory control and data acquisition (SCADA) systems.

Human interactions with the automated system form another control loop outside of the primary loop of the automated system, as shown in Fig. 5.1. Here, we refer to the industrial instrument as Plant 1, and the automated system as Plant 2.

It is a common practice to trust the decision of human operator based on superiority of human judgment compared to autonomy. However, there are circumstances

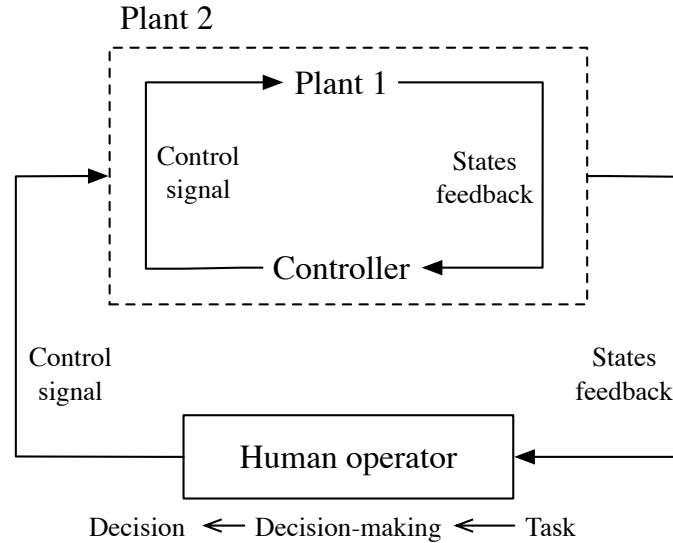


Figure 5.1: Common Human-in-the-loop control scheme

where the reliability of human decision is questionable, such as when emergencies happen, the quality of the working environment deteriorates, the human operator has been working for long hours, or when the human operator suffers from any physical or mental problem. Therefore, in certain important contexts, a special decision support system may be necessary. As known, the decision support system has been widely adopted in different scenarios, and has been an important application of artificial intelligence (AI) and expert systems technology [37, 38]. Examples range from car autopilot systems to electrical power companies online evaluation tools that predict system's near future states. Thus far, such decision support systems only act as a reference for human operators to make decisions. For instance, the decision support system may alert the operator and provide a list of recommended actions for the operator to take, such as fault diagnosis of possible locations, or emergency shut-down/braking. However, employing the cognitive decision model, the quality of human judgment and thus the reliability of his/her decisions can be evaluated, which

allows the system to reevaluate human decision and even not to follow it.

Here, we propose an augmented supervisory decision-making process, in which the human decision model introduced in the previous sections is used to evaluate the reliability of the human operator's decisions, and accordingly the operator's decision and the decision support system's output are integrated. As shown in Fig. 5.2, the decision support system plays the role of an AI operator, whose decision is denoted as  $\text{Decision}_A$ . Similarly, the human operator's decision is denoted as  $\text{Decision}_H$ . The human operator is paired with a supervisory controller to evaluate his/her judgment quality and then integrate his/her  $\text{Decision}_H$  with the decision support system's  $\text{Decision}_A$  into a final decision. Here, we simply choose one of the decisions as the final decision.

## 5.2 Case study

Let us consider a simple case, i.e., the human operator and the decision support system only need to determine whether or not to interrupt the current automated process. Furthermore, let us assume that each decision is only right or wrong, and there is nothing in between. With this assumption we can replace the qualitative term *reliability* with quantitative term *accuracy* and further normalize the accuracy of a decision into *probability* of making correct decision.

Next, we assume that the accuracy of  $\text{Decision}_A$  is provided along with  $\text{Decision}_A$  by the decision support system. The accuracy can be given based on the recorded performance of the system. By the help of the cognitive model, we would be able to justify an accuracy measure pertained to human decision. Thus, the so-called supervisory system is responsible for determining which decision to choose according to the accuracies of the two options. Computation of the accuracy of the human opera-

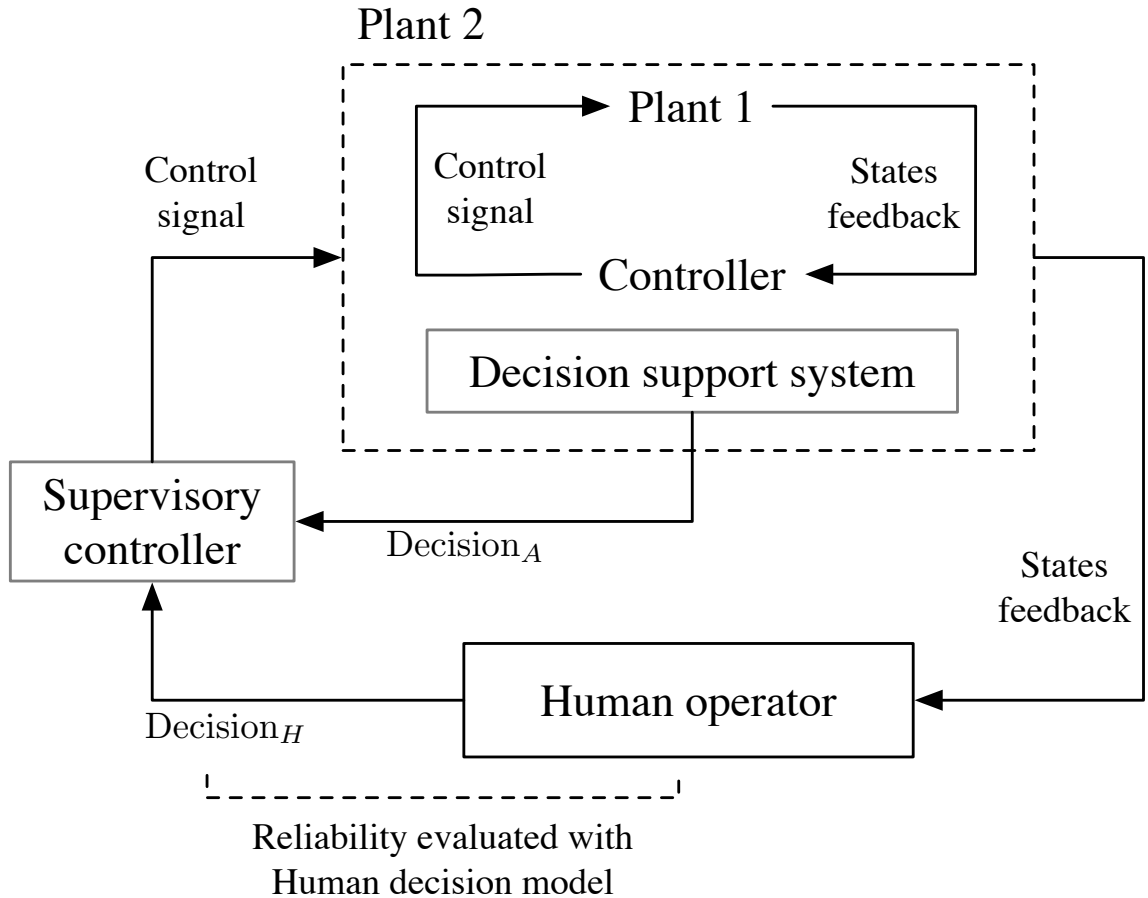


Figure 5.2: Human-cognition-in-the-loop control framework

tor's  $Decision_H$  along with the supervisory dispatching task is described in the next subsection.

The supervisory controller comparing tasks is implemented as follows. Given each decision A or H with their pertaining accuracies  $a_A$  and  $a_H$ , the probability of selecting  $Decision_A$  is set to  $p_A = (1 - a_H)a_A$  and thus the probability of taking the human operator's  $Decision_H$  is  $p_H = 1 - p_A$ . The overall expected accuracy of the augmented human-cognition-in-the-loop decision-making process is therefore given by  $a = p_H a_H + p_A a_A$ . Table 5.1 shows the behavioral pattern of the augmented decision-making process. It can be seen that when  $a_A > a_H$ , the overall accuracy  $a$  increases

Table 5.1: Accuracy of the augmented decision-making process

$a_H/a_A$	30%	60%	90%
30%	$p_A = 21\%, a = 30\%$	$p_A = 42\%, a = 42.6\%$	$p_A = 63\%, a = 67.8\%$
60%	$p_A = 12\%, a = 56\%$	$p_A = 24\%, a = 60\%$	$p_A = 36\%, a = 70.8\%$
90%	$p_A = 3\%, a = 88.2\%$	$p_A = 6\%, a = 88.2\%$	$p_A = 9\%, a = 90\%$

significantly; while when  $a_A < a_H$ , the overall accuracy  $a$  decreases only slightly. In practice, we may configure the system to choose  $\text{Decision}_H$  whenever  $a_A < a_H$ , so that the overall accuracy never decreases.

### 5.2.1 Human decision accuracy

In order to assign an accuracy measure to human decision, we need to limit ourselves to a specific task in which human attention as well as his/her internal states and work area specification are well defined. Here we simulate 2AFC framework with random dot experiment [39] in which the operator is required to make a decision based on the single cue, i.e., to detect a direction of motion of dots correctly. Our assumption here is that the operator choose the Take the Best strategy and his/her vision is the best cue at the time. Next we build a neuronal model as described in section 2.4 to emulate the process of decision-making in the sensory-motory brain areas. Note that, this is basically a single cue double choice task and can be abstracted with DDM in the form of (3.11). The complexity of a task is simply defined by the proportion of dots moving in the desired correct direction and random moving dots. The model consists of three types of neuronal population: primary visual cortex (V1) that gathers the information  $S_i$ , the middle temporal area (MT), and the lateral intraparietal cortex (LIP). The detailed description of the model can be found in [40]. Visual stimulus is given in the form of gray scale video feed and the performance of the model in detection of the direction is analyzed. The human operator's accuracy  $a_H$  is estimated using the

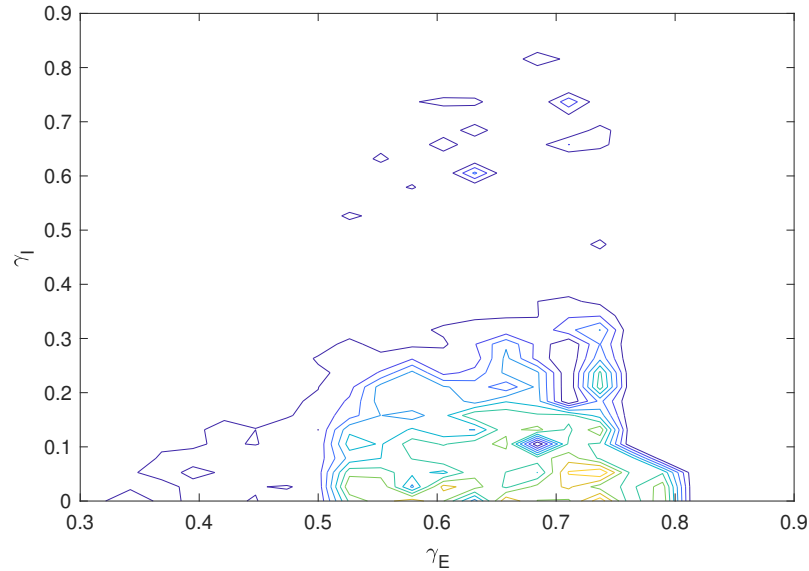


Figure 5.3: The region of operator high performance in  $\Gamma$  plane for moving dot task with complexity 50%

reward rate 2.30.

To obtain the best performance area in the  $\Gamma$  plane, we simulate the reward rate of the detection task over the range of inhibitory and excitatory gains, i.e.,  $(\gamma_I^i, \gamma_E^i)$  tuple as described in Sections 2 and 3. An example of high accuracy region for the task with complexity 50% is given in Fig. 5.3. The main outcome of this simulation is to provide a clue of the quality of human decision in different situations and a variety of job complexities. Fortunately there are some technologies available that can roughly determine the condition of human internal state by using parameters such as skin conductance and hear bit and in more advanced setup EEG signals. If by any means this condition can be mapped to the  $\Gamma$  reference plane, we can think of designing a controller to keep the operator performance in the vicinity of high performance region rather than just choosing between  $\text{Decision}_A$  and  $\text{Decision}_H$ .

### 5.2.2 Controller design

To achieve this goal we equip the so-called supervisory controller with work dispatching capability. Let us assume that a sequence of tasks  $\mathbf{m}_1, \mathbf{m}_2, \dots$  arrive at the control center (where the human operator and decision support system make decisions) one after another, where  $\mathbf{m}_i$  is a vector containing all relevant information of task  $i$  including a measure for task complexity  $m_i$ . The accuracy  $a_H(\mathbf{m}_i, \Gamma_i)$  of the human operator not only depends on the complexity  $m_i$  of task  $\mathbf{m}_i$ , but also his/her internal state  $\Gamma_i = \{\gamma_I^i, \gamma_E^i\}$  at the time of task  $\mathbf{m}_i$ . Since the operator is equipped with sensors that show his/her decision accuracy in  $\Gamma$  plain for the incoming task, the supervisory controller has the updated data of operator decision accuracy  $a_H$  by looking into his/her  $\Gamma$  plain profile. Note that large neural models for human accuracy measurements are offline models and can be updated periodically based on operator workload or his/her physical or mental condition.

To give an example we ran the neural model simulation on Tesla K40 GPU with K40MGPU's for each node in the Holland Computing Center (HCC) at University of Nebraska-Lincoln (UNL) to obtain sample  $\Gamma$  profiles. The MATLAB 2017a script was run on iMAC, intelCore i5, with 8 GB memory and macOS X version 10.12.5. Furthermore, we assume that the accuracy  $a_A$  of Decision<sub>A</sub> is given by  $a_A(m_i) = 0.95 \times m_i$ , such that accuracy  $a_A$  for the decision support system solving a simplest task  $m_i = 0.95$  is 90%. Tasks with complexities  $m_i, i = 1, 2, \dots$ , are uniformly randomly generated in the range  $[0.75, 0.95]$  and the supervisory controller dispatches them to one operator with a given  $\Gamma$  profile. To simulate the effect of stress and fatigue, we assume that the assignment of tasks affects the human operator's performance in the following way. If the human operator is assigned task  $\mathbf{m}_i$ , his/her internal state  $\Gamma_i$  will diverge from the ridge of high performance by a random distance  $\delta\Gamma_i^0$  after

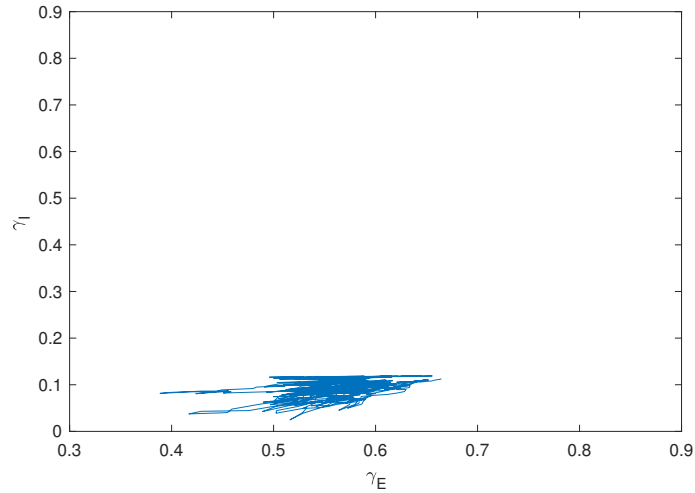
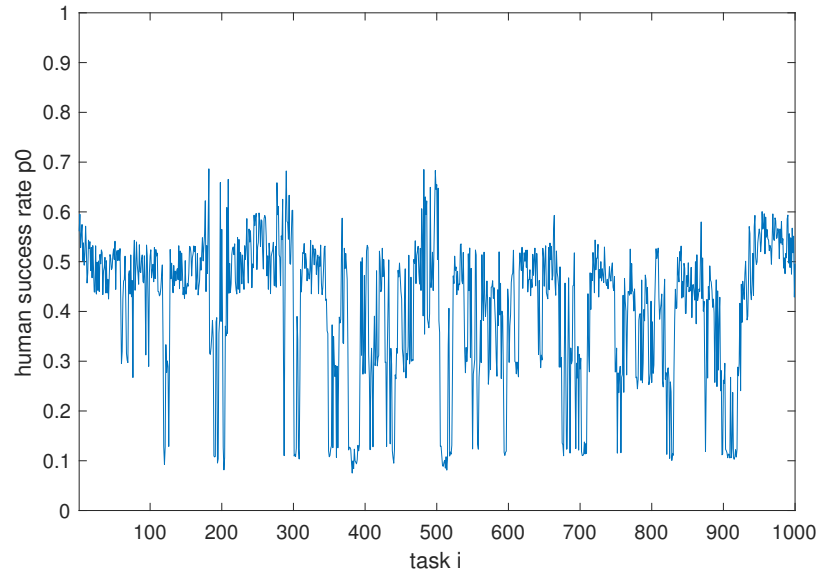
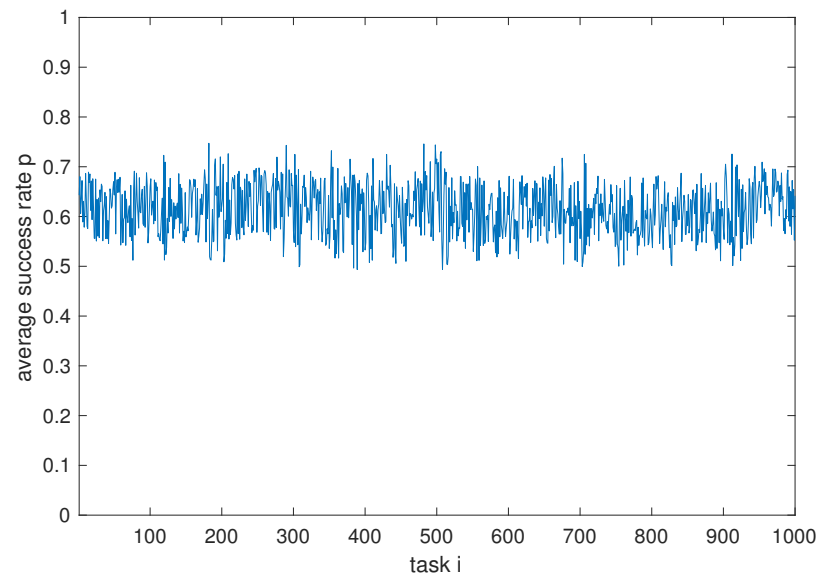


Figure 5.4:  $\Gamma$  gain plain trajectory of operator

completing the task; if the human operator skips task  $\mathbf{m}_i$ , his/her internal state will be brought closer to the ridge by a random  $\delta\Gamma_i^1$ .

It can be seen from Fig. 5.4 that the system ensures that the  $\gamma_E$  and  $\gamma_I$  gains are kept close to the region of the best performance. As the operator continues to work, his/her accuracy fluctuates, as shown in Fig. 5.5, which is a representative situation under emergencies. In addition, it is clear that the overall accuracy is kept above 0.5, and with a much smaller variance due to the effect of the supervisory controller. As compared in Fig. 5.5 and Fig. 5.6, through proper arrangement of the assignment of tasks and a decent decision support system, a higher and much more stable overall accuracy  $a$  can be achieved.

Figure 5.5: Human operator's accuracy  $a_H$ Figure 5.6: Overall accuracy  $a$

## Chapter 6

### Experiment

In the previous chapters we proposed a control framework that incorporates human decision model and its accuracy into the control loop. To do so, we assumed that human biological data that maps the decision performance, here reward rate, onto gamma plane is available. We also noted that the effect of external parameters such as emergencies and internal states such as stress and fatigue on decision performance are well studied and can be used by our platform. In this section we aim to design an experiment that validate our approach. In this way, we relied on type of information that could be gathered with today's conventional technologies, i.e. instead of cellular level gamma plane gain-performance relation we used more accessible biophysiological data such as heart beat and skin conductances. In our experiment, we tried to change decision maker internal states by manipulation her stress and anxiety level and show the dynamics of changing strategy during the course of experiment. In brief, the aims for this experiment are twofold. First, to validate operationalizations of stress by assessing whether gathered physiological data show clear evidences of change of stress level. Second, to determine whether stressful condition induces more heuristic processing and choice.

## 6.1 Effect of stress

Among human factors, one critical aspect that may influence decision making strategy is stress. Stress is used to describe experiences that are challenging emotionally and physiologically [41]. Higher cognitive areas of the brain that play a key role in decision making are target of stress, hence the acute and chronic effects of stressful experiences influence how they respond. The effect of stress in daily life is twofold. “Good stress” generally refers to those experiences that accompanied by sense of accomplishment, whereas “bad stress” or “being stressed out” refers to the sense of lack of control and mastery and leads to irritating, emotionally draining and physically exhausting condition.

As described before, emergencies impose limits on time to make a decision and on the flow of information to the decision maker. Therefore emergency situations are likely to impose stress on decision makers. It is assumed that stress influences important components of information flow by altering: 1) perceptions of the information and 2) how attention will be allocated to the factors relevant to making decisions. Moderate levels of stress actually enhance aspects of cognition [42]. However, higher levels can negatively impact perception [43] and attention [44]. Also, experiment results in [45] concluded that the effect of stress are beneficial when the task requires exclusive focusing on target information, while tasks that require integration of information from several sources are vulnerable to the adverse effects of stress.

As described in chapter 4, our proposed cognitive model is capable of embedding stress into the decision models. Employing dynamic cue weights, we proposed a method to mirror the effect of stress on *perception* and *attention*. Since we are interested in modeling actual human decision making, empirically validating the capabilities of proposed model is important. That is, in addition to testing theoretically

which classes of models perform well, the need to test whether these models capture the decisions that people actually make. Many studies have investigated the circumstances under which people use optimizing versus heuristic strategies to make judgments and decisions [46,47]. In particular, people seem to shift to more heuristic strategies under high time pressure [48,49]. Here instead, we are focused on imposing acute stress via physical stressor and high demand cognition tasks.

## 6.2 Experiment set-up

Our experiment set-up is inspired by the work presented in [50]. The referenced study was focused on high-arousal negative affective states that are typically associated with anxiety, fear and disgust, which represented by the term *emotional stress*. In contrary, our experiment is focused on *cognitive stress* which include information overload, accelerated sense of time, self-criticism and a sense of being out of control that is intensified by physical stress. The main goal is to investigate the effect of stress on changing the strategy of selecting candidate with specific set of skills.

In this study the well-established Montreal imaging stress task [51] along with cold pack stressor [52] were employed to induce acute stress in healthy participants. Individual self-rated stress response in the form of visual analog scale (VAS) [on the scale of 0 = “not at all” to 100 = “extremely”] were used to report the subjective impression of feeling, stress and anxiety level through the course of experiment. Previous studies (e.g. [53]) showed strong correlation between subjective impression of stress and some biological data, commonly used to objectively assess the level of stress. In this experiment, VAS measure is accompanied by measuring skin conductance, saliva alpha-amylase content and the change of blood pressure activity to investigate the effectiveness of the stressor tasks both subjectively and objectively, because

Table 6.1: Attributes and benefits for choice task

Attribute	Benefit
Conscientiousness	82%
Intelligence	80%
Initiative	76%
Creativity	69%
Communicative skills	57%
Agreeableness	44%

while they're often correlated, it is important to measure the physiology to avoid bias with subjective self-report. The selection of skin conductance and blood activity bio-markers are based on data available by measuring device. The saliva analysis was meant to confirm the results rigorously. Participant were asked to perform main decision tasks in two separate sessions before and after the stressor tasks.

### 6.2.1 Decision-making task

The decision-making task consists of a series of MouselabWEB matrices [54]. Each matrix will represent a pool of job applications, with a column for each applicant(see Fig. 6.1). The rows represent attributes of the applicants, and the cell of the matrix is each applicant's quality score between 1 to 5. The candidates are rated based on their qualifications in six cues, which are: conscientiousness, intelligence, initiative, creativity, communication skills, and agreeableness. However, the information in the cells will be covered, such that participants must use the mouse to place the cursor over a cell to reveal its contents. Once the cursor leaves the cell, the contents are covered again. The attributes differ in their abilities to predict worker productivity. Table 6.1 shows the predictive benefits of the attribute scores. It assumed that according to previous hires, candidates with high quality scores for attributes with high benefit values are more likely to be productive workers (pre-determined cue

**Candidate Choice-trail**

Imagine you have to make a choice between the following six candidates. Study the qualifications of each candidate and their grade between one to five carefully and make a choice by pressing the button below the candidate you prefer.

	Candidate 1	Candidate 2	Candidate 3	Candidate 4	Candidate 5	Candidate 6
Conscientiousness						
Intelligence						
Initiative		4				
Creativity						
Communication Skills						
Agreeableness						

**Benefit table**

Attribute	Benefit
Conscientiousness	82%
Intelligence	80%
Initiative	76%
Creativity	69%
Communicative skills	57%

Figure 6.1: choice task screen

validities). The participant must choose the best applicant from the pool and must search for information to make this choice. MouselabWEB allows us to measure the search behavior (e.g., which cells were entered for how long and which cell was entered next). Each time the task is administered, participants will experience between six pools of applicants. Note that the order of cues are the same for all participants and no feed back is given about their performance on selecting candidates during the experiment.

### 6.2.2 Stressor task

To impose stress on participants, we combined two stressors. First, we had the participants complete the cold pressor arm wrap task in which we wrapped their dominant arm in a cold pack (1 degree Celsius/35 degrees Fahrenheit) for up to 2 minutes. The wrap is constructed from heavy fabric with a cooled gel (CryoMax

pack) affixed to its inner surface. A plastic sheet placed between the participants skin and the cold pack. This entire apparatus will be strapped onto the participants arm with velcro affixed to the outer surface of the arm wrap.

After the cold pressor arm wrap task, we used the Montreal imaging stress task, which asks participants to solve increasingly difficult math problems under time pressure. We incentivized participants to try hard at the tasks by telling them that they can receive \$20 if they get all of the problems correct and a lower amount if they are incorrect. The program also provides negative feedback if they are incorrect by showing the decreasing performance bar at the top of the screen.

### **6.2.3 Biological data**

Three types of biological data were collected to measure the level of stress in addition to visual analogue scale. The reason of analyzing biological data is to show if participants are aware of their stress level. The physiological measures of stress and their corresponding technologies that used in this study are:

1. Salivary alpha-amylase (sAA)
2. Skin response; electrodermal activity (EDA)
3. Blood activity; photoplethysmography (PPG)

Salivary biomarkers have received special attention since they are readily accessible and easily obtained. Salivary alpha-amylase (sAA) has been proposed as a sensitive biomarker for stress-related changes in the body that reflect the activity of the sympathetic nervous system (SNS), and a growing body of research is accumulating to support the validity and reliability of this parameter [55].

More recent research relied on skin measurements for stress detection because of easy instrument interface [56]. The skin response primarily focused on is electrodermal activity (EDA), more known as galvanic skin response (GSR). During increased stress, perspiration increases, causing resistance to current flow to drop, inversely affecting conductivity of skin. Skin conductance naturally increases over time, so transient increases are targeted for EDA, i.e. the rapid transient peaks that occur due to stressor. Recorded values are typically in the range of microsiemens ( $\mu\text{S}$ ).

Inter-beat interval (IBI) and heart rate variability (HRV) are commonly used factors to examine stress [57]. IBI and HRV provides more information than HR alone. HRV is the measure of standard deviation in IBI of successive R waves in a heart beat. In stressful situations, HRV is a product of change in autonomic nerve activity, which is composed of sympathetic and parasympathetic modulation. The function of the sympathetic nervous system (SNS) as it relates to the heart is to speed HR to provide an increase in blood supply to the body. Photoplethysmography (PPG) is optical technique to detect blood volume changes in microvasculature. With this optical approach, heart rate (HR) and blood volume pulse (BVP) can be calculated. Hence, PPG provides a cheaper alternative to ECG measurements.

For skin conductance and PPG measurements we used Empatica's E4 wristband [58]. The E4 wristband contains multiple sensors that allow for convenient and comfortable sensing on the wrist. The saliva analysis were performed on Salivary Bioscience Laboratory (UNL SBL).

#### **6.2.4 Method**

Twenty young adults (13 men, 7 women) participated in the study. Participants were students of various departments at the University of Nebraska - Lincoln and

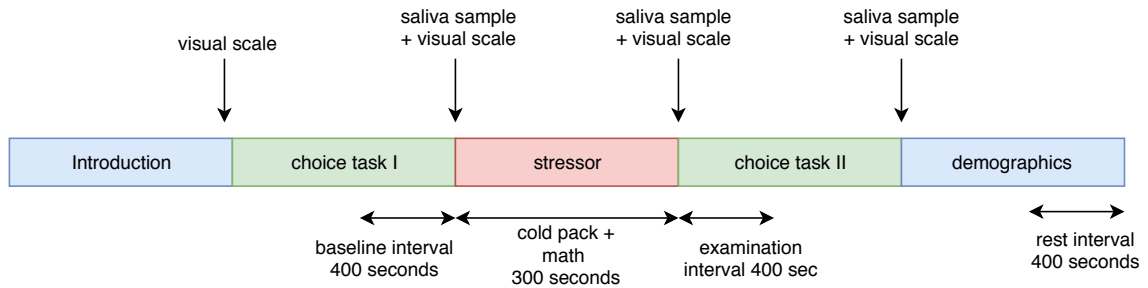


Figure 6.2: Time line of experiment

were recruited through email, online recruiting system and flyers. They were paid flat show-up fee of \$5 and up to more \$15 based on their performance of Montreal imaging stress task.

When scheduling, we asked participants not to eat or drink anything 10 minutes before the session. Upon arrival to the lab, participants provide informed consent and rinse their mouths out with water at a nearby water fountain. When they return to the testing room, we attached an Empatica E4 wristband to measure PPG and skin conductance. The participant asked to complete a questionnaire about issues related to the saliva collection and a series of visual analog scales rating their current mood, stress level and anxiety level from 0 to 100. Next, we have participants complete a decision-making task (described above) for 15 cases, followed by the visual analog scales. Then, we collected a saliva sample via passive drool. Next, participants will experience the cold pack stressor task for 2 minutes, followed by math task and the visual analog scales, and a saliva sample. Participants then performed the decision-making task again, followed by the visual analog scales, and a saliva sample. Finally, participants completed the perceived stress scale [59], perceived stress reactivity scale [60], and maximizing scale [61], along with demographic questions (gender, race/ethnicity, nationality, college major, etc.) The general time line of experiment is given in Fig. 6.2.

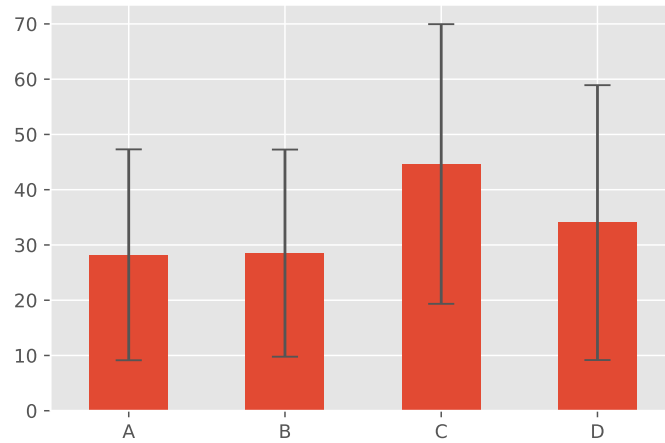


Figure 6.3: VAS results

## 6.3 Stressor task results

We are seeking to validate the hypothesis, claims that the stressor task was successful in increasing the level of stress in participants, processing the collected data. We analyzed VAS and biomarkers gathered in different instances indicated in experiment time line.

### 6.3.1 Visual analog scale (VAS)

Figure 6.3 shows the average levels of stress and their variances, indicated by participants at 4 different instances, namely at the start (A), before (B) and after (C) stressor task and at the end of choice task 2 (D). We select our null hypothesis as the scores at points B and C has no meaningful difference.

Since the number of participants are not large enough to draw significant conclusion about the effect of stress on the scores between points B and C, instead of regular t-test (gives p-value = 0.02), we used Bayesian estimation [62] to provide complete distributions of credible values for the effect size, group means and their difference,

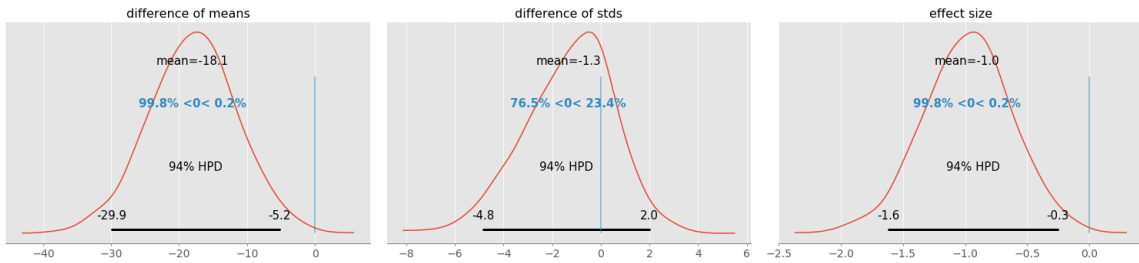


Figure 6.4: Estimated distribution of differences and effect size, Highest Posterior Density (HPD) Interval is selected to be 94%

standard deviations and their difference, and the normality of the data. To do so, we chose a Student-t distribution to describe the distributions of the scores in groups B and C with the degree of freedom  $\nu$  exponentially distributed with the mean value of 30. This allocates high prior probability over the regions of the parameter that describe the range from normal to heavy-tailed data under the Student-T distribution. For the sake of simplicity, we assumed the same degree of freedom for both groups. We choose each group mean to be normally distributed with mean value of empirical mean ( $\bar{X}$ ) and standard deviation of twice empirical standard deviation i.e.  $\mu_k \sim \mathcal{N}(\bar{x}, 2s)$  for  $k = 1, 2$ . It is also assumed the each group has a prior standard deviation distributed uniformly between  $[1, 10]$ . Having prior distribution with the above mentioned parameters in hand, now we can fit each group to the distribution and find some useful information such as the distribution of difference between means and standard deviation of two groups. As a joint measure of the groups, it is also common to estimate the effect size, which is the difference in means scaled by the pooled estimates of standard deviation.

As shown in Fig. 6.4 participant subjective impression of their stress level were moderately changed in average before and after stress task. The variances, although remained the same. Fig. 6.5 summarizes the VAS stress response before and after stressor task.

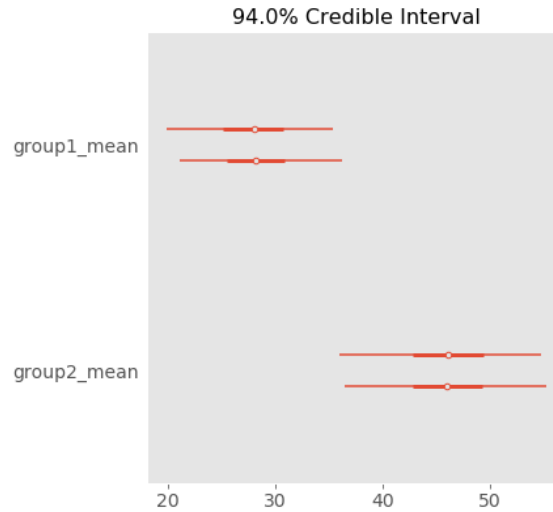


Figure 6.5: Change of the average value of stress level in VAS; group1: before stress, group2: after stress. Difference of mean =  $18.05 \pm 6.51$ , Difference of stds =  $1.34 \pm 1.84$

### 6.3.2 Inter-beat interval (IBI)

Inter-beat interval (IBI) data is collected with E4 wrist band which utilizes photoplethysmography to detect the length of time interval between two consecutive heart beats. The data is collected throughout the experiment and analyzed in three instances of 400 seconds before the stress task as baseline, 400 seconds after the stress task and the last 400 seconds of the experiment

Common measures that evaluate the effect of stress on IBI categorized in three major groups, i.e. time domain measures, frequency domain measures and non-linear measures. In [57] a complete survey of relevant studies and selected measures is given. There is strong evidence that suggests IBI is impacted by stress and can be used for the objective assessment of psychological stress, however reports on the effect of stress on different measures are not conclusive. Here, based on the similarity of our experiment to some other reports in terms of stressor tasks [63,64] and recording time interval, we selected three frequency measures, namely low frequency (LF) band [0.04, 0.15 Hz] and high frequency (HF) band [0.15, 0.4 Hz] power content and the ratio of LF/HF

to be analyzed. We used the normalized value for LF and HF band power in order to make the Bayesian estimation method converge. Note that, with small data sets, due to high fluctuation in absolute values, performing posterior probability estimation is not accurate. In time domain, we chose to analyze the standard deviation (SDNN) and root mean of squared of differences (RMSSD) of the IBI series.

For the baseline interval, 400 seconds before the start of stress task is selected in hope that all participant were experiencing the same cognitive condition after diminishing transients at the start of the experiment. The stress interval is selected to be the 400 seconds after the start of stressor task. Finally we analyzed the last 400 seconds of experiment when participants were asked to complete demographic and personality questions without any stress factor in effect.

### 6.3.2.1 Frequency domain analysis

Figure 6.6 depicts the frequency analysis of sample IBI performed by Python PyHRV library. As mentioned before, the absolute and normalized power of the sequence in each frequency band and the ratio of the power of low frequency and high frequency band are calculated in each time interval.

Figure 6.7 summarize the differences among frequency domain measures in three instances, i.e. baseline, stress and the end as defined above. We performed same Bayesian estimation techniques to investigate any significant change in these three measures. As indicated in Fig. 6.8 there is meaningful difference between the mean value of LF norm at baseline and stress periods. Our results show slight decrease in low frequency power content after imposing stress. The reverse effect is observed for the HF norm. Here, a slight decrease in power content is observable.

Since both normalized low and high frequency power content changed after impos-

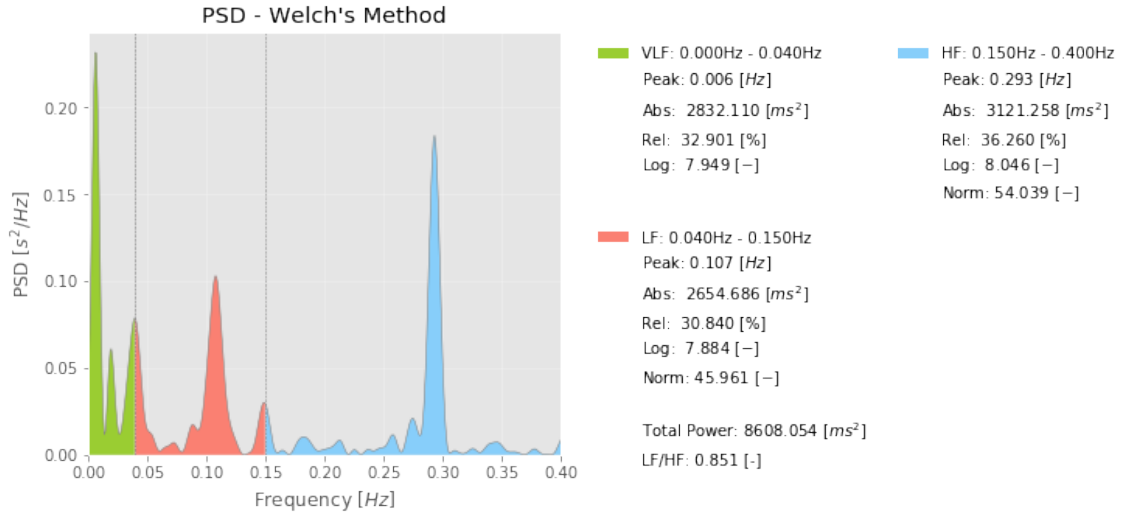


Figure 6.6: Sample frequency domain analysis of IBI in 400 seconds period

ing stress, we expect a meaningful change of LF/HF ratio, however the ratio measure is not significantly effected by stress as shown by the statistical model results. The difference of the mean of the ratios are  $0.06 \pm 0.39$ .

To get better perspective, we repeated the same statistical analysis to compare the difference estimated distributions at baseline and the end of the experiment. As presented in Fig. 6.9, we observed the same trend for LF and HF norms, even with more distinction in the difference of mean value. Regarding to LF/HF ratio, the amount of decrease is more than before. Fig. 6.10 summarizes the IBI frequency domain results in more clear setup.

### 6.3.2.2 Time domain analysis

We performed the same statistical analysis for SDNN and RMSSD measures at three instances; baseline, stress and end interval. The results are shown in Fig. 6.11. As expected, the estimated difference is more distinctive between the baseline and end of experiment. Both measures show slight decline.

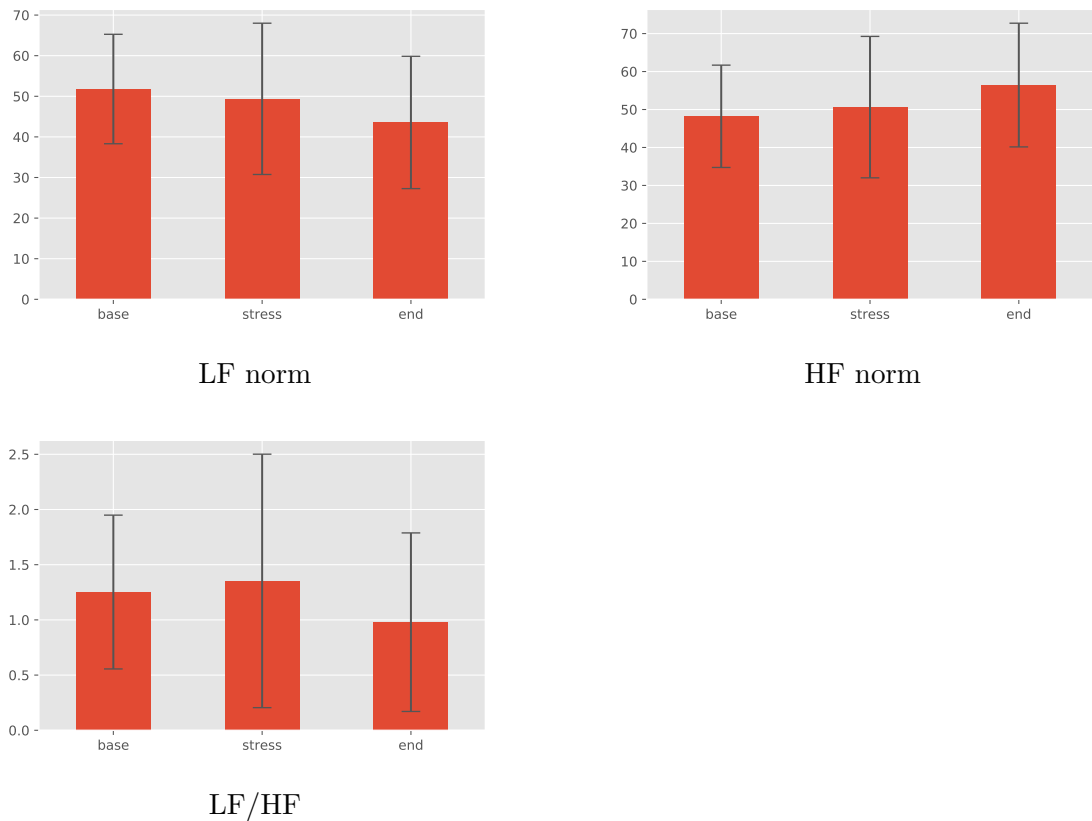


Figure 6.7: Change of frequency measures in three 400 sec. intervals; baseline, stress and end

### 6.3.3 Salivary Alpha-Amylase (sAA)

As mentioned in the experiment time line, saliva samples were collected in three instances. The first one was the end of first choice task which is considered as baseline. The second sample was collected after the stressor tasks and before the start of second choice task. The final sample is collected at the end of second choice task. Fig 6.12 shows the box plot of the salivary alpha-amylase (sAA) in (U/mL) in aforementioned three instances. While the median and average of sAA did not change significantly, the stress plot shows the larger number of samples reside in inter-quartile range. The statistical modeling of sAA did not show any significant change of average or stan-

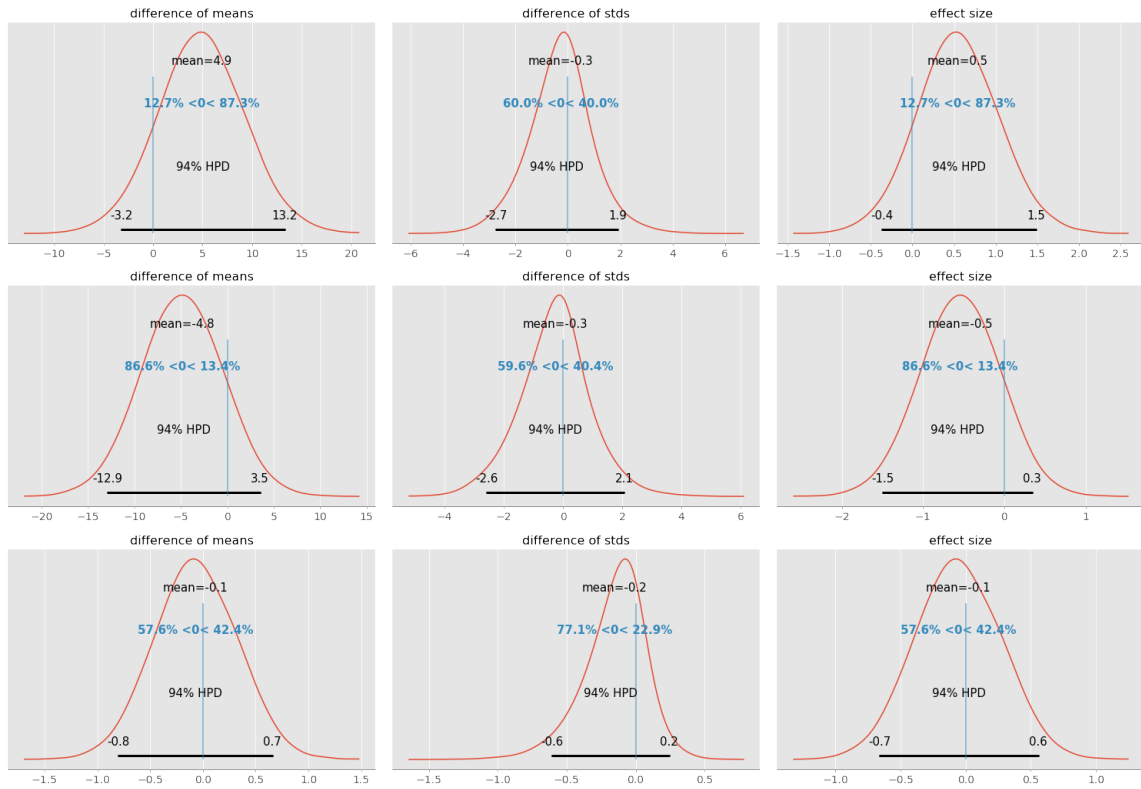


Figure 6.8: Estimated distribution of difference (group1-group2) average, standard deviation and effect size of LFnorm (top) and HFnorm (middle) and LF/HF ratio (bottom) in IBI trail; group1: baseline, group2: stress

standard deviations among three instances. For instance, the estimated mean difference between baseline and end group was  $1.31 \pm 5.70$  and between baseline and stress was  $1.82 \pm 6.91$ .

### 6.3.4 Skin conductance (EDA)

Sudden increase of skin conductance were recorded for 16 out of 20 participants that experienced stressor task. The conductance measure of one participants did not show any sudden change while two others show multiple surges. Fig 6.13 shows two sample graphs of normalized skin conductances.

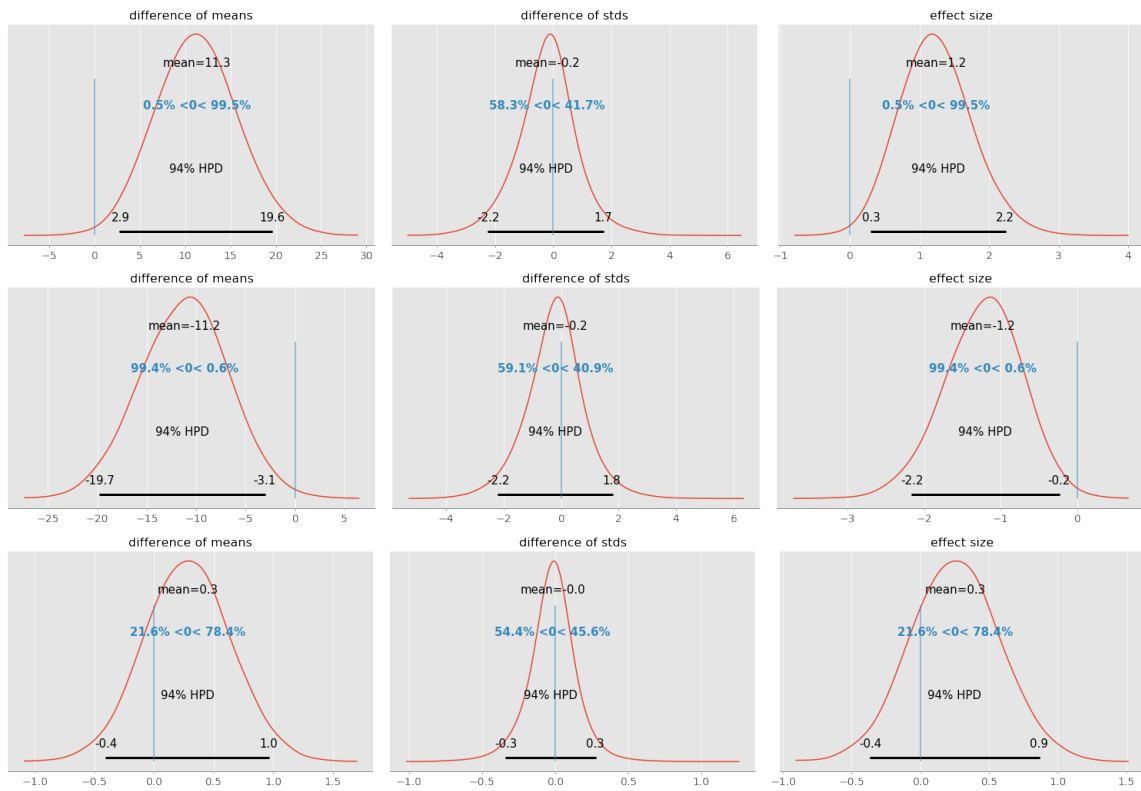


Figure 6.9: Estimated distribution of difference (group1-group2) average, standard deviation and effect size of LFnorm (top) and HFnorm (middle) and LF/HF ratio (bottom) in IBI trail; group1: baseline, group2: end

### 6.3.5 Effect of stressor; Discussion

The VAS, IBI and EDA results support our claim about the effectiveness of stressor task. However the following considerations should be taken into account. Based on the presented results, data gathered with E4 wrist band can be used to indicate the stressful condition of participants. More specifically, frequency response parameters of heart-beat variability in low and high frequency bands showed measurable changes after imposing physical and mental stressor. While the effect begins in a short period of time (400 seconds) after the start of stressor task, it gets more prominent when the participants continue to work (choice task 2). This steady increase of effects can be attributed to long time constant, with respect to selected time interval to assess the

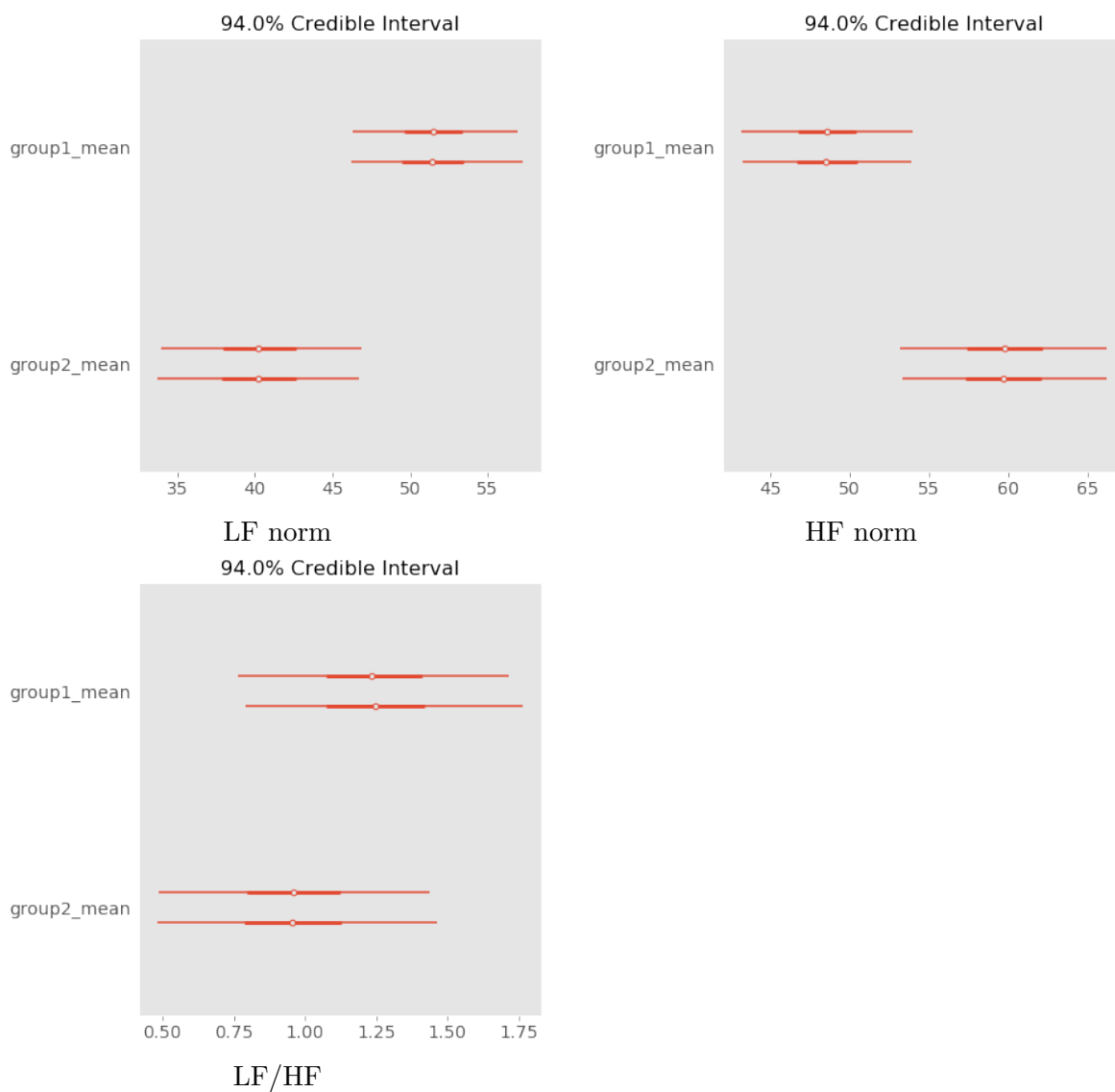


Figure 6.10: Estimated difference (group1-group2) of mean and its standard deviation for LFnorm, HFnorm and LF/HF ratio in IBI trail; group1: baseline, group2: end

data, or accumulating effect of stress and fatigue, performing cognitive demanding job.

In spite of several reports of sAA as a stress biomarker, our results of sAA analysis were not conclusive. Another important issue is analyzing sAA, which need lab works and can not be performed in near online fashion. Thus we would not advise using

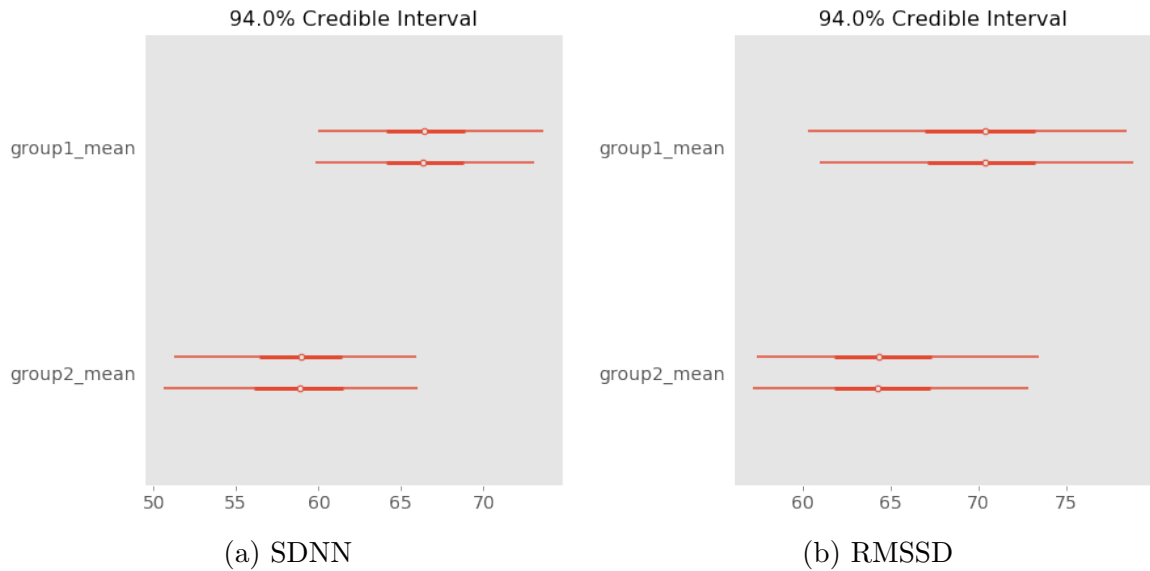


Figure 6.11: Estimated difference (group1-group2) of mean and its standard deviation for SDNN and RMSSD; group1: baseline, group2: end

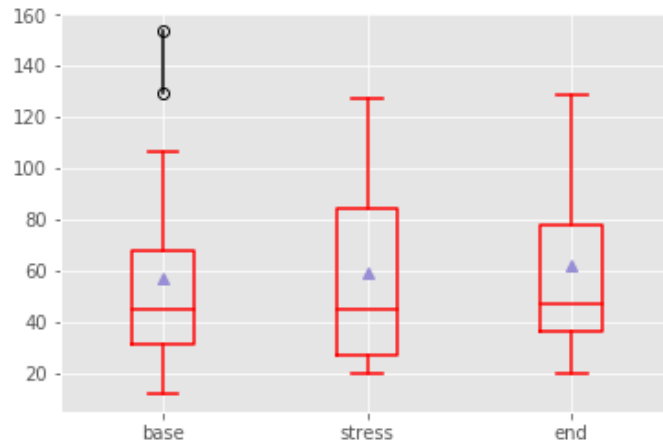


Figure 6.12: Box plot of sAA

sAA as stress indicator in our control framework. The reason that we include such analysis here was to confirm the effectiveness of stressor task via more sophisticated method, which somehow was not successful.

Sensitivity of skin conductance (EDA) to stress is less stable than IBI, since it relies on sudden change and the effect diminishes fast compare to more steady effect

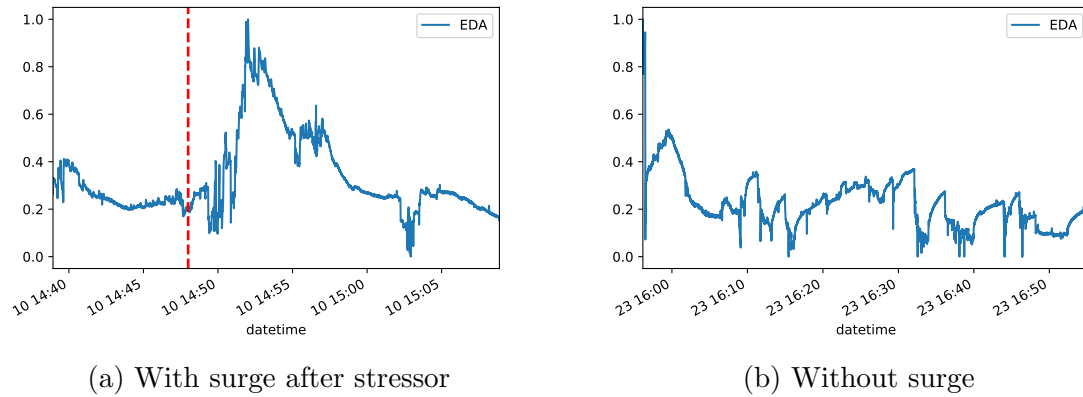


Figure 6.13: Sample EDA graphs for two participants; red line indicates the start of stressor task

of IBI. Although 85% of our small group showed transient surge in their EDA report right after stressor task, some smaller abrupt changes were detected in other non-relevant times for 3 participants. According to our results, we recommend using EDA as a complementary measure along with IBI to annotate the start of increasing stress level. It is worthy to note that almost all participants were aware of their level of stress according to VAS results.

### 6.3.6 Decision task results

To analyze the decision task data, we took three approaches. In the first one, the effect of stress on the length of time, spent on data acquisition and the frequency of reaching each data point, summed over all participants were investigated. Here, our hypothesis postulates that by imposing stress, the time of data acquisition and frequency of reaching data decreased, implying transition from WADD to heuristics.

In the second approach, we focused on each participant strategy in processing data and making decision in sessions one and two. Since the data were prioritize based on their values, reaching out to boxes with high-value data more frequently and

spending lengthier time investigating them, while ignoring boxes with less valuable data indicates heuristically leaning strategy. In contrast, looking for all cues and employing them in the decision process is a sign of WADD strategy.

The third approach is based on transition among boxes. Row transition is the sign of attribute based search, while column transition is about searching different attributes of a same candidate and more likely compromise low score in one cue with higher scores of other cues. In that sense, consecutive row transition implies leaning toward heuristics and vice-versa. To characterize this, we used search index [65] defined as:

$$\text{search index} = \frac{\text{alternative-based transitions} - \text{attribute-based transitions}}{\text{alternative-based transitions} + \text{attribute-based transitions}}$$

Higher index means using WADD strategy and lower one indicates heuristic strategy.

Figure. 6.14 shows the general trend of retrieving data in the process of making decision summed over all participants in tasks one and two. The graphs depict total time and frequency of visiting for each data point in the matrix. The results indicates decreased amount of time and frequency of reaching data in general. The same trend observed if data were grouped by each decision, in task one and two as depicted in Fig. 6.15. Here, the sum of time and frequency of visiting data points for 15 tasks in each session, for each participant is presented. To analyze the relationship between average value of measured parameters, an independent sample t-test was conducted. There was a significant difference in total time measured in session 1 (mean = 230616 msec , SD = 95035.667 ) and total time measured in session 2 (mean= 153171 msec , SD = 71706.386 ) ;  $t(12) = 3.903$ ,  $p = 0.0002$  with 99.8% confidence. The same trend observed in total frequency of reaching data points in session 1 (mean = 449.86, SD = 193.17) and session 2 (mean = 370 , SD = 173.81 );  $t(9) = 1.836$ ,  $p = 0.071$  with 95%

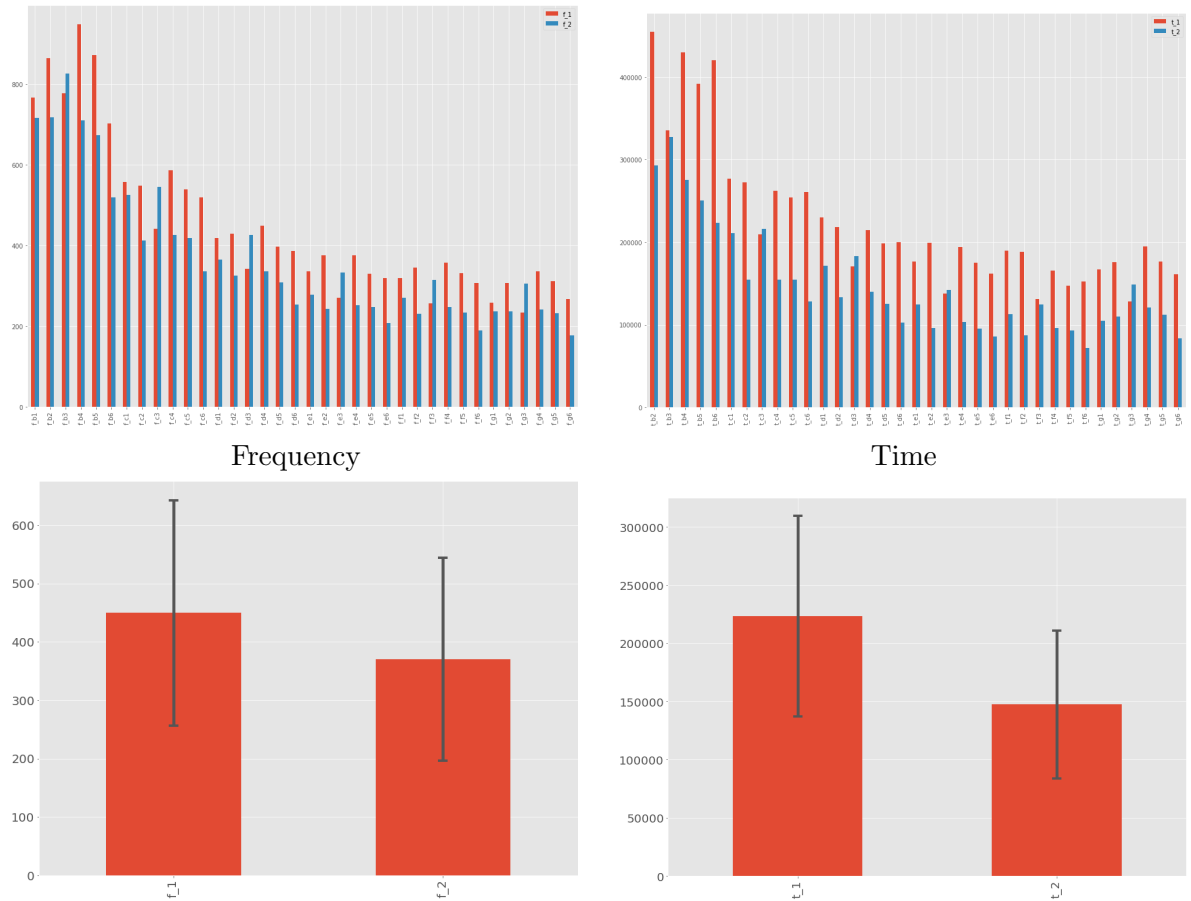


Figure 6.14: Time and frequency of retrieving data, summed over all participants, choice tasks 1 and 2

confidence. Based on the results, participants spend more time and more frequently accessed to the data in session 1 (on average) which support the hypothesis of WADD against heuristics.

As mentioned before, the time and frequency of accessing data of each row (attribute base search) can be interpreted as the tendency of using heuristics. We grouped the average time and frequency of data acquisition for 15 choices, based on each cue among all participants. The results are depicted in Fig. 6.16. As expected most valuable cue, indicated by letter ‘b’, were assessed more in both sessions. Time and frequency were decreased steadily based on the values of cues from cue ‘b’

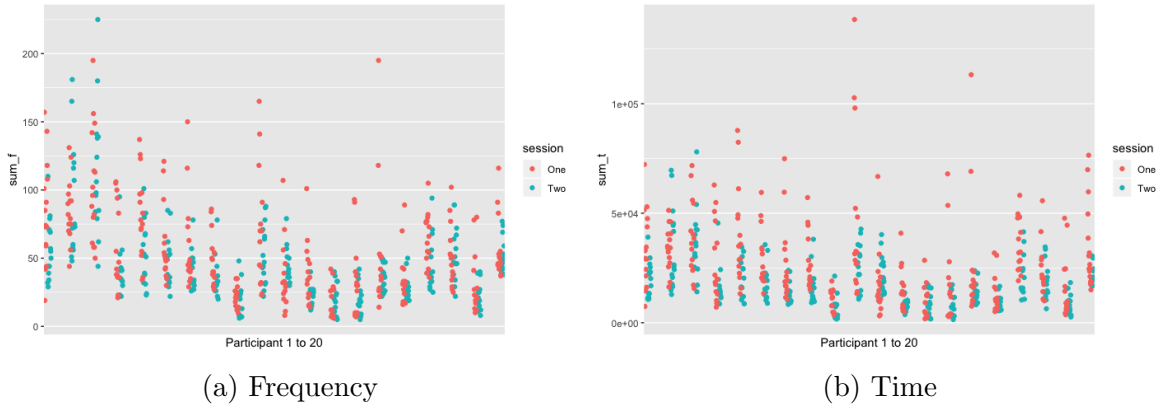


Figure 6.15: Time and frequency of retrieving data for each decision task, summed over all participants, choice tasks 1 and 2

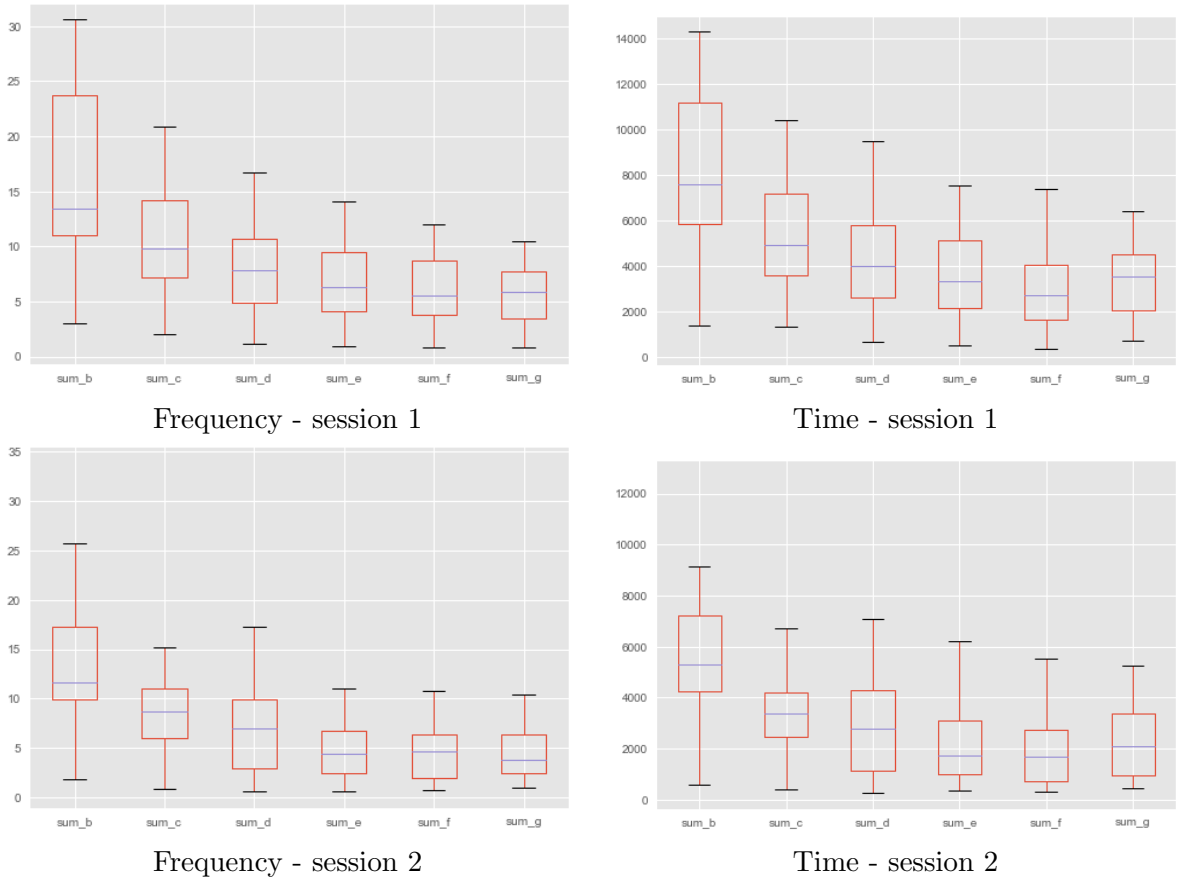


Figure 6.16: Sum of time and frequency of retrieving data, averaged for each participant, choice tasks 1 and 2. The value of cues decreases from left to right

to 'g' respectively.

Another interesting feature is the difference of total allocated time between most valuable cue and the least valuable one in each session, i.e.(  $\text{sum\_b} - \text{sum\_g}$ ). Since the total time and frequency of reaching data are different in sessions one and two, we normalized the calculated difference by dividing it to the total time and total frequency of each session. There is no significant difference in normalized total time difference measured in session 1 (mean = 0.2454 , SD = 0.2364 ) and total normalized time difference measured in session 2 (mean= 0.2623 , SD = 0.2541 ) ;  $t() = 0.8439$ ,  $p = 0.3990$ . In terms of frequency, the difference is even less stark compare to time;  $t() = 0.7584$ ,  $p = 0.4485$ . The average normalized frequency difference in session 1 was 0.2620 with SD = 0.2282 and for session 2 was 0.2767 with SD = 0.2490.

The results of analyzing search index are mixed as presented in Fig. 6.17. While some participants showed clear indication of changing strategy from higher index values in session 1 to lower ones in session 2, others showed the reverse trend. According to t-test results there is no significant difference between average search index in session 1 (mean = 0.144, SD = 0.407) and session 2 (mean = 0.1211, SD = 0.450) with  $p = 0.867$ .

The final piece of data that we analyzed is the accuracy of decisions made in sessions 1 and 2. Since the data were designed in way that there is a best choice in each task, based on WADD strategy, it was possible to calculate the percentage of correct answer of each participant in each session. According to the results there is a significant difference between the number of correct answers of each participants in 15 choice tasks in session 1 (mean = 0.16 , SD = 0.077) and same number of tasks in session 2 (mean = 0.13, SD = 0.057);  $t(4) = 1.506$ ,  $p = 0.141$  with 80% confidence.

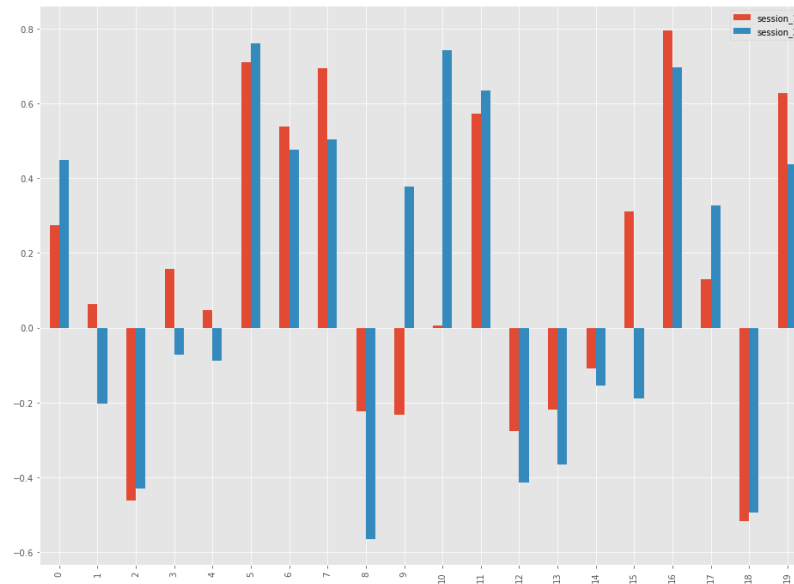


Figure 6.17: Search index of participants in session 1 and 2

### 6.3.6.1 Decision task results; Discussion

Based on our results, total time spend on making decision and frequency of visiting data points have strong correlation with the level of stress. Both measures showed significant decrease in session 2 on average. Since one of the main difference between WADD and heuristics is the amount of cognitive effort required in decision process, one can conclude that the strategy changed from WADD to heuristics, going from session 1 to 2. The decision accuracy results showed that the change of strategy worsen the level of accuracy, however not in a strong way, meaning the stress factor played a relatively destructive role. In other word the notion of good stress which lead to better concentration and more accurate decision is not the case here.

Another investigated parameter is the length of time difference spent on most and least valuable cues. In order to compare the level of difference, we normalized it by dividing to the average total time and frequency for task in each session. While in both session, most valuable cue is visited more, in session 2 the difference was more

Table 6.2: Summary of choice task results

measure	mean (session_1)	mean (session_2)	t	p-val
total time	230616 $\pm$ 95035	153171 $\pm$ 71706	3.903	$2 \times 10^{-4}$
total frequency	449.86 $\pm$ 193.17	370 $\pm$ 173.81	1.836	0.071
norm. diff. time	0.2454 $\pm$ 0.2364	0.2623 $\pm$ 0.2541	0.8439	0.3990
norm. diff. Freq.	0.2620 $\pm$ 0.2282	0.2767 $\pm$ 0.2490	0.7584	0.4485
search index	0.144 $\pm$ 0.407	0.121 $\pm$ 0.450	–	0.867
accuracy	0.16 $\pm$ 0.077	0.13 $\pm$ 0.057	1.506	0.141

observable on average, however we were not successful to capture a significant change as an indication of the change of strategy to heuristics, in which the less valuable cues are more probable to ignore. Another measure that not respond well to our change of strategy hypothesis was search index. We expected the large number of transitions based on alternatives (here candidate) as a sign of WADD while the large number of transitions based on cues indicates heuristic approach. However our results were not consistent with such explanation. Table 6.2 summarized the results.

## Chapter 7

### Conclusion

Human operator may influence the system in different levels as a function of indigenous system states or exogenous factors such as emergencies and stress. Traditionally, it is also assumed that in normal situation, automated system can complete the designated task automatically. However the trained human operator has the authority to differ from the automation and issue commands that change plant state trajectories. This scheme requires the operator be constantly aware of the states of system and notice any anomaly sufficiently soon, thus the issued corrections guarantee the safe operation, the condition that not always hold specially during emergencies, and the basic assumption that vindicates human operator full authority is jeopardized.

Our approach in solving this problem is to proposed a complementary control which adds a model of human decision to the controller, capable of predicting human command's accuracy in the near future. Using insights from mathematical and computational neuroscience as well as behavioral normative modeling approach, this work proposed a comprehensive model for general multi-cue multi-choice task to be utilized in the human in the loop control framework. This model also includes a layer of strategy selection to cover a range of strategies from weighted additive to heuristics in a continuous fashion. The LC-NE dynamics in adaptive gain theory

provided a platform to form a closed loop control system that collects bio-physically relevant data and use it to make prediction in terms of the strategy and accuracy. The outcome of decision unit can either be presented to the operator as a directive or may adjust the issued command toward better results. In this study, a controller was designed to dispatch the tasks between the system and the operator to keep the operator close to the best performance region. A case study for a simple one-attribute task was simulated showed the effectiveness of the proposed controller.

One major assumption in designing complementary control unit was that the feedback physiological signals can be mapped onto NE-LC gamma plane and hence the quality of decision at each time is known to controller. In the experiment section, we relaxed this assumption and showed that by using commercially available technologies, it is possible to infer the decision strategy and accuracy. To do so, we first proved that by means of physical and mental stressor task, it is possible to manipulate the level of stress in participants. By analyzing the heart beat variability data in frequency domain we were able to detect the stressful situation objectively. Second, we proved the change of strategy from more comprehensive WADD to simpler heuristics by processing the total time and frequency of assessing data points.

Transforming the way that people interact with complex engineered systems is the primary objective of developing focused research for cyber-physical systems or CPS. However, without touching human factors that might affect the whole system life process, this type of research merely results in a one-way, non-personalized solution. Due to significantly increasing presence of CPS in a human living environment to improve quality of life (e.g., smart buildings and communities), ignoring human factors in analysis and synthesis of sophisticated CPS becomes implausible. Alternatively, with the recent advances in cognitive computing (both algorithms and hardware) and hierarchical autonomous technology (condition monitoring and hybrid control), it becomes

possible to incorporate human factors into complex cyber-physical system-of-systems engineering. Inspired by this observation, new two-way human-system engineering in modeling, supervision, and synthesis for human-in-the-loop cyber-physical networks is required. This work deemed to fulfill this goal, by proposing a cognitive hierarchical synthesis framework that address human, cyber, and physical system interaction through behavioral dynamics, decision making, and hybrid control techniques. The proposed framework will provide a brand new vision on human roles in system engineering that may in turn benefit CPS for humanization of system operation, supervision, and control processes. Future research would include more diverse normative models for selecting strategies and more involved connectionist models that include a variety of biophysical factors. Also increasing the number of participants will add more confidence to the reported results.

## Appendix A

### Expectation and variance of multi-cue multi-choice model

We have proposed the following leaky integrator race model to describe the dynamics of multi-cue multi-choice tasks. This model combines the race model and time and order scheduling concept as follows:

$$\begin{aligned}
 dx_i(t) = & \left( -k_{i,m(t)}x_i(t) - \sum_{j \neq i} w_{i,j,m(t)}x_j(t) + S_{i,m(t)} \right) dt \\
 & + \sigma_i d\mathbf{W}_i(t), \quad m(t) \in \mathcal{M}, \quad t_{l-1} \leq t < t_l
 \end{aligned} \tag{A.1}$$

where  $k_{i,m}$  depends on both choice  $i$  and cue  $m$ ,  $w_{i,j,m}$  depends on choice  $i$ , choice  $j$ , and cue  $m$ , and  $w_{i,j,m} = w_{j,i,m}$ .

The model can be slightly simplified by ignoring the non uniform impact of tasks on different integrators as follows:

$$\begin{aligned}
 dx_i(t) = & \left( -k_{m(t)}x_i(t) - \sum_{j \neq i} w_{m(t)}x_j(t) + S_{i,m(t)} \right) dt \\
 & + \sigma_i d\mathbf{W}_i(t), \quad m(t) \in \mathcal{M}, \quad t_{l-1} \leq t < t_l
 \end{aligned} \tag{A.2}$$

Note that task with index  $m$  is selected according to cue ordering schedule and

processed during the assigned time interval. The criteria of absolute threshold or max-versus-next or max-versus-average are considered to select the choice among the members of a decision vector stacked by  $x_i$ .

In this section, we develop some mathematical preliminaries used for asymptotic analysis of mean-value and variance of the multi-cue multi-choice model A.1 using the paracontraction-based semiconvergence theory developed in [66, 67]. Throughout the paper, let  $\mathbb{R}^{n \times m}$  denote the set of all  $n$ -by- $m$  real matrices,  $\mathbb{R}^n$  the set of all  $n$ -dimensional real column vectors, and  $\|\cdot\|$  the vector/matrix 2-norm.

## A.1 Paracontraction

**Definition 1** *Let  $W : \mathcal{D} \rightarrow \mathbb{R}^{n \times n}$  and  $\mathcal{D} \subseteq \mathbb{R}^m$ .  $W$  is called parameter-dependent paracontracting (PDPC) at  $z \in \mathcal{D}$  if for any  $x \in \mathbb{R}^n$ ,  $\|W(z)x\| \leq \|x\|$  and the equality holds if and only if  $W(z)x = x$  at  $z \in \mathcal{D}$ .  $W$  is called PDPC if it is PDPC at every point in  $\mathcal{D}$ .*

Definition 1 is an extension of matrix paracontraction to parameter-dependent matrix functions. It is clear that if  $W$  is a constant matrix, then PDPC becomes the definition of paracontraction in [68, 69]. References [66, 67] discuss the relationship between paracontraction and discrete-time semistability, and give some necessary and sufficient conditions to connect both, which will be summarized as follows. Reference [66] further uses this condition to design optimal semistable controllers for network systems. Note that our condition of PDPC is slightly different from pseudo-contraction in [70] or set-contraction in [71] or uniform paracontraction in [72] since A.1 is a parameter-dependent system across  $L$  time spans with possibly time-varying

parameters, given the fact that A.1 consists of  $L$  piecewise stochastic differential equations with each one having a possibly different expectation, variance, and threshold.

The next result gives the necessary and sufficient conditions to check paracontraction practically. To state it, let  $\text{rank}(A)$  denote the rank of matrix  $A$ ,  $A^T$  denote the transpose of  $A$ , and  $\ker(A)$  denote the null space of  $A$ .

**Lemma 1** *Let  $W : \mathcal{D} \rightarrow \mathbb{R}^{n \times n}$  and  $\mathcal{D} \subseteq \mathbb{R}^m$ . Then the following statements are equivalent:*

*i)  $W$  is PDPC.*

*ii)  $\|W(z)\| \leq 1$  and  $\text{rank}(W^T(z)W(z) - I_n) = \text{rank}(W(z) - I_n + W^T(z) - I_n) =$*   
 $\text{rank} \begin{bmatrix} W^T(z)W(z) - I_n \\ W(z) - I_n + W^T(z) - I_n \end{bmatrix}$  *for every  $z \in \mathcal{D}$ .*

*iii)  $\|W(z)\| \leq 1$  and  $\text{rank}(W^T(z)W(z) - I_n) = \text{rank}(W(z) - I_n) = \text{rank} \begin{bmatrix} W^T(z)W(z) - I_n \\ W(z) - I_n \end{bmatrix}$*   
*for every  $z \in \mathcal{D}$ .*

*Proof.* The equivalence between *i)* and *ii)* follows from Remark 3.2 of [67] and the fact that  $\ker(A) = \ker(B)$  if and only if  $\text{rank}(A) = \text{rank}(B) = \text{rank} \begin{bmatrix} A \\ B \end{bmatrix}$  for  $A \in \mathbb{R}^{n \times m}$  and  $B \in \mathbb{R}^{n \times l}$ . The equivalence between *i)* and *iii)* follows from Lemma 3.2 of [67] and the fact that  $\ker(A) = \ker(B)$  if and only if  $\text{rank}(A) = \text{rank}(B) = \text{rank} \begin{bmatrix} A \\ B \end{bmatrix}$ .  $\square$

## A.2 Asymptotic Analysis of Discrete-Time Systems

### A.2.1 Discrete-time switched linear systems

In this section, we will discuss some asymptotic properties of discrete-time switched linear systems with time-varying parameters and external inputs given by the sequential form

$$X_{k+1} = W_{p_k}(z_k)X_k + b_{p_k}(z_k), \quad k = 0, 1, 2, \dots \quad (\text{A.3})$$

where  $X_k \in \mathbb{R}^q$  is the state,  $W_{p_k}(\cdot) \in \mathbb{R}^{q \times q}$ ,  $\{p_k\}_{k=0}^\infty \subseteq \Sigma$ ,  $\Sigma$  is an index set,  $\{z_k\}_{k=0}^\infty \subseteq \mathcal{D} \subseteq \mathbb{R}^m$  is the parameter set, and  $b_{p_k}(\cdot) \in \mathbb{R}^q$  is the external input.

Note that  $\ker(W_{p_k}(z_k) - I_q)$  is a subspace for every  $k \geq 0$  and every  $z_k \in \mathcal{D}$ . Since a subspace cannot lie in any subspace of lesser dimension, it follows that there exists a positive integer  $N = N_{z_k}$  such that  $\bigcap_{k=N}^\infty \ker(W_{p_k}(z_k) - I_q) = \bigcap_{k=l}^\infty \ker(W_{p_k}(z_k) - I_q)$  for all  $l \geq N$ . Similarly, it follows that there exists a positive integer  $N = N_z$  such that  $\bigcap_{k=N}^\infty \ker(W_{p_k}(z) - I_q) = \bigcap_{k=l}^\infty \ker(W_{p_k}(z) - I_q)$  for all  $l \geq N$ . In general,  $N_{z_k}$  and  $N_z$  may not be equal. Nevertheless, we found out that both are equal for the discrete-time system that we will construct for asymptotic approximation of A.1 later (see the proof of Theorem 1). Hence, in this work we make the following standing assumption:

**Assumption 1** *For (A.3), there exists a positive integer  $N$  such that  $\bigcap_{k=N}^\infty \ker(W_{p_k}(z_k) - I_q) = \bigcap_{k=l}^\infty \ker(W_{p_l}(z_k) - I_q) = \bigcap_{k=N}^\infty \ker(W_{p_k}(z) - I_q) = \bigcap_{k=l}^\infty \ker(W_{p_l}(z) - I_q)$  for all  $l \geq N$ , any  $z_k \in \mathcal{D}$ , and any  $z \in \mathcal{D}$ .*

Assumption 1 implies that the fixed-point subspace of the parameter-dependent ma-

trix sequence  $\{W_{p_k}(z_k)\}_{k=0}^{\infty}$  will be similar to that of a parameter-independent matrix sequence after certain time period. A sufficient condition to guarantee Assumption 1 is that there exists a positive integer  $N$ , independent of  $z_k \in \mathcal{D}$  and  $z \in \mathcal{D}$ , such that  $\ker(W_{p_k}(z_k) - I_q) = \ker(W_{p_k}(z) - I_q)$  for all  $k \geq N$ , any  $z_k \in \mathcal{D}$ , and any  $z \in \mathcal{D}$ . The following result gives an alternative, more general condition to guarantee Assumption 1.

**Lemma 2** Consider (A.3), where  $W_{p_k}(\cdot) \in \mathbb{R}^{q \times q}$ ,  $p_k \in \Sigma$ , and  $z_k \in \mathcal{D}$ . Let  $J_{p_k} \subseteq \Sigma$  be an admissible set such that every element in  $J_{p_k}$  appears infinitely often in the sequence  $\{p_k\}_{k=0}^{\infty}$  for (A.4). If  $J_{p_k} = \{1, 2, \dots, j\}$  and  $\text{rank}(A) = \text{rank}(B) = \text{rank} \begin{bmatrix} A \\ B \end{bmatrix}$ , where

$$A = \begin{bmatrix} W_1(w_1) - I_q \\ W_2(w_2) - I_q \\ \vdots \\ W_j(w_j) - I_q \end{bmatrix}, \quad B = \begin{bmatrix} W_1(w_{j+1}) - I_q \\ W_2(w_{j+1}) - I_q \\ \vdots \\ W_j(w_{j+1}) - I_q \end{bmatrix}$$

for every  $w_i \in \mathcal{D}$ ,  $i = 1, 2, \dots, j + 1$ , then Assumption 1 holds.

*Proof.* Since  $J_{p_k} = J = \{1, 2, \dots, j\}$  is independent of  $z_k$ , it follows from the definition of  $J_{p_k}$  that there exists a positive integer  $N_{z_k}$  such that  $\bigcap_{k=N_{z_k}}^{\infty} \ker(W_{p_k}(z_k) - I_q) = \bigcap_{k=l}^{\infty} \ker(W_{p_k}(z_k) - I_q) = \bigcap_{p \in J} \ker(W_p(z_{n_p}) - I_q)$  for every  $z_k \in \mathcal{D}$  and every  $l \geq N_{z_k}$ . Let  $N = \min\{N_{z_k} : \bigcap_{k=N_{z_k}}^{\infty} \ker(W_{p_k}(z_k) - I_q) = \bigcap_{p \in J} \ker(W_p(z_{n_p}) - I_q), \forall z_k \in \mathcal{D}\}$ . Such an  $N$  is well defined due to the facts that  $J_{p_k}$  is independent of  $z_k$  and  $J_{p_k} = J$ . Then  $\bigcap_{k=N}^{\infty} \ker(W_{p_k}(z_k) - I_q) = \bigcap_{k=l}^{\infty} \ker(W_{p_l}(z_k) - I_q) = \bigcap_{p \in J} \ker(W_p(z_{n_p}) - I_q)$  for all  $l \geq N$  and any  $z_k \in \mathcal{D}$ .

Note that the rank condition holds if and only if  $\bigcap_{p \in J} \ker(W_p(w_p) - I_q) = \bigcap_{p \in J} \ker(W_p(w_{j+1}) - I_q)$  for every  $w_i \in \mathcal{D}$ ,  $i = 1, 2, \dots, j+1$  (recall that  $\ker(A) = \ker(B)$  if and only if  $\text{rank}(A) = \text{rank}(B) = \text{rank} \begin{bmatrix} A \\ B \end{bmatrix}$ ). Note that by taking  $z_k = w_{j+1}$  for all  $k = 0, 1, 2, \dots$ , we have  $\bigcap_{k=N}^{\infty} \ker(W_{p_k}(w_{j+1}) - I_q) = \bigcap_{k=l}^{\infty} \ker(W_{p_l}(w_{j+1}) - I_q) = \bigcap_{p \in J} \ker(W_p(w_{j+1}) - I_q)$  for every  $w_{j+1} \in \mathcal{D}$  and every  $l \geq N$ . Finally, since  $z_k \in \mathcal{D}$  is arbitrary, taking  $z_{n_p} = w_p$ ,  $p \in J$ , yields the conclusion.  $\square$

Under Lemma 2, let  $N$  be the minimum one such that  $\bigcap_{k=N}^{\infty} \ker(W_{p_k}(z_k) - I_q) = \bigcap_{k=l}^{\infty} \ker(W_{p_l}(z_k) - I_q)$  for all  $l \geq N$  and all  $z_k \in \mathcal{D}$ . Now, using superposition for linear systems and Assumption 1, we can decompose (A.3) into two subsystems

$$x_{k+1} = W_{p_k}(z_k)x_k, \quad x_0 = X_0, \quad k = 0, 1, 2, \dots \quad (\text{A.4})$$

$$y_{k+1} = y_k + \prod_{i=0}^k W_{p_{k-i}}(z_{k-i})b_{p_k}(z_k), \quad y_0 = 0, \quad (\text{A.5})$$

where  $X_k = x_k + y_k$ ,  $K = RR^T \prod_{i=0}^{N-1} W_{p_{N-1-i}}(z_{N-1-i})$ ,  $R = [\mathbf{s}_1, \mathbf{s}_2, \dots, \mathbf{s}_r] \in \mathbb{R}^{q \times r}$ ,  $\{\mathbf{s}_1, \mathbf{s}_2, \dots, \mathbf{s}_r\}$  be an orthonormal basis for  $\bigcap_{k=N}^{\infty} \ker(W_{p_k}(z_k) - I_q)$ ,  $r = \dim(\bigcap_{k=N}^{\infty} \ker(W_{p_k}(z_k) - I_q))$ , and  $\dim S$  denotes the dimension of subsapce  $S$ . We call (A.4) the *homogeneous subsystem* of (A.3) and (A.5) the *non-homogeneous subsystem* of (A.3).

## A.2.2 Homogeneous subsystem

In this subsection, we consider the convergence behavior of the homogeneous subsystem (A.4), i.e., under what conditions does (A.4) converge asymptotically? To this end, define the *positive limit set* of (A.4) with respect to  $\{z_k\}_{k=0}^{\infty}$  as  $\omega_p(x_0, \{z_k\}) = \{x^* \in \mathbb{R}^q : \exists \{x_{q_k}\}_{k=0}^{\infty} \subseteq \{x_k\}_{k=0}^{\infty}, \lim_{k \rightarrow \infty} x_{q_k} = x^*\}$  for every  $x_0 \in \mathbb{R}^q$  and every

$\{z_k\}_{k=0}^\infty \subseteq \mathcal{D}$ , where  $x^*$  is called an *accumulation point* of (A.4). Finally, the *omega limit set*  $\Omega_p(x_0)$  of (A.4) is defined as  $\Omega_p(x_0) = \bigcup_{z_k \in \mathcal{D}} \omega_p(x_0, \{z_k\})$ .

The next result shows that the positive limit set  $\omega_p(x_0, \{z_k\})$  of (A.4) is embedded in this subspace when the matrices in (A.4) are PDPC.

**Lemma 3** Consider (A.4), where  $W_{p_k}(\cdot) \in \mathbb{R}^{q \times q}$  is PDPC,  $p_k \in \Sigma$ , and  $z_k \in \mathcal{D}$ .

Assume that Assumption 1 holds,  $W_{p_k}(\cdot)$  is continuous,  $\Sigma$  is finite, and  $\mathcal{D}$  is compact.

Then for every  $x_0 \in \mathbb{R}^q$  and every  $z_k \in \mathcal{D}$ ,  $\omega_p(x_0, \{z_k\})$  is nonempty and  $\Omega_p(x_0) \subseteq \bigcup_{z \in \mathcal{D}} \bigcap_{k=N}^\infty \ker(W_{p_k}(z) - I_q)$ .

*Proof.* Consider (A.4) and let  $x_0 \in \mathbb{R}^q$  and  $z_k \in \mathcal{D}$ . Since  $W_{p_k}(\cdot)$  is PDPC, it follows from Lemma 1 and (A.4) that  $\|x_{k+1}\| \leq \|x_k\|$  for every  $k = 0, 1, 2, \dots$ , which implies that  $\{x_k\}_{k=0}^\infty$  is bounded and, hence, has an accumulation point  $x^* \in \omega_p(x_0, \{z_k\})$ . Thus,  $\omega_p(x_0, \{z_k\})$  is nonempty. Let  $\{x_{q_k}\}_{k=0}^\infty$  be a subsequence of  $\{x_k\}_{k=0}^\infty$  such that  $\lim_{k \rightarrow \infty} x_{q_k} = x^*$ .

We claim that  $x^* \in \bigcup_{z \in \mathcal{D}} \bigcap_{k=N}^\infty \ker(W_{p_k}(z) - I_q)$ . Suppose that  $x^* \notin \bigcup_{z \in \mathcal{D}} \bigcap_{k=N}^\infty \ker(W_{p_k}(z) - I_q)$ . Note that  $p_k \in \Sigma$  and by assumption,  $\Sigma$  is finite. Let  $J \subseteq \Sigma$  be the set of all positive integers that appear infinitely often in  $\{p_k\}_{k=N}^\infty$ . Without loss of generality, assume that  $J = \{1, \dots, n\}$ . Then for every  $k \geq N$ , there exists  $\sigma \in J$  such that  $x^* \in \ker(W_{p_k}(z) - I_q)$  for  $p_k < \sigma$  and  $x^* \notin \ker(W_{p_k}(z) - I_q)$  for  $p_k \geq \sigma$ . Since every element in  $J$  appears infinitely often in  $\{p_k\}_{k=N}^\infty$ , for each  $k \geq N$  there exists a smallest integer  $r_k \geq q_k \geq N$  such that  $p_{r_{k+1}} \geq \sigma$  and  $\lim_{k \rightarrow \infty} x_{r_k}$  exists. Note that  $x_{r_k} - x^* = W_{\alpha_1}(z_{\alpha_1})W_{\alpha_2}(z_{\alpha_2}) \cdots W_{\alpha_p}(z_{\alpha_p})(x_{q_k} - x^*)$  for some  $1 \leq \alpha_i < \sigma$ ,  $1 \leq i \leq p$ , we have  $\|x_{r_k} - x^*\| \leq \|x_{q_k} - x^*\|$  for all  $k \geq N$ , which shows that  $\lim_{k \rightarrow \infty} x_{r_k} = x^*$ . Now there is at least one number in  $\{\sigma, \sigma + 1, \dots, n\}$  that occurs

infinitely often among the numbers  $p_{r_{k+1}}$ ,  $k \geq N$ . Without loss of generality, assume that this number is  $\sigma$ .

Consider a new sequence  $\{y_k\}_{k=N}^\infty$  of  $\{x_{r_k}\}_{k=N}^\infty$  for which  $p_{r_{k+1}} = \sigma$ . Then both  $\{y_k\}_{k=N}^\infty$  and  $\{W_\sigma(z_k)y_k\}_{k=N}^\infty$  are subsequences of  $\{x_k\}_{k=N}^\infty$ . Since  $z_k \in \mathcal{D}$  and  $\mathcal{D}$  is compact, it follows that there exists a subsequence  $\{z_{n_k}\}_{k=N}^\infty$  of  $\{z_k\}_{k=N}^\infty$  such that  $\lim_{k \rightarrow \infty} z_{n_k} = z^* \in \mathcal{D}$ . Hence,  $\|x^*\| = \lim_{k \rightarrow \infty} \|y_{n_k}\| = \lim_{k \rightarrow \infty} \|W_\sigma(z_{n_k})y_{n_k}\| = \|W_\sigma(z^*)x^*\|$ . Now it follows from the PDPC of  $W_\sigma(\cdot)$  that  $x^* = W_\sigma(z^*)x^*$ , which contradicts the fact that  $x^* \notin \ker(W_{p_k}(z^*) - I_q)$  for all  $p_k \geq \sigma$  and  $z^* \in \mathcal{D}$ . Thus,  $x^* \in \bigcup_{z \in \mathcal{D}} \bigcap_{k=N}^\infty \ker(W_{p_k}(z) - I_q)$ .  $\square$

Hence, Lemma 3 indicates the possible structures for all the limit points of (A.4). If  $\bigcap_{k=N}^\infty \ker(W_{p_k}(z) - I_q) = \{\mathbf{0}\}$  and  $\Sigma$  is finite, then by Lemma 3,  $\lim_{k \rightarrow \infty} x_k = \mathbf{0}$ . Otherwise, if  $\bigcap_{k=N}^\infty \ker(W_{p_k}(z) - I_q) \neq \{\mathbf{0}\}$ , then we have the following decomposition result for  $x_m$  when  $m$  is sufficiently large.

**Lemma 4** Consider (A.4), where  $W_{p_k}(\cdot) \in \mathbb{R}^{q \times q}$  is PDPC,  $p_k \in \Sigma$ , and  $z_k \in \mathcal{D}$ . Assume that Assumption 1 holds and  $\bigcap_{k=N}^\infty \ker(W_{p_k}(z) - I_q) \neq \{\mathbf{0}\}$  for  $z \in \mathcal{D}$ . Then for every  $m \geq N$  and every  $z_k \in \mathcal{D}$ ,  $x_m$  of (A.4) can be decomposed as

$$\begin{aligned} x_m &= RR^T x_{N-1} + (W_{p_m}(z_m) - RR^T) \\ &\quad (W_{p_{m-1}}(z_{m-1}) - RR^T) \cdots (W_{p_N}(z_N) - RR^T) x_{N-1}. \end{aligned} \quad (\text{A.6})$$

*Proof.* By the definition of  $R$  and Assumption 1, we have  $(W_{p_m}(z) - I_q)R = \mathbf{0}_{q \times r}$  and hence,  $(W_{p_m}(z_m) - I_q)R = \mathbf{0}_{q \times r}$  for every  $m \geq N$ , where  $\mathbf{0}_{q \times r}$  denotes the  $q \times r$  matrix whose entries are all zeros. Next, it follows from Corollary 3.2 of [67] that  $\ker(W_{p_m}^T(z_m) - I_q) = \ker(W_{p_m}(z_m) - I_q)$  for every  $m \geq N$ . Now  $(W_{p_m}^T(z_m) - I_q)R =$

$\mathbf{0}_{q \times r}$  for every  $m \geq N$ . Hence,  $R^T W_{p_m}(z_m) = (W_{p_m}^T(z_m)R)^T = R^T$ . Therefore, for every  $i \geq N$ , we have  $(W_{p_{i+1}}(z_{i+1}) - RR^T)(W_{p_i}(z_i) - RR^T) = W_{p_{i+1}}(z_{i+1})W_{p_i}(z_i) - RR^T$ . By induction,

$$\begin{aligned} & \prod_{i=0}^m W_{p_{m-i}}(z_{m-i}) - RR^T \prod_{i=0}^{N-1} W_{p_{N-1-i}}(z_{N-1-i}) \\ &= \left( \prod_{i=0}^{m-N} W_{p_{m-i}}(z_{m-i}) - RR^T \right) \left( \prod_{i=0}^{N-1} W_{p_{N-1-i}}(z_{N-1-i}) \right) \\ &= \left( \prod_{i=0}^{m-N} (W_{p_{m-i}}(z_{m-i}) - RR^T) \right) \left( \prod_{i=0}^{N-1} W_{p_{N-1-i}}(z_{N-1-i}) \right). \end{aligned} \quad (\text{A.7})$$

Right-multiplying  $x_0$  on both sides of (A.7) yields (A.6).  $\square$

Note that the decomposition (A.6) has multiple structures  $W_{p_m}(z_m) - RR^T$  for every  $m \geq N$ . The following result gives a PDPC property for them.

**Lemma 5** Consider (A.4), where  $W_{p_k}(\cdot) \in \mathbb{R}^{q \times q}$  is PDPC,  $p_k \in \Sigma$ , and  $z_k \in \mathcal{D}$ .

Assume that Assumption 1 holds and  $\bigcap_{k=N}^{\infty} \ker(W_{p_k}(z) - I_q) \neq \{\mathbf{0}\}$  for  $z \in \mathcal{D}$ . Then for every  $i \geq N$ ,  $W_{p_i}(z_i) - RR^T$  is PDPC for any  $z_i \in \mathcal{D}$ .

*Proof.* Let  $R = [\mathbf{s}_1, \mathbf{s}_2, \dots, \mathbf{s}_r] \in \mathbb{R}^{q \times r}$ ,  $\text{span}\{\mathbf{s}_{r+1}, \mathbf{s}_{r+2}, \dots, \mathbf{s}_q\} = \text{span}\{\mathbf{s}_1, \mathbf{s}_2, \dots, \mathbf{s}_r\}^\perp$ , and  $Q = [\mathbf{s}_{r+1}, \mathbf{s}_{r+2}, \dots, \mathbf{s}_q] \in \mathbb{R}^{q \times (q-r)}$ , where  $q - r = \dim(\text{span}\{\mathbf{s}_1, \mathbf{s}_2, \dots, \mathbf{s}_r\}^\perp)$  and  $\text{span}S$  denotes the span of set  $S$ . Next, let  $x \notin \ker(W_{p_k}(z_k) - RR^T - I_q)$ ,  $k \geq N$ . Then  $x = Ry_1 + Qy_2$  for some  $y_1 \in \mathbb{R}^{r \times 1}$  and some  $y_2 \in \mathbb{R}^{(q-r) \times 1}$ . Note that  $W_{p_k}(z_k)R = R$  for all  $k \geq N$ . Then it follows that  $(W_{p_k}(z_k) - RR^T)x = W_{p_k}(z_k)Qy_2$ . Hence,  $x \notin \ker(W_{p_k}(z_k) - RR^T - I_q)$  if and only if  $W_{p_k}(z_k)Qy_2 \neq Ry_1 + Qy_2$ , or, equivalently,  $(W_{p_k}(z_k) - I_q)Qy_2 \neq Ry_1$ . Note that it follows from Corollary 3.2 of [67] that  $\text{ran}(W_{p_k}(z_k) - I_q) \cap \ker(W_{p_k}(z_k) - I_q) = \{\mathbf{0}_{q \times 1}\}$ . Since  $(W_{p_k}(z_k) - I_q)Qy_2 \in$

$\text{ran}(W_{p_k}(z_k) - I_q)$  and  $Ry_1 \in \ker(W_{p_k}(z_k) - I_q)$ , it follows that  $(W_{p_k}(z_k) - I_q)Qy_2 \neq Ry_1$  if and only if either  $(W_{p_k}(z_k) - I_q)Qy_2 \neq \mathbf{0}_{q \times 1}$  or  $Ry_1 \neq \mathbf{0}_{q \times 1}$ .

If  $(W_{p_k}(z_k) - I_q)Qy_2 \neq \mathbf{0}_{q \times 1}$ , then it follows from the PDPC of  $W_{p_k}(z_k)$  that  $\|W_{p_k}(z_k)Qy_2\|^2 < \|Qy_2\|^2 \leq \|Ry_1\|^2 + \|Qy_2\|^2 = \|Ry_1 + Qy_2\|^2$ , i.e.,  $\|(W_{p_k}(z_k) - RR^T)x\| < \|x\|$ . Therefore, by definition,  $W_{p_k}(z_k) - RR^T$  is PDPC for every  $k \geq N$ .

Alternatively, if  $Ry_1 \neq \mathbf{0}_{q \times 1}$ , then  $\|Ry_1\| > 0$ . Since  $W_{p_k}(z_k)$  is PDPC, it follows that  $\|W_{p_k}(z_k)Qy_2\|^2 \leq \|Qy_2\|^2 < \|Ry_1\|^2 + \|Qy_2\|^2 = \|Ry_1 + Qy_2\|^2$ , i.e.,  $\|(W_{p_k}(z_k) - RR^T)x\| < \|x\|$ . Hence, using the similar arguments as above, one can show that  $W_{p_k}(z_k) - RR^T$  is PDPC for every  $k \geq N$  in this case.  $\square$

When  $\Sigma$  is finite, Lemma 5 can be further strengthened as follows.

**Lemma 6** Consider (A.4), where  $W_{p_k}(\cdot) \in \mathbb{R}^{q \times q}$  is PDPC,  $p_k \in \Sigma$ , and  $z_k \in \mathcal{D}$ .

Assume that Assumption 1 holds,  $\bigcap_{k=N}^{\infty} \ker(W_{p_k}(z) - I_q) \neq \{\mathbf{0}\}$  for  $z \in \mathcal{D}$ , and  $\Sigma$  is finite.

i) Then for any  $z_k = z \in \mathcal{D}$  when  $k \geq N$ ,  $\max_{k \geq N} \|(W_{p_k}(z) - RR^T)x\| < \|x\|$  for all  $x \notin \ker(W_{p_k}(z) - RR^T - I_q)$ .

ii) If, in addition,  $W_{p_k}(\cdot)$  is continuous for every  $k \geq N$  and  $\mathcal{D}$  is compact, then for every  $k \geq N$ ,  $\max_{k \geq N} \max_{z_k \in \mathcal{D}} \|(W_{p_k}(z_k) - RR^T)x\| < \|x\|$  for all  $x \notin \ker(W_{p_k}(z_k) - RR^T - I_q)$ .

*Proof.* i) Let  $x \in \mathbb{R}^q$ . Note that it follows from the proof of Lemma 5 that  $x \notin \ker(W_{p_k}(z) - RR^T - I_q)$  if and only if  $(W_{p_k}(z) - I_q)Qy_2 \neq \mathbf{0}_{q \times 1}$  or  $Ry_1 \neq \mathbf{0}_{q \times 1}$ , where  $x = Ry_1 + Qy_2$ .

If  $(W_{p_k}(z) - I_q)Qy_2 \neq \mathbf{0}_{q \times 1}$ , then it follows from the PDPC of  $W_{p_k}(z)$  that  $\max_{k \geq N} \|W_{p_k}(z)Qy_2\| = \|W_{p_k^*}(z)Qy_2\| < \|Qy_2\| \leq (\|Ry_1\|^2 + \|Qy_2\|^2)^{1/2} = \|Ry_1 + Qy_2\|$ , i.e.,  $\max_{k \geq N} \|(W_{p_k}(z) - RR^T)x\| < \|x\|$ .

Alternatively, if  $Ry_1 \neq \mathbf{0}_{q \times 1}$ , then  $\|Ry_1\| > 0$ . Thus, it follows from the PDPC of  $W_{p_k}(z)$  that  $\max_{k \geq N} \|W_{p_k}(z)Qy_2\| = \|W_{p_k^*}(z)Qy_2\| \leq \|Qy_2\| < (\|Ry_1\|^2 + \|Qy_2\|^2)^{1/2} = \|Ry_1 + Qy_2\|$ , i.e.,  $\max_{k \geq N} \|(W_{p_k}(z) - RR^T)x\| < \|x\|$ .

ii) The proof is similar to that of i), and hence, is omitted.  $\square$

Based on Lemma 5, we have the following further result on the structure of  $\bigcap_{k=N}^{\infty} \ker(W_{p_k}(z_k) - RR^T - I_q)$ .

**Lemma 7** Consider (A.4), where  $W_{p_k}(\cdot) \in \mathbb{R}^{q \times q}$  is PDPC,  $p_k \in \Sigma$ , and  $z_k \in \mathcal{D}$ .

Assume that Assumption 1 holds and  $\bigcap_{k=N}^{\infty} \ker(W_{p_k}(z) - I_q) \neq \{\mathbf{0}\}$  for  $z \in \mathcal{D}$ . Then for every  $m \geq N$  and every  $z_k \in \mathcal{D}$ ,  $\bigcap_{k=m}^{\infty} \ker(I_q - W_{p_k}(z_k) + RR^T) = \{\mathbf{0}\}$ .

*Proof.* Let  $x \in \mathbb{R}^q$ . If  $x \in \bigcap_{i=m}^{\infty} \ker(I_q - W_{p_i}(z_i) + RR^T)$ , then  $W_{p_i}(z_i)x = (I_q + RR^T)x$  for every  $i \geq m$ . Since  $\|W_{p_i}(z_i)x\|^2 = \|x\|^2 + 2\|R^T x\|^2 + \|RR^T x\|^2$  and  $\|W_{p_i}(z_i)x\| \leq \|x\|$ , it follows that  $R^T x = \mathbf{0}_{r \times 1}$ . Hence, by the PDPC of  $W_{p_i}(\cdot)$ ,  $W_{p_i}(z_i)x = x$ , which implies that  $x \in \ker(W_{p_i}(z_i) - I_q)$  for every  $i \geq m$ . Consequently,  $x \in \bigcap_{i=m}^{\infty} \ker(W_{p_i}(z_i) - I_q)$ , where  $m \geq N$ . Since  $\bigcap_{k=N}^{\infty} \ker((W_{p_k}(z_k) - I_q) = \bigcap_{k=m}^{\infty} \ker(W_{p_k}(z_k) - I_q)$  for every  $m \geq N$  and the column vectors of  $R$  form an orthonormal basis for  $\bigcap_{k=N}^{\infty} \ker(W_{p_k}(z_k) - I_q)$ , it follows that there exists  $y \in \mathbb{R}^r$  such that  $x = Ry$ . Since  $R^T x = \mathbf{0}_{r \times 1}$ , it follows that  $R^T Ry = \mathbf{0}_{r \times 1}$ ; and, hence,  $Ry = \mathbf{0}_{q \times 1}$ . Finally,  $x = Ry = \mathbf{0}_{q \times 1}$ .  $\square$  Using the above results, one can have the following result on the convergence of (A.4) with a finite index set.

**Lemma 8** Consider (A.4), where  $W_{p_k}(\cdot) \in \mathbb{R}^{q \times q}$  is PDPC,  $p_k \in \Sigma$ , and  $z_k \in \mathcal{D}$ .

Assume that Assumption 1 holds and  $\Sigma$  is finite.

i) Then for any  $x_0 \in \mathbb{R}^q$  and any  $z_k = z \in \mathcal{D}$  when  $k \geq N$ ,  $\lim_{k \rightarrow \infty} x_k =$

$$RR^T x_{N-1} \in \bigcap_{k=N}^{\infty} \ker(W_{p_k}(z) - I_q).$$

ii) If, in addition,  $W_{p_k}(\cdot)$  is continuous for every  $k \geq N$  and  $\mathcal{D}$  is compact, then for

$$\text{any } x_0 \in \mathbb{R}^q \text{ and any } z_k \in \mathcal{D}, \lim_{k \rightarrow \infty} x_k = RR^T x_{N-1} \in \bigcap_{k=N}^{\infty} \ker(W_{p_k}(z_k) - I_q).$$

*Proof.* Let  $z_k \in \mathcal{D}$ . First, if  $\bigcap_{k=N}^{\infty} \ker(W_{p_k}(z_k) - I_q) = \{\mathbf{0}\}$ , then it follows from Lemma 3 that  $\lim_{k \rightarrow \infty} x_k = \mathbf{0}$ . Now we assume that  $\bigcap_{k=N}^{\infty} \ker(W_{p_k}(z_k) - I_q) \neq \{\mathbf{0}\}$ .

Define  $\mathcal{W}_m$  as

$$\begin{aligned} \mathcal{W}_m &= \left( \prod_{i=0}^{m-N} (W_{p_{m-i}}(z_{m-i}) - RR^T) \right) \\ &\quad \times \left( \prod_{i=0}^{N-1} W_{p_{N-1-i}}(z_{N-1-i}) \right) \end{aligned}$$

for every  $m \geq N$ . Then it follows from Lemma 4 that for every  $x_0 \in \mathbb{R}^q$  and every  $m \geq N$ ,

$$\mathcal{W}_m x_0 = x_m - RR^T x_{N-1}. \quad (\text{A.8})$$

We claim that for any  $x \in \mathbb{R}^q$ ,  $\lim_{m \rightarrow \infty} \mathcal{W}_m x = \mathbf{0}_{q \times 1}$ . Suppose, conversely, that there exists  $\mathbf{x} \in \mathbb{R}^q$  such that  $\mathcal{W}_m \mathbf{x}$  does not converge to  $\mathbf{0}_{q \times 1}$  as  $m \rightarrow \infty$ . By Lemma 5,  $W_{p_k}(z_k) - RR^T$  is PDPC for every  $k \geq N$ . Since  $\|W_{p_k}(z_k)\| \leq 1$  due to Lemma 1, we have:

$$\|\mathcal{W}_m \mathbf{x}\| \leq \left( \prod_{i=0}^{m-N} \|W_{p_{m-i}}(z_{m-i}) - RR^T\| \right) \left( \prod_{i=0}^{N-1} \|W_{p_{N-1-i}}(z_{N-1-i})\| \right) \|\mathbf{x}\| \leq \|\mathbf{x}\|$$

Thus,  $\{\mathcal{W}_m \mathbf{x}\}_{m=N}^{\infty}$  is a bounded sequence in  $\mathbb{R}^q$ . It follows from Bolzano-Weierstrass

Theorem that there exists a subsequence  $\{m_k\}_{k=0}^\infty$  such that  $\lim_{k \rightarrow \infty} \mathcal{W}_{m_k} \mathbf{x} = \mathbf{w} \neq \mathbf{0}_{q \times 1}$ , where  $m_0 \geq N$ .

Let  $\mathcal{W}_{m_k} \mathbf{x} = s_k \mathbf{w} + \mathbf{d}_k$ , where  $\mathbf{d}_k \in \text{span}\{\mathbf{w}\}^\perp$ . Note that  $\mathbf{w}^\top \mathcal{W}_{m_k} \mathbf{x} = s_k \|\mathbf{w}\|^2$  and  $\mathbf{d}_k^\top \mathcal{W}_{m_k} \mathbf{x} = \|\mathbf{d}_k\|^2$ . Taking the limit on both sides of these two equations yields  $\lim_{k \rightarrow \infty} s_k = 0$  and  $\lim_{k \rightarrow \infty} \mathbf{d}_k = \mathbf{0}_{q \times 1}$ . Next, it follows from Lemma 7 that  $\bigcap_{i=m_k}^\infty \ker(I_q - W_{p_i}(z_i) + RR^\top) = \{\mathbf{0}_{q \times 1}\}$  for every  $k = 0, 1, 2, \dots$ . Since  $\mathbf{w} \neq \mathbf{0}_{q \times 1}$ , it follows that  $\mathbf{w} \notin \bigcap_{i=m_k}^\infty \ker(I_q - W_{p_i}(z_i) + RR^\top)$ . Hence, for every  $k = 0, 1, 2, \dots$ , there exists  $i > m_k$  such that  $\mathbf{w} \notin \ker(I_q - W_{p_i}(z_i) + RR^\top)$ . Let  $n_k = \min\{i : i > m_k, \mathbf{w} \notin \ker(I_q - W_{p_i}(z_i) + RR^\top)\}$ . Then it follows that

$$\begin{aligned} \mathcal{W}_{n_k} \mathbf{x} &= \left( \prod_{i=0}^{n_k - m_k - 1} (W_{p_{n_k - i}}(z_{n_k - i}) - RR^\top) \right) \\ &\quad \times \left( \prod_{i=0}^{m_k - N} (W_{m_k - i}(z_{m_k - i}) - RR^\top) \right) \\ &\quad \times \left( \prod_{i=0}^{N-1} W_{p_{N-1-i}}(z_{N-1-i}) \right) \mathbf{x} \\ &= s_k (W_{p_{n_k}}(z_{n_k}) - RR^\top) \mathbf{w} \\ &\quad + \left( \prod_{i=0}^{n_k - m_k - 1} (W_{p_{n_k - i}}(z_{n_k - i}) - RR^\top) \right) \mathbf{d}_k. \end{aligned} \quad (\text{A.9})$$

*i)* Note that by assumption,  $z_k = z \in \mathcal{D}$  for all  $k \geq N$ . Taking the norm on both sides of (A.9) yields

$$\|\mathcal{W}_{n_k} \mathbf{x}\| \leq |s_k| \max_{n_k \geq N} \|(W_{p_{n_k}}(z) - RR^\top) \mathbf{w}\| + \|\mathbf{d}_k\|. \quad (\text{A.10})$$

Since  $\mathbf{w} \notin \ker(I_q - W_{p_{n_k}}(z) + RR^\top)$ , it follows from Lemma 6 that  $\max_{n_k \geq N} \|(W_{p_{n_k}}(z) -$

$RR^T\mathbf{w}\| < \|\mathbf{w}\|$ . Hence, by (A.10),

$$\begin{aligned}
\limsup_{k \rightarrow \infty} \|\mathcal{W}_{n_k} \mathbf{x}\| &\leq \limsup_{k \rightarrow \infty} |s_k| \max_{n_k \geq N} \|(W_{p_{n_k}}(z) - RR^T)\mathbf{w}\| \\
&\quad + \limsup_{k \rightarrow \infty} \|\mathbf{d}_k\| \\
&\leq \max_{n_k \geq N} \|(W_{p_{n_k}}(z) - RR^T)\mathbf{w}\| \\
&< \|\mathbf{w}\|. \tag{A.11}
\end{aligned}$$

Note that  $\|\mathcal{W}_{n_k} \mathbf{x}\|$  is monotonically decreasing in terms of  $k$ . Then it follows that  $\lim_{k \rightarrow \infty} \|\mathcal{W}_{n_k} \mathbf{x}\| = \|\mathbf{w}\|$ . Consequently, for any subsequence  $\{s_k\}_{k=0}^\infty$  of  $\{n_k\}_{k=0}^\infty$ ,  $\lim_{k \rightarrow \infty} \|\mathcal{W}_{s_k} \mathbf{x}\| = \|\mathbf{w}\|$ . On the other hand, it follows from (A.11) that there exists a subsequence  $\{q_k\}_{k=0}^\infty$  of  $\{n_k\}_{k=0}^\infty$  such that  $\lim_{k \rightarrow \infty} \|\mathcal{W}_{q_k} \mathbf{x}\| < \|\mathbf{w}\|$ , which is a contradiction. Hence,  $\lim_{m \rightarrow \infty} \mathcal{W}_m x_0 = \mathbf{0}_{q \times 1}$  for every  $x_0 \in \mathbb{R}^q$ . Finally, by (A.8),  $\lim_{m \rightarrow \infty} x_m = \lim_{m \rightarrow \infty} \mathcal{W}_m x_0 + RR^T x_{N_z-1} = RR^T x_{N_z-1} = x_\infty$  and  $x_\infty \in \bigcap_{k=N}^\infty \ker(W_{p_k}(z) - I_q)$  due to Lemma 3.

*ii)* The proof of the second part is similar to that of *i)* by replacing  $W_{p_k}(z)$  and  $\max_{n_k \geq N} \|(W_{p_{n_k}}(z) - RR^T)\mathbf{w}\|$  with  $W_{p_k}(z_k)$  and  $\max_{n_k \geq N} \max_{z_k \in \mathcal{D}} \|(W_{p_{n_k}}(z_k) - RR^T)\mathbf{w}\|$  for all  $k \geq N$ , respectively.  $\square$

Now combining Lemmas 1 and 8, we have the following convergence result for (A.4).

**Theorem 1** *Consider (A.4), where  $W_{p_k}(\cdot) \in \mathbb{R}^{q \times q}$ ,  $p_k \in \Sigma$ , and  $z_k \in \mathcal{D}$ . Assume that Assumption 1 holds and  $\Sigma$  is finite. Furthermore, assume that for every  $p \in \Sigma$  and every  $z \in \mathcal{D}$ ,  $\|W_p(z)\| \leq 1$  and  $\text{rank}(W_p^T(z)W_p(z) - I_q) = \text{rank}(W_p(z) - I_q) = \text{rank} \begin{bmatrix} W_p^T(z)W_p(z) - I_q & W_p^T(z) - I_q \end{bmatrix}$ .*

i) Then for any  $x_0 \in \mathbb{R}^q$  and any  $z_k = z \in \mathcal{D}$  when  $k \geq N$ ,  $\lim_{k \rightarrow \infty} x_k =$

$$RR^T x_{N-1} \in \bigcap_{k=N}^{\infty} \ker(W_{p_k}(z) - I_q).$$

ii) If, in addition,  $W_{p_k}(\cdot)$  is continuous for every  $k \geq N$  and  $\mathcal{D}$  is compact, then for

$$\text{any } x_0 \in \mathbb{R}^q \text{ and any } z_k \in \mathcal{D}, \lim_{k \rightarrow \infty} x_k = RR^T x_{N-1} \in \bigcap_{k=N}^{\infty} \ker(W_{p_k}(z_k) - I_q).$$

*Proof.* The results are the direct consequence of Lemmas 1 and 8.  $\square$

**Remark 1** Unlike the existing results in the literature [68–71, 73–75] where the existence of the limit for (A.4) is only confirmed, but not explicitly calculated, Theorem 1 has two advantages of 1) giving a clue on how to verify paracontraction practically, since both conditions  $\|W_p(z)\| \leq 1$  and  $\text{rank}(W_p^T(z)W_p(z) - I_q) = \text{rank}(W_p(z) - I_q) = \text{rank} \begin{bmatrix} W_p^T(z)W_p(z) - I_q & W_p^T(z) - I_q \end{bmatrix}$  in Theorem 1 can be checked numerically by using the singular value decomposition of  $W_p(z)$ , and 2) having the explicit limit expression  $\lim_{k \rightarrow \infty} x_k = RR^T x_{N-1}$ , which turns out to be a crucial property of studying the convergence performance of (A.5) for the sake of asymptotic approximation of the first and second moment equations for (3.14), while the existing results do not have this property, and hence, cannot be used for asymptotic approximation of (3.14).

### A.2.3 Non-homogeneous subsystem

To discuss the convergence property of (A.5), first note that under Assumption 1, if  $\bigcap_{k=N}^{\infty} \ker(W_{p_k}(z) - I_q) = \bigcap_{k=N}^{\infty} \ker(W_{p_k}(z_k) - I_q) = \mathbb{R}^q$ , then it follows that  $W_{p_k}(z) = W_{p_k}(z_k) = I_q$  for all  $k \geq N$ . In this case, it follows from (A.5) that  $y_k = \sum_{j=0}^k \prod_{i=0}^j W_{p_{j-i}}(z_{j-i}) b_{p_j}(z_j)$  for all  $k < N$  and  $y_k = \sum_{j=0}^{N-1} \prod_{i=0}^j W_{p_{j-i}}(z_{j-i}) b_{p_j}(z_j) +$

$(\prod_{i=0}^{N-1} W_{p_{N-1-i}}(z_{N-1-i})) (\sum_{j=N}^k b_{p_j}(z_j))$  for all  $k \geq N$ . Hence, the asymptotic property of  $y_k$  is closely related to the term  $\sum_{j=N}^k b_{p_j}(z_j)$ , i.e., if  $\sum_{j=N}^{\infty} b_{p_j}(z_j)$  converges, then  $\lim_{k \rightarrow \infty} y_k$  exists.

Now we consider the case where  $\bigcap_{k=N}^{\infty} \ker(W_{p_k}(z) - I_q) = \bigcap_{k=N}^{\infty} \ker(W_{p_k}(z_k) - I_q) \neq \mathbb{R}^q$  under Assumption 1 and  $W_{p_k}(\cdot)$  is PDPC. The key idea here is to derive an appropriate upperbound for  $\prod_{i=0}^{m-N} (W_{p_{m-i}}(z_{m-i}) - RR^T)$  by utilizing its PDPC property proved in Lemmas 5 and 7.

**Lemma 9** *Consider (A.5), where  $W_{p_k}(\cdot) \in \mathbb{R}^{q \times q}$  is PDPC,  $p_k \in \Sigma$ ,  $z_k \in \mathcal{D}$ , and  $b_{p_k} \in \mathbb{R}^q$ . Assume that Assumption 1 holds and  $\Sigma$  is finite. Furthermore, assume that for every  $z \in \mathcal{D}$ ,  $\bigcap_{k=N}^{\infty} \ker(W_{p_k}(z) - I_q) \neq \mathbb{R}^q$ .*

i) *For any  $z_k = z \in \mathcal{D}$  when  $k \geq N$ , there exists a subsequence  $\{m_k\}_{k=0}^{\infty} \subseteq \{N, N+1, \dots\}$  such that  $m_0 = N$ ,  $1 \leq m_{k+1} - m_k \leq M$  for all  $k \geq 0$  and some  $M \geq 1$ , and  $c(z) = \max_{k \geq 0} \|\prod_{i=0}^{m_{k+1}-m_k} (W_{p_{m_{k+1}-i}}(z) - RR^T)\| < 1$ .*

ii) *If, in addition,  $W_{p_k}(\cdot)$  is continuous for every  $k \geq N$  and  $\mathcal{D}$  is compact, then there exists a subsequence  $\{m_k\}_{k=0}^{\infty} \subseteq \{N, N+1, \dots\}$  such that  $m_0 = N$ ,  $1 \leq m_{k+1} - m_k \leq M$  for all  $k \geq 0$  and some  $M \geq 1$ , and*

$$\bar{c} = \max_{k \geq 0} \max_{z_k \in \mathcal{D}} \|\prod_{i=0}^{m_{k+1}-m_k} (W_{p_{m_{k+1}-i}}(z_{m_{k+1}-i}) - RR^T)\| < 1.$$

*Proof.* Let  $x \in \mathbb{R}^q$  and  $x \neq 0$ . It follows from Lemma 7 that for any  $m \geq N$ ,  $x \notin \bigcap_{k=m}^{\infty} \ker(I_q - W_{p_k}(z_k) + RR^T)$ . Hence, for given  $m_0 = N$ , there exists  $m_1 \geq m_0 + 1$  such that  $x \notin \ker(I_q - W_{p_{m_1}}(z_{m_1}) + RR^T)$ . Let  $m_1$  be the minimum one of such a positive integer. By Lemma 5,  $W_{p_k}(z_k) - RR^T$  is PDPC for every  $k \geq N$ . Hence, if  $\prod_{i=0}^{m_1-1-m_0} (W_{p_{m_1-1-i}}(z_{m_1-1-i}) - RR^T)x \neq 0$ , then  $\|\prod_{i=0}^{m_1-1-m_0} (W_{p_{m_1-1-i}}(z_{m_1-1-i}) -$

$RR^T)x\| = \|(W_{p_{m_1}}(z_{m_1}) - RR^T) \prod_{i=0}^{m_1-1-m_0} (W_{p_{m_1-1-i}}(z_{m_1-1-i}) - RR^T)x\| < \|\prod_{i=0}^{m_1-1-m_0} (W_{p_{m_1-1-i}}(z_{m_1-1-i}) - RR^T)x\| \leq \|\prod_{i=0}^{m_1-1-m_0} (W_{p_{m_1-1-i}}(z_{m_1-1-i}) - RR^T)\| \|x\| \leq \|x\|$ . Otherwise, if  $\prod_{i=0}^{m_1-1-m_0} (W_{p_{m_1-1-i}}(z_{m_1-1-i}) - RR^T)x = 0$ , then  $\|\prod_{i=0}^{m_1-1-m_0} (W_{p_{m_1-1-i}}(z_{m_1-1-i}) - RR^T)x\| = 0 < \|x\|$ . Thus,

$$\begin{aligned} & \left\| \prod_{i=0}^{m_1-1-m_0} (W_{p_{m_1-1-i}}(z_{m_1-1-i}) - RR^T) \right\| \\ &= \max_{x \neq 0} \frac{\|\prod_{i=0}^{m_1-1-m_0} (W_{p_{m_1-1-i}}(z_{m_1-1-i}) - RR^T)x\|}{\|x\|} < 1. \end{aligned}$$

Similarly, for this  $m_1$ , one can construct a minimum positive integer  $m_2 \geq m_1 + 1$  such that  $x \notin \ker((I_q - W_{p_{m_2}}(z_{m_2}) + RR^T)$  and  $\|\prod_{i=0}^{m_2-m_1} (W_{p_{m_2-i}}(z_{m_2-i}) - RR^T)\| < 1$ . By induction, we have a subsequence  $\{m_k\}_{k=0}^\infty$  such that  $m_{k+1} - m_k \geq 1$  and  $\|\prod_{i=0}^{m_{k+1}-m_k} (W_{p_{m_{k+1}-i}}(z_{m_{k+1}-i}) - RR^T)\| < 1$  for all  $k \geq 0$ .

Next, we claim that  $\limsup_{k \rightarrow \infty} (m_{k+1} - m_k) < \infty$ . Suppose that this is not true. Let  $J_{z_k}$  be the one defined in Lemma 2. Clearly  $1 \leq |J_{z_k}| \leq |\Sigma| < \infty$ , where  $|S|$  denotes the cardinality of  $S$ . Then it follows that for  $\varepsilon = |\Sigma|$ , there exists  $K \geq 1$  such that  $m_{K+1} - m_K \geq \varepsilon + 2 = |\Sigma| + 2$  and  $J_{z_k} \subseteq \{p_{m_k} : K \leq k \leq K+1\}$ . By the definition of  $m_k$ , we have  $x \notin \ker(I_q - W_{p_{m_K}}(z_{m_K}) + RR^T)$ ,  $x \notin \ker(I_q - W_{p_{m_{K+1}}}(z_{m_{K+1}}) + RR^T)$ , and  $x \in \ker(I_q - W_{p_{m_k}}(z_{m_k}) + RR^T)$  for  $x \neq 0$  and  $m_K + 1 \leq k \leq m_{K+1} - 1$ . Hence,  $x \in \bigcap_{k=m_K+1}^{m_{K+1}-1} \ker(I_q - W_{p_k}(z_k) + RR^T) \subseteq \bigcap_{m \in J_{z_k}} \ker(I_q - W_m(z_k) + RR^T)$ . Thus,  $\bigcap_{m \in J_{z_k}} \ker(I_q - W_m(z_k) + RR^T) \neq \{\mathbf{0}\}$ . On the other hand, for sufficiently large  $K$ ,  $m_K + 1 \leq N' \leq m_{K+1} - 1$ , and every  $\ell \geq N'$ ,  $\bigcap_{k=N'}^\infty \ker(I_q - W_{p_k}(z_k) + RR^T) = \bigcap_{k=\ell}^\infty \ker(I_q - W_{p_k}(z_k) + RR^T) = \bigcap_{m \in J_{z_k}} \ker(I_q - W_m(z_k) + RR^T)$ . By Lemma 7,  $\bigcap_{m \in J_{z_k}} \ker(I_q - W_m(z_k) + RR^T) = \{\mathbf{0}\}$ , which is a contradiction. Therefore,  $\limsup_{k \rightarrow \infty} (m_{k+1} - m_k) < \infty$ .

i) For  $z_k = z \in \mathcal{D}$  when  $k \geq N$ , it follows that  $\|\prod_{i=0}^{m_{k+1}-m_k} (W_{p_{m_{k+1}-i}}(z) - RR^T)\| < 1$  for all  $k \geq 0$  since  $m_k \geq N$  for all  $k \geq 0$ . In this case,  $\max_{k \geq 0} \|\prod_{i=0}^{m_{k+1}-m_k} (W_{p_{m_{k+1}-i}}(z) - RR^T)\| < 1$ .

$RR^T\| < 1$  due to the facts that  $1 \leq m_{k+1} - m_k \leq M$ ,  $\|W_{p_{m_{k+1}-i}}(z) - RR^T\| \leq 1$ ,  $p_{m_{k+1}-i} \in \Sigma$ , and  $\Sigma$  is finite.

ii) For  $z_k \in \mathcal{D}$ , since  $\|\prod_{i=0}^{m_{k+1}-m_k} (W_{p_{m_{k+1}-i}}(z_{m_{k+1}-i}) - RR^T)\| < 1$  for every  $k \geq 0$ ,  $z_k$  is arbitrary, and  $\mathcal{D}$  is compact, it follows that there exist  $z_k^* \in \mathcal{D}$  and  $\{m_k^*\}_{k=0}^\infty$  such that  $\max_{z_k \in \mathcal{D}} \|\prod_{i=0}^{m_{k+1}-m_k} (W_{p_{m_{k+1}-i}}(z_{m_{k+1}-i}) - RR^T)\| = \|\prod_{i=0}^{m_{k+1}^*-m_k^*} (W_{p_{m_{k+1}^*-i}}(z_{m_{k+1}^*-i}^*) - RR^T)\| < 1$  for every  $k \geq 0$ . Hence,  $\max_{k \geq 0} \|\prod_{i=0}^{m_{k+1}^*-m_k^*} (W_{p_{m_{k+1}^*-i}}(z_{m_{k+1}^*-i}^*) - RR^T)\| < 1$  due to the facts that  $1 \leq m_{k+1}^* - m_k^* \leq M$ ,  $\|W_{p_{m_{k+1}^*-i}}(z_{m_{k+1}^*-i}^*) - RR^T\| \leq 1$ ,  $p_{m_{k+1}^*-i} \in \Sigma$ , and  $\Sigma$  is finite.  $\square$

Lemma 9 regroups the product  $\prod_{i=0}^{m-N} (W_{p_{m-i}}(z_{m-i}) - RR^T)$  according to a constructed subsequence  $\{m_k\}_{k=0}^\infty$  to have a desired upperbound. Using this result and summation of infinite series, we have a convergence property for (A.5).

**Lemma 10** Consider (A.5), where  $W_{p_k}(\cdot) \in \mathbb{R}^{q \times q}$  is PDPC,  $p_k \in \Sigma$ ,  $z_k \in \mathcal{D}$ , and  $b_{p_k} \in \mathbb{R}^q$ . Assume that Assumption 1 holds and  $\Sigma$  is finite. Furthermore, assume that for every  $z \in \mathcal{D}$ ,  $\bigcap_{k=N}^\infty \ker(W_{p_k}(z) - I_q) \neq \mathbb{R}^q$ .

i) If  $\sup_{k \geq N+1} \|b_{p_k}(z_k)\| < \infty$ , then for any  $x_0 \in \mathbb{R}^q$  and any  $z_k = z \in \mathcal{D}$  when  $k \geq N$ ,

$$\lim_{k \rightarrow \infty} (y_k - RR^T (\prod_{i=0}^{N-1} W_{p_{N-1-i}}(z_{N-1-i})) (\sum_{j=N+1}^k b_{p_j}(z_j)) - \sum_{k=0}^N \prod_{i=0}^k W_{p_{k-i}}(z_{k-i}) b_{p_k}(z_k)) = y_\infty$$

exists and  $\|y_\infty\| \leq M \frac{c(z)}{(1-c(z))^2} \mathcal{Y}_N$ , where  $M = \sup_{k \geq 0} (m_{k+1} - m_k)$  and  $\mathcal{Y}_N = \|\prod_{i=0}^{N-1} W_{p_{N-1-i}}(z_{N-1-i})\| \sup_{k \geq N+1} \|b_{p_k}(z_k)\|$ .

ii) If  $\sup_{k \geq N+1} \|b_{p_k}(z_k)\| < \infty$ , and in addition,  $W_{p_k}(\cdot)$  is continuous for every  $k \geq N$

and  $\mathcal{D}$  is compact, then for any  $x_0 \in \mathbb{R}^q$  and any  $z_k \in \mathcal{D}$ ,

$$\lim_{k \rightarrow \infty} (y_k - RR^T (\prod_{i=0}^{N-1} W_{p_{N-1-i}}(z_{N-1-i})) (\sum_{j=N+1}^k b_{p_j}(z_j)) - \sum_{k=0}^N \prod_{i=0}^k W_{p_{k-i}}(z_{k-i}) b_{p_k}(z_k)) = y_\infty$$

exists and  $\|y_\infty\| \leq M \frac{\bar{c}}{(1-\bar{c})^2} \mathcal{Y}_N$ .

*Proof.* *i)* Consider (A.7). Since  $z_k = z \in \mathcal{D}$  when  $k \geq N$ , it follows that

$$\begin{aligned}
& \left\| \sum_{k=1}^{\infty} \sum_{m=m_1}^{m_k} \left( \prod_{i=0}^{m-m_0} (W_{p_{m-i}}(z_{m-i}) - RR^T) \right) \right. \\
& \quad \times \left. \left( \prod_{i=0}^{m_0-1} W_{p_{m_0-1-i}}(z_{m_0-1-i}) \right) \right\| \\
& \leq \sum_{k=1}^{\infty} \sum_{m=m_1}^{m_k} \left\| \prod_{i=0}^{m-m_0} (W_{p_{m-i}}(z_{m-i}) - RR^T) \right\| \\
& \leq \sum_{k=1}^{\infty} \sum_{j=1}^k (m_j - m_{j-1}) (c(z))^k \\
& \leq \sum_{k=1}^{\infty} kM (c(z))^k \\
& = M \frac{c(z)}{(1-c(z))^2} \tag{A.12}
\end{aligned}$$

where we used the fact that  $\sum_{k=1}^{\infty} kx^k = x/(1-x)^2$  for  $|x| < 1$ . Then it follows from (A.12) that  $\sum_{m=N}^{\infty} (\prod_{i=0}^{m-N} (W_{p_{m-i}}(z_{m-i}) - RR^T)) (\prod_{i=0}^{N-1} W_{p_{N-1-i}}(z_{N-1-i}))$  converges.

Note that it follows from (A.5) that for  $m \leq N$ ,  $y_m = \sum_{k=0}^m (\prod_{i=0}^k W_{p_{k-i}}(z_{k-i}) b_{p_k}(z_k))$ .

Hence, it follows from (A.7) that for all  $m \geq N+1$ ,

$$\begin{aligned}
& y_m - RR^T (\prod_{i=0}^{N-1} W_{p_{N-1-i}}(z_{N-1-i})) (\sum_{j=N+1}^m b_{p_j}(z_j)) = \sum_{k=0}^N \prod_{i=0}^k W_{p_{k-i}}(z_{k-i}) b_{p_k}(z_k) + \\
& \sum_{j=N+1}^m \mathcal{W}_j b_{p_j}(z_j). \text{ Note that}
\end{aligned}$$

$$\begin{aligned}
& \left\| \sum_{j=N+1}^{\infty} \mathcal{W}_j b_{p_j}(z_j) \right\| = \left\| \sum_{j=N+1}^{\infty} \left( \prod_{i=0}^{j-N} (W_{p_{j-i}}(z_{j-i}) - RR^T) \right) \right. \\
& \quad \times \left. \left( \prod_{i=0}^{N-1} W_{p_{N-1-i}}(z_{N-1-i}) \right) b_{p_j}(z_j) \right\| \\
& \leq \sum_{k=1}^{\infty} \sum_{j=1}^k (m_j - m_{j-1}) (c(z))^k \mathcal{Y}_N \\
& \leq M \frac{c(z)}{(1-c(z))^2} \mathcal{Y}_N.
\end{aligned}$$

Consequently,

$$\lim_{k \rightarrow \infty} (y_k - RR^T \left( \prod_{i=0}^{N-1} W_{p_{N-1-i}}(z_{N-1-i}) \right) \left( \sum_{j=N+1}^k b_{p_j}(z_j) \right) - \sum_{k=0}^N \prod_{i=0}^k W_{p_{k-i}}(z_{k-i}) b_{p_k}(z_k)) = y_\infty$$

and  $\|y_\infty\| \leq M \frac{c(z)}{(1-c(z))^2} \mathcal{Y}_N$ . The proof of *ii*) is similar to that of *i*), and hence, is omitted.  $\square$

**Theorem 2** Consider (A.5), where  $W_{p_k}(\cdot) \in \mathbb{R}^{q \times q}$ ,  $p_k \in \Sigma$ ,  $z_k \in \mathcal{D}$ , and  $b_{p_k} \in \mathbb{R}^q$ . Assume that Assumption 1 holds and  $\Sigma$  is finite. Furthermore, assume that for every  $z \in \mathcal{D}$ ,  $\bigcap_{k=N}^{\infty} \ker(W_{p_k}(z) - I_q) \neq \mathbb{R}^q$ , and for every  $p \in \mathcal{M}$  and every  $z \in \mathcal{D}$ ,  $\|W_p(z)\| \leq 1$  and  $\text{rank}(W_p^T(z)W_p(z) - I_q) = \text{rank}(W_p(z) - I_q) = \text{rank} \begin{bmatrix} W_p^T(z)W_p(z) - I_q & W_p^T(z) - I_q \end{bmatrix}$ .

*i*) If  $\sup_{k \geq N+1} \|b_{p_k}(z_k)\| < \infty$ , then for any  $x_0 \in \mathbb{R}^q$  and any  $z_k = z \in \mathcal{D}$  when  $k \geq N$ ,

$$\lim_{k \rightarrow \infty} (y_k - RR^T \left( \prod_{i=0}^{N-1} W_{p_{N-1-i}}(z_{N-1-i}) \right) \left( \sum_{j=N+1}^k b_{p_j}(z_j) \right) - \sum_{k=0}^N \prod_{i=0}^k W_{p_{k-i}}(z_{k-i}) b_{p_k}(z_k)) = y_\infty$$

exists and  $\|y_\infty\| \leq M \frac{c(z)}{(1-c(z))^2} \mathcal{Y}_N$ .

*ii*) If  $\sup_{k \geq N+1} \|b_{p_k}(z_k)\| < \infty$ , and in addition,  $W_{p_k}(\cdot)$  is continuous for every  $k \geq N$

and  $\mathcal{D}$  is compact, then for any  $x_0 \in \mathbb{R}^q$  and any  $z_k \in \mathcal{D}$ ,

$$\lim_{k \rightarrow \infty} (y_k - RR^T \left( \prod_{i=0}^{N-1} W_{p_{N-1-i}}(z_{N-1-i}) \right) \left( \sum_{j=N+1}^k b_{p_j}(z_j) \right) - \sum_{k=0}^N \prod_{i=0}^k W_{p_{k-i}}(z_{k-i}) b_{p_k}(z_k)) = y_\infty$$

exists and  $\|y_\infty\| \leq M \frac{\bar{c}}{(1-\bar{c})^2} \mathcal{Y}_N$ .

*Proof.* The results are the direct consequence of Lemmas 1 and 10.  $\square$

### A.3 Asymptotic Approximation of Mean-Value Multi-Cue Multi-Choice Tasks

#### A.3.1 Asymptotic approximation of expectation

It is known that the O-H process (3.11) has the following asymptotic approximations on expectation and variance in the long run:  $\lim_{t \rightarrow \infty} \mathbb{E}[x(t)] = \mu/\lambda$  and  $\lim_{t \rightarrow \infty} \mathbb{E}[x^2(t)] = \sigma^2/(2\lambda)$ , where  $\mathbb{E}$  denotes the expectation operator. Now a natural question about the multi-cue multi-choice task model (A.2) or the extended version (A.1) is that whether or not (A.2) or (A.1) has a similar asymptotic approximations of expectation and variance in the long run.

Consider the extended multi-cue multi-choice model (A.1). Let  $n$  denote the number of choices  $i$ , i.e.,  $i = 1, 2, \dots, n$ , and define  $t_{L+1} = \infty$ . Since index  $m \in \mathcal{M}$  is selected according to the cue ordering and assigned time interval  $[t_{l-1}, t_l)$ , a piecewise constant switching signal  $\alpha : \mathbb{R} \rightarrow \mathcal{M}$  is defined as  $\alpha(t) = m$  for  $t \in [t_{l-1}, t_l)$ ,  $l = 1, 2, \dots, L + 1$ . Then  $x_{i,m}(t)$  in (3.14) can be characterized by  $x_{i,\alpha(t)}(t)$ . Let  $X_{\alpha(t)}(t) = [x_{1,\alpha(t)}(t), x_{2,\alpha(t)}(t), \dots, x_{n,\alpha(t)}(t)]^T \in \mathbb{R}^n$  be a column vector stacking  $x_{i,m}(t)$  together, where  $(\cdot)^T$  denotes the transpose operation. Then (A.1) can be rewritten as a vector-valued differential equation form:

$$dX_{\alpha(t)}(t) = A_{\alpha(t)}X_{\alpha(t)}(t)dt + S_{\alpha(t)}dt + Bd\mathbf{W}(t) \quad (\text{A.13})$$

where  $k_{i,\alpha(t)} \in \mathbb{R}$ ,  $w_{i,j,\alpha(t)} \in \mathbb{R}$ ,  $A_{\alpha(t)} = -\sum_{i=1}^n k_{i,\alpha(t)} \mathbf{e}_i \mathbf{e}_i^T - \sum_{i=1}^n \sum_{j=1, j \neq i}^n w_{i,j,\alpha(t)} \mathbf{e}_i \mathbf{e}_j^T$ ,  $w_{i,j,\alpha(t)} = w_{j,i,\alpha(t)}$ ,  $\mathbf{e}_i$  denotes the  $i$ th column of  $I_n$ ,  $S_{\alpha(t)} = [S_{1,\alpha(t)}, S_{2,\alpha(t)}, \dots, S_{n,\alpha(t)}]^T \in \mathbb{R}^n$ ,  $B \in \mathbb{R}^{n \times n}$  is an  $n$ -by- $n$  diagonal matrix whose  $i$ th diagonal element is  $\sigma_i$ , and  $\mathbf{W}(t) = [\mathbf{W}_1(t), \mathbf{W}_2(t), \dots, \mathbf{W}_n(t)]^T \in \mathbb{R}^n$ . Note that  $A_{\alpha(t)}$  is symmetric and when

$k_{i,\alpha(t)} = k_{\alpha(t)}$  and  $w_{i,j,\alpha(t)} = w_{\alpha(t)}$ , (A.1) becomes (A.2), and hence, in this case  $A_{\alpha(t)} = (w_{\alpha(t)} - k_{\alpha(t)})I_n - w_{\alpha(t)}\mathbf{e}\mathbf{e}^T$ , where  $\mathbf{e}$  denotes the  $n$ -dimensional column vector whose elements are all ones.

Let  $Y(t) = \mathbb{E}[X_{\alpha(t)}(t)]$ . Then it follows from [76] that the first moment equation for (A.1) is given by

$$\dot{Y}(t) = A_{\alpha(t)}Y(t) + S_{\alpha(t)}. \quad (\text{A.14})$$

Using the variation of constants formula, (A.14) has the following solution form for every  $t \geq s$ :

$$Y(t) = e^{\int_s^t A_{\alpha(\tau)} d\tau} Y(s) + \int_s^t e^{-\int_s^\tau A_{\alpha(\sigma)} d\sigma} S_{\alpha(\tau)} d\tau. \quad (\text{A.15})$$

Now we consider two cases.

**Case 1)**  $\text{rank} \begin{bmatrix} A_m & -S_m \end{bmatrix} = \text{rank}(A_m)$  for every  $m \in \mathcal{M}$ . In this case, the equation  $A_m X = -S_m$  has a solution  $X = Y_m^*$  for every  $m \in \mathcal{M}$ . Let  $\alpha(t) = m_l \in \mathcal{M}$  for  $t \in [t_{l-1}, t_l]$ ,  $l = 1, 2, \dots, L+1$ , and define  $\Phi_{m_l}(t, t_{l-1}) = e^{\int_{t_{l-1}}^t A_{\alpha(\tau)} d\tau} = e^{A_{m_l}(t-t_{l-1})}$  for  $t \in [t_{l-1}, t_l]$ ,  $l = 1, 2, \dots, L+1$ . Then it follows from (A.14) that for every  $l = 1, 2, \dots, L+1$ ,

$$Y(t) - Y_{m_l}^* = \Phi_{m_l}(t, t_{l-1})(Y(t_{l-1}) - Y_{m_{l-1}}^*), \quad t \in [t_{l-1}, t_l]. \quad (\text{A.16})$$

Next, we will give a sufficient condition on how an asymptotic approximation of the expectation for (A.2) and (A.1) is achieved, i.e., a condition to guarantee the existence of  $\lim_{t \rightarrow \infty} (Y(t) - Y_{m_l}^*)$ .

**Corollary 1** Consider (A.2) and (3.14). Assume that  $\text{rank} \begin{bmatrix} A_p & -S_p \end{bmatrix} = \text{rank}(A_p)$  for every  $p \in \mathcal{M}$ . Let  $A_p Y_p^* = -S_p$  for every  $p \in \mathcal{M}$ .

i) For (A.1), assume that for every  $p \in \mathcal{M}$ ,  $A_p = -\sum_{i=1}^n k_{i,p} \mathbf{e}_i \mathbf{e}_i^T - \sum_{i=1}^n \sum_{j=1, j \neq i}^n w_{i,j,p} \mathbf{e}_i \mathbf{e}_j^T$  is negative-semidefinite. Then for any  $0 < T_D \leq t_l - t_{l-1} \leq T_\Delta$ ,  $l = 1, 2, \dots, L$ ,  $\lim_{t \rightarrow \infty} (Y(t) - Y_{m_l}^*) = RR^T (Y(t_{N-1}) - Y_{m_{N-1}}^*)$ , where  $Y(t)$  is given by (A.15), the column vectors of  $R$  form an orthonormal basis for  $\bigcap_{l=N}^{\infty} \ker(\Lambda_{m_l}(z)T_{m_l}^{-1})$ ,  $z \in [T_D, T_\Delta]$ ,  $N$  is given by Assumption 1,  $T_p \in \mathbb{R}^{n \times n}$  is an orthogonal matrix to diagonalize  $-\sum_{i=1}^n k_{i,p} \mathbf{e}_i \mathbf{e}_i^T - \sum_{i=1}^n \sum_{j=1, j \neq i}^n w_{i,j,p} \mathbf{e}_i \mathbf{e}_j^T$ , and  $\Lambda_p(z)$  is the corresponding diagonal matrix.

ii) For (A.2), assume that for every  $p \in \mathcal{M}$ ,  $\max\{w_p, (1-n)w_p\} \leq k_p$ . Then for any  $0 < T_D \leq t_l - t_{l-1} \leq T_\Delta$ ,  $l = 1, 2, \dots, L$ ,  $\lim_{t \rightarrow \infty} (Y(t) - Y_{m_l}^*) = RR^T (Y(t_{N-1}) - Y_{m_{N-1}}^*)$ , where the column vectors of  $R$  form an orthonormal basis for  $\bigcap_{l=N}^{\infty} \ker(\Lambda_{m_l}(z)T^{-1})$ ,  $z \in [T_D, T_\Delta]$ , and  $T \in \mathbb{R}^{n \times n}$  is an orthogonal matrix to diagonalize  $(w_p - k_p)I_n - w_p \mathbf{e} \mathbf{e}^T$ .

*Proof.* i) Let  $\lambda_{i,p}$ ,  $i = 1, \dots, n$ , be the eigenvalues of  $A_p = -\sum_{i=1}^n k_{i,p} \mathbf{e}_i \mathbf{e}_i^T - \sum_{i=1}^n \sum_{j=1, j \neq i}^n w_{i,j,p} \mathbf{e}_i \mathbf{e}_j^T$ . Then it follows from the symmetry of  $A_p$  that there exists an orthogonal matrix  $T_p \in \mathbb{R}^{n \times n}$  such that  $A_p = T_p \text{diag}(\lambda_{1,p}, \lambda_{2,p}, \dots, \lambda_{n,p}) T_p^{-1}$ , where  $\text{diag}$  denotes a diagonal matrix and  $p \in \mathcal{M}$ . Now we have  $\Phi_{m_l}(t, t_{l-1}) - I_n = e^{A_{m_l}(t-t_{l-1})} - I_n = T_{m_l} \Lambda_{m_l}(t - t_{l-1}) T_{m_l}^{-1}$ , where  $\Lambda_{m_l}(t - t_{l-1}) = \text{diag}(e^{\lambda_{1,m_l}(t-t_{l-1})} - 1, e^{\lambda_{2,m_l}(t-t_{l-1})} - 1, \dots, e^{\lambda_{n,m_l}(t-t_{l-1})} - 1)$ ,  $t \in [t_{l-1}, t_l]$ . Hence, for any  $0 < T_D \leq z_l = t_l - t_{l-1} \leq T_\Delta$ ,  $l = 1, 2, \dots, L$ , and any  $z > 0$ ,  $\ker(\Phi_{m_l}(t, t_{l-1}) - I_n) = \ker(T_{m_l} \Lambda_{m_l}(z_l) T_{m_l}^{-1}) = \ker(T_{m_l} \Lambda_{m_l}(z) T_{m_l}^{-1})$  holds for  $t \in [t_{l-1}, t_l]$  and  $l = 1, 2, \dots, L+1$ .

Thus, if  $L < \infty$ , then for  $N = L+1$ ,  $\bigcap_{l=N}^{L+1} \ker(T_{m_l} \Lambda_{m_l}(z_l) T_{m_l}^{-1}) = \bigcap_{l=N}^{L+1} \ker(T_{m_l} \Lambda_{m_l}(z) T_{m_l}^{-1})$  for any  $z_l \in [T_D, T_\Delta]$  and any  $z \in [T_D, T_\Delta]$ . Therefore, Assumption 1 holds. Otherwise, if  $L = \infty$ , then for sufficiently large  $N$  and any  $m \geq N$ ,  $\bigcap_{l=N}^{\infty} \ker(T_{m_l} \Lambda_{m_l}(z_l) T_{m_l}^{-1}) = \bigcap_{l=N}^{\infty} \ker(T_{m_l} \Lambda_{m_l}(z) T_{m_l}^{-1}) = \bigcap_{l=m}^{\infty} \ker(T_{m_l} \Lambda_{m_l}(z) T_{m_l}^{-1})$  for any  $z_l \in [T_D, T_\Delta]$  and any  $z \in [T_D, T_\Delta]$ . Therefore, Assumption 1 holds (the verification of Assumption 1 can also be done by using Lemma 2).

Hence,  $\|e^{A_p \delta}\| = e^{(\max_{1 \leq i \leq n} \lambda_{i,p}) \delta}$  for every  $\delta \geq 0$ . Thus,  $\|e^{A_p \delta}\| \leq 1$  for every  $\delta \geq 0$  if and only if  $\max_{1 \leq i \leq n} \lambda_{i,p} \leq 0$ .

On the other hand, note that  $\text{rank}(e^{2A_p \delta} - I_n) = \text{rank}(T_p \text{diag}(e^{2\lambda_{1,p} \delta} - 1, e^{2\lambda_{2,p} \delta} - 1, \dots, e^{2\lambda_{n,p} \delta} - 1) T_p^{-1}) = \text{rank}(T_p \text{diag}(e^{\lambda_{1,p} \delta} - 1, e^{\lambda_{2,p} \delta} - 1, \dots, e^{\lambda_{n,p} \delta} - 1) T_p^{-1}) = \text{rank}(e^{A_p \delta} - I_n)$ . Moreover,

$$\begin{aligned} \text{rank} \begin{bmatrix} e^{2A_p \delta} - I_n & e^{A_p \delta} - I_n \end{bmatrix} &= \text{rank} \begin{bmatrix} e^{2A_p \delta} - I_n \\ e^{A_p \delta} - I_n \end{bmatrix} = \\ \text{rank} \begin{bmatrix} T_p \text{diag}(e^{2\lambda_{1,p} \delta} - 1, e^{2\lambda_{2,p} \delta} - 1, \dots, e^{2\lambda_{n,p} \delta} - 1) T_p^{-1} \\ T_p \text{diag}(e^{\lambda_{1,p} \delta} - 1, e^{\lambda_{2,p} \delta} - 1, \dots, e^{\lambda_{n,p} \delta} - 1) T_p^{-1} \end{bmatrix} &= \\ \text{rank}(T_p \text{diag}(e^{\lambda_{1,p} \delta} - 1, e^{\lambda_{2,p} \delta} - 1, \dots, e^{\lambda_{n,p} \delta} - 1) T_p^{-1}) &= \text{rank}(e^{A_p \delta} - I_n) \end{aligned}$$

for every  $\delta \geq 0$ . Now let  $W_p(z) = e^{A_p z}$ , where  $z \in \mathcal{D}$  and  $\mathcal{D} = [T_D, T_\Delta]$ . Then the conclusion is a direct consequence of Theorem 1.

*ii)* The conclusion is a direct consequence of *i)* and the fact that for every  $p \in \mathcal{M}$ ,  $A_p = (w_p - k_p)I_n - w_p \mathbf{e} \mathbf{e}^T$  has the diagonalization form  $T^{-1} A_p T = \text{diag}((1-n)w_p - k_p, w_p - k_p, \dots, w_p - k_p)$ .  $\square$

**Case 2)**  $\text{rank} \begin{bmatrix} A_m & -S_m \end{bmatrix} \neq \text{rank}(A_m)$  for some  $m \in \mathcal{M}$ . In this case, the equation  $A_m X = -S_m$  does not have a solution  $X$  for some  $m \in \mathcal{M}$ . Hence, one cannot use

Corollary 1 to establish the convergence for  $Y(t)$ . Note that it follows from (A.15) that  $Y(t) = \Phi_{m_l}(t, t_{l-1})Y(t_{l-1}) + \int_{t_{l-1}}^t \Phi_{m_l}^{-1}(\tau, t_{l-1})d\tau S_{m_l}$ . Next, it also follows from the proof of Corollary 1 that  $\Phi_{m_l}^{-1}(\tau, t_{l-1}) = e^{-A_{m_l}(\tau-t_{l-1})} = \Phi_{m_l}(-\tau, -t_{l-1})$  for all  $\tau \in [t_{l-1}, t_l]$ . Let  $b_{m_l}(t, t_{l-1}) = \int_{t_{l-1}}^t \Phi_{m_l}^{-1}(\tau, t_{l-1})d\tau S_{m_l}$  for every  $t \in [t_{l-1}, t_l]$ . Similar to (A.4) and (A.5), we can decompose  $Y(t)$  into the following two subsystems for every  $t \in [t_{l-1}, t_l]$

$$Y_1(t) = \Phi_{m_l}(t, t_{l-1})Y_1(t_{l-1}), \quad Y_1(t_0) = Y(t_0) \quad (\text{A.17})$$

$$\begin{aligned} Y_2(t) = & Y_2(t_{l-1}) + b_{m_l}(t, t_{l-1}) \\ & + \Phi_{m_l}(t, t_{l-1})b_{m_{l-1}}(t_{l-1}, t_{l-2}) \\ & + \Phi_{m_l}(t, t_{l-1}) \sum_{s=1}^{l-2} \prod_{k=0}^{s-1} \Phi_{m_{l-1-k}}(t_{l-1-k}, t_{l-2-k}) \\ & \times b_{m_{l-1-s}}(t_{l-1-s}, t_{l-2-s}), \quad Y_2(0) = 0 \end{aligned} \quad (\text{A.18})$$

where  $Y(t) = Y_1(t) + Y_2(t)$ . Then the following conclusion is immediate.

**Corollary 2** Consider (A.2) and (A.1). Assume that  $\text{rank} \begin{bmatrix} A_p & -S_p \end{bmatrix} \neq \text{rank}(A_p)$

for some  $p \in \mathcal{M}$ .

i) For (A.1), assume that for every  $p \in \mathcal{M}$ ,  $A_p = -\sum_{i=1}^n k_{i,p} \mathbf{e}_i \mathbf{e}_i^T - \sum_{i=1}^n \sum_{j=1, j \neq i}^n w_{i,j,p} \mathbf{e}_i \mathbf{e}_j^T$

is negative-semidefinite. Then for any  $0 < T_D \leq t_l - t_{l-1} \leq T_\Delta$ ,  $l = 1, 2, \dots, L$ ,

$\lim_{t \rightarrow \infty} (Y(t) - RR^T Y_1(t_{N-1}) - RR^T (\prod_{i=0}^{N-1} W_{m_{N-1-i}}(z_{N-1-i})) (\sum_{j=N+1}^l b_{m_j}(z_j)) - \sum_{k=0}^N \prod_{i=0}^k W_{m_{k-i}}(z_{k-i}) b_{m_k}(z_k))$  exists, where  $W_p(z) = e^{A_p z}$ ,  $z_k = t_k - t_{k-1}$ , and  $b_{m_k}(z_k) = b_{m_k}(t_k, t_{k-1})$ .

ii) For (A.2), assume that for every  $p \in \mathcal{M}$ ,  $\max\{w_p, (1-n)w_p\} \leq k_p$ . Then for

any  $0 < T_D \leq t_l - t_{l-1} \leq T_\Delta$ ,  $l = 1, 2, \dots, L$ ,  $\lim_{t \rightarrow \infty} (Y(t) - RR^T Y_1(t_{N-1}) - RR^T (\prod_{i=0}^{N-1} W_{m_{N-1-i}}(z_{N-1-i})) (\sum_{j=N+1}^l b_{m_j}(z_j)) - \sum_{k=0}^N \prod_{i=0}^k W_{m_{k-i}}(z_{k-i}) b_{m_k}(z_k))$  exists.

*Proof.* Note that  $b_{m_k}(t_k, t_{k-1}) = e^{-A_{m_k}(t_k - t_{k-1})}$ . Hence, for any  $t_k - t_{k-1} \in [T_D, T_\Delta]$ ,  $\|e^{-A_{m_k}(t_k - t_{k-1})}\| \leq \max_{p \in \mathcal{M}} e^{-\min_{1 \leq i \leq n} \lambda_{i,p} T_\Delta} < \infty$ . The results now are the direct consequence of Theorem 2 for (A.18) and Corollary 1 for (A.17).  $\square$

### A.3.2 Asymptotic approximation of variance

Let  $Z(t) = E[X_{\alpha(t)}(t)X_{\alpha(t)}^T(t)]$  denote the second moment matrix. Then it follows from [76] that the second moment equation for (A.1) is given by

$$\begin{aligned} \dot{Z}(t) &= A_{\alpha(t)}Z(t) + Z(t)A_{\alpha(t)}^T + U(t)Y^T(t) + Y(t)U^T(t) \\ &\quad + BB^T \end{aligned} \tag{A.19}$$

Define the covariance matrix  $V(t) = Z(t) - Y(t)Y^T(t)$ . Then it follows from (A.14) and (A.19) that

$$\dot{V}(t) = A_{\alpha(t)}V(t) + V(t)A_{\alpha(t)}^T + BB^T \tag{A.20}$$

Equation (A.20) is a (switched) Lyapunov differential equation [77]. It follows from Lemma 3.1 of [77] that for any  $t \geq s$ ,

$$\begin{aligned} \text{vec } V(t) &= \left( e^{\int_s^t A_{\alpha(\tau)} d\tau} \otimes e^{\int_s^t A_{\alpha(\tau)} d\tau} \right) \text{vec } V(s) \\ &\quad + \left( \int_s^t e^{-\int_s^\tau A_{\alpha(\sigma)} d\sigma} \otimes e^{-\int_s^\tau A_{\alpha(\sigma)} d\sigma} d\tau \right) \text{vec } BB^T \end{aligned} \tag{A.21}$$

where  $\text{vec}$  denotes the vectorization operation [78, p. 439] and  $\otimes$  denotes the Kronecker product.

Similar to (A.17) and (A.18), we can decompose  $\text{vec } V(t)$  into the following two subsystems for every  $t \in [t_{l-1}, t_l)$

$$U_1(t) = \Phi_{m_l}(t, t_{l-1})U_1(t_{l-1}), \quad U_1(t_0) = \text{vec } V(0) \quad (\text{A.22})$$

$$\begin{aligned} U_2(t) = & U_2(t_{l-1}) + \mathbf{b}_{m_l}(t, t_{l-1}) \\ & + \Phi_{m_l}(t, t_{l-1})\mathbf{b}_{m_{l-1}}(t_{l-1}, t_{l-2}) \\ & + \Phi_{m_l}(t, t_{l-1}) \sum_{s=1}^{l-2} \prod_{k=0}^{s-1} \Phi_{m_{l-1-k}}(t_{l-1-k}, t_{l-2-k}) \\ & \times \mathbf{b}_{m_{l-1-s}}(t_{l-1-s}, t_{l-2-s}), \quad U_2(0) = 0 \end{aligned} \quad (\text{A.23})$$

where  $V(t) = \text{vec}^{-1}(U_1(t) + U_2(t))$ ,  $\Phi_{m_l}(t, t_{l-1}) = \Phi_{m_l}(t, t_{l-1}) \otimes \Phi_{m_l}(t, t_{l-1})$  and  $\mathbf{b}_{m_l}(t, t_{l-1}) = (\int_{t_{l-1}}^t \Phi_{m_l}^{-1}(\tau, t_{l-1}) d\tau) \text{vec } BB^T$ . Hence, by considering two cases of which  $\text{rank} \begin{bmatrix} A_p \oplus A_p & -\text{vec } BB^T \end{bmatrix} = \text{rank}(A_p \oplus A_p)$  for every  $p \in \mathcal{M}$  and  $\text{rank} \begin{bmatrix} A_p \oplus A_p & -\text{vec } BB^T \end{bmatrix} \neq \text{rank}(A_p \oplus A_p)$  for some  $p \in \mathcal{M}$ , one can have two similar results as Corollaries 1 and 2 for (A.22) and (A.23), where  $\oplus$  denotes the Kronecker sum. Since there is no specific technical difficulty here, we do not present these results here.

Finally, we define the asymptotic approximate solutions to (A.14) and (A.20). For Case 1) of (A.14), Let

$${}^1Y(t) = Y_{\alpha(t)}^* + RR^T(Y(t_{N-1}) - Y_{m_{N-1}}^*) \quad \text{for } t \geq t_{N-1}$$

and

$${}^1Y(t) = Y_{\alpha(t)}^* + RR^T(Y(t) - Y_{\alpha(t)}^*) \quad \text{for } t < t_{N-1}$$

For Case 2) of (A.14), let

$$\begin{aligned} {}^2Y(t) = & RR^TY_1(t_{N-1}) + RR^T\left(\prod_{i=0}^{N-1} W_{m_{N-1-i}}(z_{N-1-i})\right)\left(\sum_{j=N+1}^l b_{m_j}(z_j)\right) + \\ & \sum_{k=0}^N \prod_{i=0}^k W_{m_{k-i}}(z_{k-i}) b_{m_k}(z_k) + \sum_{j=N+1}^{\infty} \mathcal{W}_j b_{\alpha(t)}(z_j) \end{aligned}$$

for  $t \geq t_{N-1}$  and

$${}^2Y(t) = RR^TY_1(t) + \sum_{k=0}^l \prod_{i=0}^k W_{m_{k-i}}(z_{k-i}) b_{m_k}(z_k)$$

for  $t < t_{N-1}$ . Similarly we have  ${}^1V(t)$  and  ${}^2V(t)$  for (A.20). Then we call  ${}^iY(t)$  and  ${}^iV(t)$  the asymptotic approximate solutions to (A.14) and (A.20), respectively,  $i = 1, 2$ .

## Bibliography

- [1] E. M. Izhikevich, *Dynamical systems in neuroscience: the geometry of excitability and bursting*. MIT press, 2007.
- [2] S. Wichary and T. Smolen, “Neural underpinnings of decision strategy selection: A review and a theoretical model,” *Frontiers in Neuroscience*, vol. 10, p. 500, 2016. [Online]. Available: <https://www.frontiersin.org/article/10.3389/fnins.2016.00500>
- [3] G. Ermentrout and D. Terman, *Mathematical Foundations of Neuroscience*, ser. Interdisciplinary Applied Mathematics. Springer New York, 2010. [Online]. Available: <https://books.google.com/books?id=0fLdzaFgtjcC>
- [4] D. Purves, *Neuroscience, 6th Edition*. Sinauer Associates, 2018.
- [5] A. L. Hodgkin and A. F. Huxley, “A quantitative description of membrane current and its application to conduction and excitation in nerve,” *The Journal of Physiology*, vol. 117.4, pp. 500–544, 1952.
- [6] N. Burkitt, “A review of the integrate-and-fire neuron model: I. homogeneous synaptic input,” *Biol. Cybern.*, vol. 95, no. 1, pp. 1–19, Jun. 2006. [Online]. Available: <http://dx.doi.org/10.1007/s00422-006-0068-6>
- [7] Y. A. Kuznetsov, *Elements of applied bifurcation theory*. Springer Science & Business Media, 2013, vol. 112.

- [8] K.-F. Wong and X.-J. Wang, “A recurrent network mechanism of time integration in perceptual decisions,” *Journal of Neuroscience*, vol. 26, no. 4, pp. 1314–1328, 2006.
- [9] R. Bogacz, E. Brown, J. Moehlis, P. Holmes, and J. D. Cohen, “The physics of optimal decision making: a formal analysis of models of performance in two-alternative forced-choice tasks.” *Psychological review*, vol. 113, no. 4, p. 700, 2006.
- [10] P. Billingsley, *Probability and measure*. John Wiley & Sons, 2008.
- [11] C. L. Baker Jr and O. J. Braddick, “The basis of area and dot number effects in random dot motion perception,” *Vision Research*, vol. 22, no. 10, pp. 1253–1259, 1982.
- [12] A. Diederich and P. Oswald, “Sequential sampling model for multiattribute choice alternatives with random attention time and processing order,” *Frontiers in Human Neuroscience*, vol. 8, p. 697, 2014.
- [13] M. Usher and J. L. McClelland, “The time course of perceptual choice: the leaky, competing accumulator model.” *Psychological review*, vol. 108, no. 3, p. 550, 2001.
- [14] K. Kawazu and H. Tanaka, “A diffusion process in a brownian environment with drift,” *Journal of the Mathematical Society of Japan*, vol. 49, no. 2, pp. 189–211, 1997.
- [15] R. E. Mickens, *Nonstandard finite difference models of differential equations*. world scientific, 1994.

- [16] A. E. Raftery, "A model for high-order markov chains," *Journal of the Royal Statistical Society: Series B (Methodological)*, vol. 47, no. 3, pp. 528–539, 1985.
- [17] C. Chatfield, *The analysis of time series: an introduction*. Chapman and Hall/CRC, 2003.
- [18] W.-K. Ching, T.-K. Siu, M. K. Ng, and X. Huang, "Markov chains: models, algorithms and applications," 2013.
- [19] J. R. Busemeyer and J. T. Townsend, "Decision field theory: a dynamic-cognitive approach to decision making in an uncertain environment." *Psychological review*, vol. 100, no. 3, p. 432, 1993.
- [20] S. Wichary and T. Smolen, "Neural underpinnings of decision strategy selection: a review and a theoretical model," *Frontiers in neuroscience*, vol. 10, p. 500, 2016.
- [21] G. Aston-Jones and J. D. Cohen, "An integrative theory of locus coeruleus-norepinephrine function: adaptive gain and optimal performance," *Annu. Rev. Neurosci.*, vol. 28, pp. 403–450, 2005.
- [22] G. Gigerenzer and H. Brighton, "Homo heuristicus: Why biased minds make better inferences," *Topics in Cognitive Science*, vol. 1, no. 1, pp. 107–143, 2009. [Online]. Available: <https://onlinelibrary.wiley.com/doi/abs/10.1111/j.1756-8765.2008.01006.x>
- [23] G. Gigerenzer and W. Gaissmaier, "Heuristic decision making," *Annual Review of Psychology*, vol. 62, no. 1, pp. 451–482, 2011, PMID: 21126183. [Online]. Available: <https://doi.org/10.1146/annurev-psych-120709-145346>

- [24] G. Gigerenzer and H. Brighton, “Homo heuristicus: Why biased minds make better inferences,” *Topics in Cognitive Science*, vol. 1, no. 1, pp. 107–143, 2009. [Online]. Available: <https://onlinelibrary.wiley.com/doi/abs/10.1111/j.1756-8765.2008.01006.x>
- [25] Gigerenzer, G., Todd, P. M., and The ABC Research Group, *Evolution and cognition. Simple heuristics that make us smart*. New York, NY, US: Oxford University Press.
- [26] Mata, R. and Pachur, T. and von Helversen, B. and Hertwig, R. and Rieskamp, J. and Schooler, L. , “Ecological rationality: a framework for understanding and aiding the aging decision maker,” *Front Neurosci*, vol. 6, p. 19, 2012.
- [27] L. Martignon and U. Hoffrage, “Fast, frugal, and fit: Simple heuristics for paired comparison,” *Theory and Decision*, vol. 52, no. 1, pp. 29–71, 2002.
- [28] R. M. Yerkes and J. D. Dodson, “The relation of strength of stimulus to rapidity of habit-formation,” *Journal of comparative neurology and psychology*, vol. 18, no. 5, pp. 459–482, 1908.
- [29] P. Katz and R. Calin-Jageman, “Neuromodulation,” in *Encyclopedia of Neuroscience*, L. R. Squire, Ed. Oxford: Academic Press, 2009, pp. 497 – 503. [Online]. Available: <http://www.sciencedirect.com/science/article/pii/B9780080450469019641>
- [30] M. Usher, J. D. Cohen, D. Servan-Schreiber, J. Rajkowski, and G. Aston-Jones, “The role of locus coeruleus in the regulation of cognitive performance,” *Science*, vol. 283, no. 5401, pp. 549–554, 1999.

- [31] P. Eckhoff, K. Wong-Lin, and P. Holmes, “Dimension reduction and dynamics of a spiking neural network model for decision making under neuromodulation,” *SIAM journal on applied dynamical systems*, vol. 10, no. 1, pp. 148–188, 2011.
- [32] T. Hosokawa, S. W. Kennerley, J. Sloan, and J. D. Wallis, “Single-neuron mechanisms underlying cost-benefit analysis in frontal cortex,” *Journal of Neuroscience*, vol. 33, no. 44, pp. 17 385–17 397, 2013.
- [33] A. F. Rossi, L. Pessoa, R. Desimone, and L. G. Ungerleider, “The prefrontal cortex and the executive control of attention,” *Experimental brain research*, vol. 192, no. 3, p. 489, 2009.
- [34] S. J. Anderson, S. C. Peters, T. E. Pilutti, and K. Iagnemma, “An optimal-control-based framework for trajectory planning, threat assessment, and semi-autonomous control of passenger vehicles in hazard avoidance scenarios,” *International Journal of Vehicle Autonomous Systems*, vol. 8, no. 2-4, pp. 190–216, 2010.
- [35] R. Chipalkatty, G. Droge, and M. B. Egerstedt, “Less is more: Mixed-initiative model-predictive control with human inputs,” *IEEE Transactions on Robotics*, vol. 29, no. 3, pp. 695–703, June 2013.
- [36] B. P. Sellner, L. M. Hiatt, R. Simmons, and S. Singh, “Attaining situational awareness for sliding autonomy,” 01 2006, pp. 80–87.
- [37] K. Coussement, D. F. Benoit, and M. Antioco, “A bayesian approach for incorporating expert opinions into decision support systems: A case study of online consumer-satisfaction detection,” *Decision Support Systems*, vol. 79, pp. 24–32, 2015.

- [38] K. G. Murty, J. Liu, Y.-w. Wan, and R. Linn, “A decision support system for operations in a container terminal,” *Decision Support Systems*, vol. 39, no. 3, pp. 309–332, 2005.
- [39] M. L. Platt and P. W. Glimcher, “Neural correlates of decision variables in parietal cortex,” *Nature*, vol. 400, pp. 233 EP –, 07 1999. [Online]. Available: <https://doi.org/10.1038/22268>
- [40] M. Beyeler, M. Richert, N. D. Dutt, and J. L. Krichmar, “Efficient spiking neural network model of pattern motion selectivity in visual cortex,” *Neuroinformatics*, vol. 12, no. 3, pp. 435–454, Jul 2014.
- [41] B. S. McEwen, “Physiology and neurobiology of stress and adaptation: Central role of the brain,” *Physiological Reviews*, vol. 87, no. 3, pp. 873–904, 2007, pMID: 17615391. [Online]. Available: <https://doi.org/10.1152/physrev.00041.2006>
- [42] D. M. Diamond, M. C. Bennett, M. Fleshner, and G. M. Rose, “Inverted-u relationship between the level of peripheral corticosterone and the magnitude of hippocampal primed burst potentiation,” *Hippocampus*, vol. 2, no. 4, pp. 421–430, 1992.
- [43] L. Postman and J. S. Bruner, “Perception under stress,” *Psychological Review*, vol. 55, no. 6, pp. 314–323, 1948.
- [44] H. Braunstein-bercovitz, “Does stress enhance or impair selective attention? the effects of stress and perceptual load on negative priming,” *Anxiety, Stress, & Coping*, vol. 16, no. 4, pp. 345–357, 2003.

- [45] E. Chajut and D. Algom, "Selective attention improves under stress: implications for theories of social cognition," *J Pers Soc Psychol*, vol. 85, no. 2, pp. 231–248, Aug 2003.
- [46] J. W. Payne, J. R. Bettman, and E. J. Johnson, *The Adaptive Decision Maker*. Cambridge University Press, 1993.
- [47] A. Bröder, *The quest for take-the-best: Insights and outlooks from experimental research*. Oxford University Press, 2011, pp. 364–380.
- [48] J. W. Payne, J. R. Bettman, and E. J. Johnson, "Adaptive strategy selection in decision-making," *Journal of Experimental Psychology: Learning, Memory, and Cognition*, vol. 14, no. 3, pp. 534–552, 1988.
- [49] J. Rieskamp and U. Hoffrage, *When do people use simple heuristics, and how can we tell?* Oxford University Press, 1999, pp. 141–167.
- [50] S. Wichary, R. Mata, and J. Rieskamp, "Probabilistic inferences under emotional stress: How arousal affects decision processes," *Journal of Behavioral Decision Making*, vol. 29, no. 5, pp. 525–538, 2016. [Online]. Available: <https://onlinelibrary.wiley.com/doi/abs/10.1002/bdm.1896>
- [51] K. Dedovic, R. Renwick, N. K. Mahani, V. Engert, S. J. Lupien, and J. C. Pruessner, "The montreal imaging stress task: using functional imaging to investigate the effects of perceiving and processing psychosocial stress in the human brain," *Journal of Psychiatry and Neuroscience*, vol. 30, no. 5, p. 319, 2005.
- [52] A. H. Lewis, A. J. Porcelli, and M. R. Delgado, "The effects of acute stress exposure on striatal activity during pavlovian conditioning with monetary gains and losses," *Frontiers in behavioral neuroscience*, vol. 8, p. 179, 2014.

- [53] Y. Noto, T. Sato, M. Kudo, K. Kurata, and K. Hirota, “The relationship between salivary biomarkers and state-trait anxiety inventory score under mental arithmetic stress: a pilot study.” *Anesthesia & Analgesia*, vol. 101, no. 6, pp. 1873–1876, 2005.
- [54] Martijn Willemsen and Eric Johnson, “Mouselabweb,” available at: <http://www.mouselabweb.org>.
- [55] L. Petrakova, B. K. Doering, S. Vits, H. Engler, W. Rief, M. Schedlowski, and J.-S. Grigoleit, “Psychosocial stress increases salivary alpha-amylase activity independently from plasma noradrenaline levels,” *PLoS One*, vol. 10, no. 8, p. e0134561, 2015.
- [56] S. Greene, H. Thapliyal, and A. Caban-Holt, “A survey of affective computing for stress detection: Evaluating technologies in stress detection for better health,” *IEEE Consumer Electronics Magazine*, vol. 5, no. 4, pp. 44–56, Oct 2016.
- [57] H.-G. Kim, E.-J. Cheon, D.-S. Bai, Y. H. Lee, and B.-H. Koo, “Stress and heart rate variability: A meta-analysis and review of the literature,” *Psychiatry investigation*, vol. 15, no. 3, p. 235, 2018.
- [58] Available at: <https://www.empatica.com/research/e4>.
- [59] S. Cohen, T. Kamarck, and R. Mermelstein, “A global measure of perceived stress,” *Journal of health and social behavior*, pp. 385–396, 1983.
- [60] W. Schlotz, I. S. Yim, P. M. Zoccola, L. Jansen, and P. Schulz, “The perceived stress reactivity scale: Measurement invariance, stability, and validity in three countries.” *Psychological assessment*, vol. 23, no. 1, p. 80, 2011.

- [61] I. Dar-Nimrod, C. D. Rawn, D. R. Lehman, and B. Schwartz, “The maximization paradox: The costs of seeking alternatives,” *Personality and Individual Differences*, vol. 46, no. 5-6, pp. 631–635, 2009.
- [62] J. K. Kruschke, “Bayesian estimation supersedes the t test,” *Journal of Experimental Psychology*, vol. 142, no. 2, pp. 573–603, 2013.
- [63] J. Taelman, S. Vandeput, I. Gligorijevi, A. Spaepen, and S. Van Huffel, “Time-frequency heart rate variability characteristics of young adults during physical, mental and combined stress in laboratory environment,” in *2011 Annual International Conference of the IEEE Engineering in Medicine and Biology Society*, Aug 2011, pp. 1973–1976.
- [64] E. Filaire, H. Portier, A. Massart, L. Ramat, and A. Teixeira, “Effect of lecturing to 200 students on heart rate variability and alpha-amylase activity,” *European Journal of Applied Physiology*, vol. 108, no. 5, pp. 1035–1043, Mar 2010. [Online]. Available: <https://doi.org/10.1007/s00421-009-1310-4>
- [65] J. W. Payne, “Task complexity and contingent processing in decision making: An information search and protocol analysis,” *Organizational behavior and human performance*, vol. 16, no. 2, pp. 366–387, 1976.
- [66] Q. Hui, “Optimal semistable control in *ad hoc* network systems: A sequential two-stage approach,” *IEEE Trans. Automat. Control*, vol. 58, no. 3, pp. 779–784, 2013.
- [67] —, “Further results on paracontracting matrices and correction to ‘Optimal semistable control in *ad hoc* network systems: A sequential two-stage approach’,” *IEEE Trans. Automat. Control*, vol. 60, no. 12, pp. 3305–3309, 2015.

- [68] S. Nelson and M. Neumann, “Generalizations of the projection method with applications to SOR theory for Hermitian positive semidefinite linear systems,” *Numer. Math.*, vol. 51, no. 2, pp. 123–141, 1987.
- [69] L. Elsner, I. Koltracht, and M. Neumann, “On the convergence of asynchronous paracontractions with applications to tomographic reconstruction from incomplete data,” *Linear Alg. Appl.*, vol. 130, pp. 65–82, 1990.
- [70] Y. Su and A. Bhaya, “Convergence of pseudocontractions and applications to two-stage and asynchronous multisplitting for singular  $m$ -matrices,” *SIAM J. Matrix Anal. Appl.*, vol. 22, no. 3, pp. 948–964, 2001.
- [71] C. W. Wu, “On some properties of contracting matrices,” *Linear Alg. Appl.*, vol. 428, pp. 2509–2523, 2008.
- [72] X. Wang and Z. Cheng, “The convergence of infinite product of uniformly paracontracting matrices and its application in consensus of the Vicsek model,” *J. Sys. Sci. Math. Scis.*, vol. 33, no. 6, pp. 724–731, 2013.
- [73] L. Elsner, I. Koltracht, and M. Neumann, “Convergence of sequential and asynchronous nonlinear paracontractions,” *Numer. Math.*, vol. 62, no. 1, pp. 305–319, 1992.
- [74] P. Tseng, “On the convergence of the products of firmly nonexpansive mappings,” *SIAM J. Optimiz.*, vol. 2, no. 3, pp. 425–434, 1992.
- [75] R. Bru, L. Elsner, and M. Neumann, “Convergence of infinite products of matrices and inner-outer iteration schemes,” *Electron. Trans. Numer. Anal.*, vol. 2, pp. 183–193, 1994.

- [76] P. E. Kloeden and E. Platen, *Numerical Solution of Stochastic Differential Equations*, 2nd ed. Berlin, Germany: Springer-Verlag, 1995.
- [77] Q. Hui and Z. Liu, “Semistability-based robust and optimal control design for network systems,” Contr. Sci. Eng. Lab., Dept. Mech. Eng., Texas Tech Univ., Lubbock, TX, Tech. Rep. CSEL-07-14, 2014. [Online]. Available: <https://arxiv.org/abs/1407.6690>
- [78] D. S. Bernstein, *Matrix Mathematics*, 2nd ed. Princeton, NJ: Princeton Univ. Press, 2009.